Fabricating and Characterizing Multifunctional Graphene Nanoplatelets-based Polylactide Nanocomposites

by

Qi Zhang

A thesis submitted in partial fulfillment of the requirements for the degree of

Master of Science

Department of Mechanical Engineering
University of Alberta

Abstract

With rising environmental concerns related to plastic pollution and dependency on petrochemical resources, biopolymers have been gaining attention. Polylactide (PLA) as one biopolymer option has attracted much interest. However, the low thermal and electrical conductivities limit its full application in advanced engineering devices. The main objective of this thesis was to fabricate multifunctional PLA polymers with high conductivity and mechanical properties comparable to pure PLA polymer by incorporating graphene nanoplatelet (GNP).

Heat conduction in polymer nanocomposites is mainly controlled by the transport of phonons. A weak interfacial compatibility between filler and polymer may result in high interfacial thermal resistance and robust phonon scattering, resulting in low thermal conductivity. To improve the dispersion of pure graphene nanoplatelet (pGNP) and interfacial bonding between pGNP and PLA matrix, the surface of pGNP was non-covalent modified with tannic acid to obtain functionalized graphene nanoplatelet (fGNP). Moreover, phonon and heat transfer are more pronounced for nanofiller alignment. Therefore, in this work, the two-step processes solution-blending followed by hot compression molding was applied to prepare aligned pGNP/PLA and fGNP/PLA nanocomposites.

The analysis of Fourier transform infrared spectroscopy and X-ray diffraction of fGNP and pGNP powders suggested the success of non-covalent modification. Scanning electron microscopy results indicated improved interfacial adhesion. Moreover, alignment of pGNP and fGNP in PLA specimens was revealed by transmission electron microscopy and thermal conductivity testing. Therefore, PLA nanocomposites exhibited anisotropic thermal conductivity perpendicular and parallel to the in-plane direction of the samples. Anisotropy indices (the ratio of thermal conductivity in parallel to perpendicular direction) of 18.5 and 21.6 were ascertained for samples

with 16 wt% pGNP and 16 wt% fGNP loading, respectively. A greatly enhanced in-plane thermal conductivity of 8.65 W/mK was achieved for PLA nanocomposite with 16 wt% fGNP, which was a 43-fold and 1.5-fold increase compared to neat PLA and nanocomposite reinforced by 16 wt% pGNP, respectively.

Moreover, in-plane electrical conductivity was substantially increased, with the electrical percolation threshold of GNP between 6 and 8 wt%. With the incorporation of 16 wt% fGNP and pGNP, respective conductivities of 0.8 S/cm and 0.5 S/cm reached more than 13 orders of magnitude higher than the value of pure PLA. Besides, embedding 12 wt% GNP in nanocomposites can impart an average total electromagnetic interference shielding effectiveness of 20.71 dB (pGNP/PLA) and 27.91 dB (fGNP/PLA), respectively, which exceeds the required minimum value (20.0 dB) for commercial electromagnetic interference shielding application. Other testing revealed nanocomposites exhibiting improvement in the Young's modulus (3.51 GPa at 16 wt% fGNP) and storage moduli (12.1 GPa at 40°C for 16 wt% fGNP) as well as better thermal stability upon fGNP incorporation accompanied by strong adhesion to PLA matrix.

Overall, the simple hot-compression process combined with the non-covalent modification was effective in manufacturing multifunctional fGNP/PLA nanocomposites with improved electrical and thermal conductivity, better thermal stability, as well as mechanical properties, which may enable the applications of GNP/PLA nanocomposites in electric/electronic, automobile devices, and other potential fields requiring efficient directional thermal management.

Acknowledgments

During my studies at the University of Alberta, many people helped and instructed me. Primarily, I want to express my sincere gratitude to my supervisor Prof. Dr. Pierre Mertiny for his excellent instruction, encouragement, as well as financial support throughout my studies and research here. Without these help, this project work is hardly completed. Also, I would like to thank him for reviewing my thesis and giving much valuable advice. Under his supervision and lead, I have learned how to conduct experimental research and overcome difficulties. I will sincerely cherish forever the enjoyable time working with him. I would also like to thank Bernie Faulkner, who was a technician in the Mechanical Engineering machine shop. He supported my work immensely by making sample molds and repairing devices. Besides, I am very grateful to the technical staff of the nanoFAB for guiding me to operate the instruments there properly. I am also thankful to my workmates in my supervisor's group for their kind help. What is more, I would like to express my thanks for funding support from the Discovery Grants program (grant number RGPIN-2016-04650) of Natural Sciences and Engineering Research Council of Canada (NSERC), China Scholarship Council (CSC), and Alberta Innovates Technology Futures (AITF) Scholarships. Most of all, I give my sincere appreciation to my family for their love and support in these years.

Table of Contents

List of Tables

List of Figures

List of Abbreviations

PLA: Polylactic acid or polylactide

CNT: Carbon nanotube

ITR: Interfacial thermal resistance

0 D: 0-dimensional

1 D: 1-dimensional

2 D: 2-dimensional

GNP: Graphene or graphite nanoplatelets

pGNP: Pure graphene nanoplatelet

fGNP: Functionalized graphene nanoplatelet

TA: Tannic acid

XRD: X-ray diffraction

FTIR: Fourier transform infrared spectroscopy

TEM: Transmission electron microscopy

SEM: Scanning electron microscopy

TPS: Transient plane source

DMA: Dynamic mechanical analysis

E': Storage modulus

E'': Loss modulus

T_g: Glass transition temperatures

TGA: Thermogravimetric analysis

DSC: Differential scanning calorimetry

tanδ: Damping factor

$T_{5\%}$: Thermal decomposition temperature at 5% mass loss

$T_{10\%}$: Thermal decomposition temperature at 10% mass loss

$T_{50\%}$: Thermal decomposition temperature at 50% mass loss

T_{max}: The temperature of the maximum weight loss rate

EMI: Electromagnetic interference

SE: Shielding effectiveness

SE_T: Total electromagnetic interference shielding effectiveness

SE_R: Reflection shielding effectiveness

SE_A: Absorption shielding effectiveness

Chapter 1 – Introduction

1.1 Background

Polymers from non-renewable sources are successfully used in numerous applications, such as electronic devices and fluid containment vessels (e.g. piping). However, waste disposal and recycling and the reliance on petroleum-based products with related pollution issues are problematic [1]. Consequently, research on biodegradable polymers has been gaining significant attention [2]. Biodegradable polymers include, but are not limit to, poly(ε-caprolactone), polybutylene adipate terephthalate, polybutylene succinate, polylactic acid, poly(3-hydroxybutyrate-co-hydroxyhexanoate), and poly(3-hydroxybutyrate-co-hydroxyvalerate) [3, 4]. Among the family of sustainable biopolymers, polylactic acid, has lately attracted increasing scientific interest [5], with the advantages in thermal processibility, biocompatibility, and bioabsorbable ability [6].

Low thermal conductivity of polymers (typically 0.1 to 0.5 W/mK [7]) impedes many industrial applications, such as in heat sinks, batteries and other electronic devices entailing thermal management capability [8, 9]. Thus, tailoring a multifunctional PLA matrix is an attractive proposition. Multifunctionality, in this context, entails a cost-effective material composition having improved thermal conductivity and mechanical strength comparable with neat PLA polymer to meet the requirements for given engineering applications. In the following sections of this introductory chapter, background information on polylactide, nano-reinforcements, and factors affecting the thermal conductivity are described.

1.2 Basic of polylactide biopolymer

Poly (lactic acid), also named polylactide, hydrophobic aliphatic thermoplastic polyester, is generally synthesized either via polycondensation of lactic acid monomer or ring-opening polymerizing lactide (cyclic dimer of lactic acid) [10, 11]. The first study to produce PLA material was researched in the 1845 by polycondensing the lactic acid monomer, and the low molecular weight of PLA is produced in 1932. Soon, in 1945, PLA product is industrially applied in the medical application [12-14]. The lactic acid can be easily derived from the fermenting of

renewable sources such as cornstarch, sugarcane, or potato [15]. Thus, the PLA is also the bio-based polymer.

The existence of chiral carbon in lactic acid, L-(+)-lactic acid and D-(−)-lactic acid, can introduce three stereoisomeric structures of PLA, which is the poly-(L-lactic acid) (PLLA), poly-(D-lactic acid) (PDLA), and poly-(D,L-lactic acid) (PDLLA) [16, 17]. The L-(+)-lactic acid isomer is the major form of lactic acid [18]. Conventional plastic manufacturing processes, such as thermo-compression forming, injection, extrusion or blow molding, and electron spinning, can be utilized to fabricate PLA products [19]. The mechanical properties of PLA (2.5 kJ/m^2 impact strength, 3-4 GPa Young's modulus, and 50-70 MPa tensile strength [20]) are comparable to a range of commodity petrochemical-derived polyolefin materials, such as polyethylene terephthalate (PET), polystyrene (PS), and polypropylene (PP) [21-24], with values shown in Table 1. PLA is seen as a potential alternative to these petroleum-based polymers. PLA has been applied for various applications, within industrial and academic communities, such as industrial packaging, biomedical devices, automotive industries, and agricultural areas [25-27].

Table 1. The mechanical properties comparison of PLA and some petroleum-based polymers

Physical properties	PLA	PS	PET	PP
Young's modulus (GPa)	3.5-3.8	2.3-3.2	2.8-4.2	1.1-1.6
Elongation at break (%)	4-240	1.2-3	30-300	70-600
Tensile strength (MPa)	48-55	34-50	48-72	20-40
Glass transition temperature (°C)	40-70	70-115	73-80	-10
Notched izod impact (kJ/m^2)	2.0	1.2	35	6

1.3 Polylactide-based composites

Some drawbacks of PLA polymer, such as poor electrical and thermal conductivities, low service temperature and crystallization, and being a weak gas barrier, may limit industrial applications [28, 29]. Many approaches, including adding plasticizers [30], mixing with other polymers [31], and

incorporating small amounts of fillers [32] have been explored to tailor PLA polymer properties and mitigate its shortcoming properties.

Among these strategies, combining PLA with nanofillers (at least one dimension size smaller than 100 nm) has been an active field of research to improve the performance of PLA while maintaining its key properties by producing nanoparticle/PLA nanocomposites [33, 34]. The numbers of studies on PLA composites are depicted in Figure 1, which were obtained from the Ei Compendex engineering database (Elsevier, Amsterdam, Netherlands), by searching abstracts for the term "PLA composites". Adding nanofillers into the polymer matrix is a practical and straightforward approach to achieving enhanced target material properties. Moreover, other properties may also be improved or at least not largely deteriorate due to the small loading of nanoparticles added to the polymer matrix.

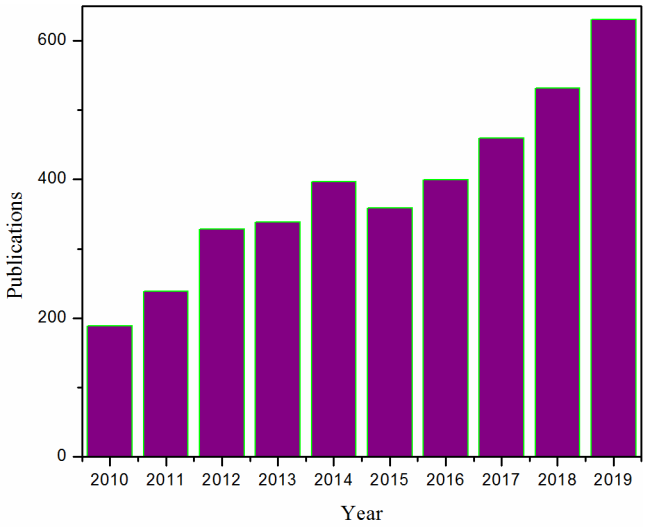

Figure 1. The number of publications of PLA-based composites from 2010 to 2019.

The most frequently used nano-reinforcements in PLA matrix include, but not limited to, nanosilica [35], layered silicate (such as nanoclay [36]), microcrystalline cellulose [37], and carbonaceous material (such as graphene or graphene derivatives [38, 39], carbon fiber [40], and carbon nanotube (CNT) [41]). To fabricate PLA nanocomposites, frequently conventional routes, including melt compounding [42], solution dissolution mixing [43], electrospinning [44], and in situ polymerization [45], have been reported. Generally, the degree of enhancement of various properties in nanofiller/polymer nanocomposites is highly dependent on several factors, including inherent characteristics and structure of the nanofiller (such as the aspect ratio, surface area,

dimension, and synergistic effect), the nanofiller dispersion morphology (random or alignment) in the polymer matrix, and the interfacial bonding between the nano-reinforcement and the polymeric matrix [46-49].

Upon reviewing the previous technical literature on nanofiller/PLA nanocomposites, it was concluded that only a limited number of studies have been concerned with improving conductivities of electrically/thermally insulating PLA, particularly in the case of graphene nanoplatelets-reinforced PLA nanocomposites.

1.4 Brief introduction of graphene (nanoplatelets)

Among the available nanofillers, carbon nano-reinforcement such as CNT and graphene are attractive choices. Graphene, discovered in 2004 [50, 51], consists of a single atomic thick layer of sp^2 hybridized conjugated carbon network hexagonally arranged in a honeycomb two-dimensional lattice structure [52, 53]. Studying graphene as the reinforcement for polymer nanocomposites has drawn considerable interest due to its impressive thermal conductivity (theoretical value of ~5000 W/mK [54]), electron mobility (200 000 $cm^2\ V^{-1}\ s^{-1}$) [55] and mechanical properties (tensile strength ~130 GPa, Young's modulus 0.5-1 TPa [56]). However, due to the high fabrication cost in mass production and low manufacturing rate of high-quality graphene, commercialized applications of single-sheet graphene-based nanocomposite products are typically not competitive [57]. One of the graphene derivatives, graphite (or graphene) nanoplatelets (GNP), also known as graphite nanoflakes or nanosheets, is a promising alternative to graphene. For example, a thermal conductivity of 6.44 $Wm^{-1}K^{-1}$ was reported for an epoxy nanocomposite with 25 vol% GNP, which is a 30 times increase over pure epoxy [58].

GNP is comprised of multiple 2-D graphene layers (thickness 5 to 10 nm [59]), stacked by Van der Waal's forces. The diameter of GNP is in the range from several to dozens of micrometers [60], with aspect ratio (100-1500) [61] and specific surface area (50-750 m^2/g) [62]. Interestingly, most of the outstanding properties of graphene are retentive in GNP, with the exceptional in-plane thermal conductivity (in order of 3000 to 5000 $W\ m^{-1}\ K^{-1}$ [63]), and ultrahigh mechanical properties (elastic modulus 1000 GPa, tensile strength 10 to 20 GPa [64]).

GNP powder can be produced by a top-down approach from the expansion of intercalated graphite. Commercial natural graphite is firstly intercalated with acid ions. Then the intercalated graphite is

thermally expanded by quick heating to above 600°C [65]. After these two processes, lastly, graphite is exposed to mechanical or ultrasonic treatment to obtain the desired sizes of final GNP [66]. Compared to the one-atom-layered graphene or carbon nanotubes, large quantities of GNP can be commercially produced cost-effectively because of the mature fabrication technologies and the low price of abundance graphite [67].

The advantages of GNP as reinforcement over other carbonaceous materials (such as CNT, carbon fiber, or graphene) are summarized as follows:

(i) Improved processability: Compared with graphene and CNT, it is easier to uniformly disperse GNP during fabricating nanofiller/polymer nanocomposites because of the lower viscosity of mixtures [68-70], which can result in more efficient reinforcement effect of the nanofiller phase.

(ii) The lower price of GNP: The cost of GNP (about 65 dollars/kg) is much lower than that of graphene (more than 500 dollars/kg) and CNT [71, 72].

(iii) The greater surface area of GNP: With higher surface area and aspect ratio than that of CNT, a stronger interfacial interaction between GNP and polymer promotes effective stress transfer to GNP from the polymer [73, 74], leading to a higher mechanical properties of nanocomposites.

(iv) The lower thermal contact resistance: Although GNP and single-wall carbon nanotube have similar intrinsic thermal conductivity, the thermal contact resistance between polymer and GNP is lower in comparison to CNT or carbon fiber [75], resulting in more effective heat transfer and improved thermal conductivity. Therefore, to achieve a specific thermal conductivity of nanocomposites, the required GNP loading is typically much lower.

(v) Specific platelet nanostructure: The planar structure of GNP is favored for creating large interaction areas to polymer and providing the two-dimensional paths for phonon transport, which contribute to higher thermal conductivity of GNP-based nanocomposites than one-dimensional carbon nanofillers counterparts [8, 63].

1.5 Graphene nanoplatelets/polylactide nanocomposites

Because of the remarkable intrinsic properties and low production costs, GNP can be considered a promising nanofiller to produce multifunctional polymer nanocomposites. In the past few years, the technical literature reviews has reported studies on the effect of GNP on different properties of various polymers, including PLA as the matrix [16, 76]. There are two primary research directions. Some researchers focus on improving the macroscopic properties of PLA, such as conductivities [77], thermal stability [78], and mechanical properties [79]. Other studies focused on studying the microstructure of GNP/PLA nanocomposites, for example, the crystallization behavior [80], and tailoring interfacial bonding [81].

Notably, tailoring PLA polymeric nanocomposites with multifunctional properties, implying reaching high electrical and thermal conductive while maintaining suitable mechanical properties, has become a significant research activity. With the multifunctionality, it is expected to pursue durable, high-performance commercial demands and replace fossil-based products in some potential markets of advanced engineering areas, such as aerospace and automotive [82], electrostatic/heat dissipation device [83, 84], electromagnetic interference shielding [85], sensor [86], electrodes [87], heat sinks [88], energy storage devices [89-91], et al. Furthermore, with comparable conductivity, GNP/polymer nanocomposites may even be applied in some areas previously using conventional metal, because of lighter weight, higher resistance to acid or alkali corrosion and more economical producing method of nanocomposites [92].

1.6 Factors influencing the thermal conductivity of nanocomposites

Although adding GNP can increase the thermal conductivity of polymer, compared with the intrinsic thermal conductivity of GNP and the mixing rule between polymer and GNP, in most cases, the experimental values reported in the literature were much lower than theoretically predicted values [93].

The actual desired conductivity achievement for nanofiller-reinforced polymer nanocomposites is ascribed to several important contributing factors, such as the type, loading, surface area and aspect ratio of the nanofiller [94, 95], synergistic effects of nanofillers [96], homogenous dispersion and distribution of the naofiller [97], crystallinity of the polymer [98], interfacial adhesion between nanofillers and the host matrix polymer [93, 99], and alignment of nanofillers [100].

1.6.1 The effect of dispersion and interfacial bonding

Due to strong π–π stacking interactions between the layer structures of GNP and the weak bonding to polymers [101, 102], GNP tends to easily restack or form agglomerations to minimize surface free energy [103, 104], thus deteriorating the inherent thermal conductivity. Moreover, due to agglomerations, interactions between GNP nanoparticles and polymer may be reduced to point contacts, which may hamper interfacial bonding between GNP and polymeric matrix. It is known that the heat conduction in polymer nanocomposites is mainly controlled by the transport of phonons (lattice vibration) [61]. The weak interfacial compatibility/coupling may cause a robust phonon scattering or acoustic impedance mismatch at the interface of GNP and polymer, imparting high interfacial thermal resistance (Kapitza resistance) [105, 106], which can reduce the thermal conductivity of the nanocomposites.

Besides applying different dispersion methods, such as powerful sonication mixing or high-shear mechanical blending, significant attention has been given to functionalizing GNP to match surface chemistries between GNP and the polymeric material [107]. Two main strategies have been implemented to modify GNP, i.e.,

(i) Producing new functional groups (such as the hydrophilic/hydrophobic groups) to GNP backbone by covalent bonding through chemical reactions [108].

(ii) Attaching small molecules on the surface of GNP by non-covalent coupling through physical stabilization, including surface adsorption, micelle formation, electrostatic interaction, hydrogen bonding, and π–π interactions [104, 109].

The former approaches (covalent bonding method) include oxygen plasma treatment [29], oxidizing with acid [110], and some ‘grafting to’ and ‘grafting from’ methods [111]. Compared with the non-covalent method, these functional groups may help to form strong and stable interfacial bonding between GNP and polymer by building covalent linkages, significantly improving the load transfer to nanofillers and the thermal stability of PLA [112-114]. However, the chemical reactions may convert the hybridization state of GNP from sp^2 carbon atoms to sp^3 configuration carbon, and produce structural defect sites on the surface, thus disrupting electron paths and damaging the structural integrity of GNP [115, 116]. Thence, properties related to the transport of electrons, phonons, and other quantum effects are deteriorated [117-119]. Moreover, this method may generate toxic wastes, equipment corrosion, and health hazards because of the

use of strong acids (such as the mixture of sulphuric acid and nitric acid) and some dangerous organic solvents [108, 120]. Therefore, to keep the high intrinsic conductivities of GNP and avoid the mentioned problems, as an alternative, non-covalent functionalization should be adopted.

This approach is carried out by building π–π stacking interactions or van der Waals force between the wrapped surface of GNP with the functional groups of dispersing surfactants or the well-defined polymers [116, 121]. Meanwhile, this functionalization approach is more accessible, non-destructive, and no disruption of electron or phonon conjugation compared to covalent one, although the stabilizing effects are limited. Graphene nanosheet (GNS) have been non-covalent functionalized by pyrene poly(glycidyl methacrylate). The thermal conductivity of modified GNP/epoxy is about 20% higher than that of pure GNP reinforced epoxy samples at 4phr (parts per hundred), due to the homogeneous dispersion of GNP and improved interaction between GNS and epoxy polymer [122].

1.6.2 The effect of GNP alignment

In addition to improving the interfacial interaction, creating aligned nanofillers can be an effective way to improve thermal conductivity. Compared with randomly dispersed nanofillers, phonon and heat transfer are more accessible along the pathway in the filler alignment direction. Moreover, because of interactions between nanoparticles, quasi-continuous transport pathways for heat flow may be established within the polymer matrix at higher filler loading. Therefore, thermal conductivity along the alignment direction may substantially increase because of the reduction of contact resistance between adjacent nanofillers and interfacial thermal resistance (ITR) [123, 124]. Moreover, beneficial filler alignment effects may allow reducing nanofiller loading needed for a specific thermal conductivity, which in turn may reduce product cost.

Notably, GNP exhibits anisotropic thermal conductivity, with a much higher intrinsic “in-plane” (~3000 to 5000 W/mK) than “through-the-thickness” value (~10 to 20 W/mK) [125]. Thus, controlling the GNP orientation may take full advantage of the excellent in-plane thermal conductivity, as an efficient heat flow along the alignment direction [126, 127].

The alignment of GNP in a polymer matrix can be achieved by several approaches, such as melt-extrusion, injection, milling or compression [126, 128-133], self-assembly [134, 135], mechanical stretching [136], and electric or magnetic fields [137-141]. Among these methods, magnetic and

electric-field alignment are attractive because of the ability to achieve filler orientation in any desired direction. However, surface modification of GNP with magnetic nanoparticles is necessary, or a powerful external magnetic field may need to be applied, which are complicated processes and may increase cost. Besides, the low breakdown voltage of polymer results in a limited usage of the electric field approach to align GNP fillers [142].

Of the aforementioned methods, hot compression force induced alignment is an attractive alternative for laboratory research because it is a rather straightforward fabrication process for actual polymer components. Besides, nanofiller surface modification is not a requirement, and the manipulation process is less technologically complicated compared to using electric and magnetic field. Moreover, this method can be conducted for series production. Wang et al. [131] fabricated GNP/cellulose nanocrystal papers using hot-compression processing. Morphology studies of the samples exhibited a high degree of GNP alignment after hot-pressing. At 75 wt% GNP loading, the samples' in-plane thermal conductivity reached 73 W/mK, compared to values of 1.2 W/mK and 47 W/mK in the through-plane direction and that of unpressed paper, respectively. In the study of Ding [143], polystyrene/graphene nanocomposites were prepared by solution mixing and hot-pressing techniques. The samples indicated distinct anisotropic thermal conductivity relating to the through-plane and in-plane directions.

1.7 Objective of this thesis

The review of the technical literature on improving the thermal conductivity of PLA polymer revealed that studies from only four research groups have been reported using GNP as the nano-reinforcement [85, 144-146]. Therefore, a need exists to investigate the effect of GNP on thermal and electrical conductivities of PLA nanocomposites. Moreover, three of these four groups prepared the GNP/PLA nanocomposites using melt compounding rather than by a solution mixing method. The latter is the simpler method for fabricating polymer nanocomposites. Moreover, small filler particles can typically be dispersed well during solution blending as opposed to melt compounding [147, 148], which may be a benefit for improving conductivity. Thus, the structures and properties of GNP/PLA nanocomposites prepared by solution mixing were comprehensively examined in the present study. Moreover, the improvement of thermal conductivity in the research of Lin et al. [146] was only modest, with a value of 0.77 W/mK at 30 wt% modified GNP. Based on knowledge of the affecting factors on thermal conductivity of polymer nanocomposites, some

novel ideas or methods were applied in this thesis to significantly improve thermal conductivity. Besides thermal conductivity, electrical conductivity and electromagnetic interference shielding effectiveness were investigated to broaden the industrial and commercial application of biodegradable PLA polymer.

The objectives of this thesis work are therefore to:

1) Investigate the feasibility of hot-compression-induced alignment of pure GNP (pGNP) in PLA nanocomposites.
2) Apply non-covalent modification to functionalize GNP (fGNP) for improved compatibility between GNP and PLA.
3) Study and compare the macroscopic properties and microstructure of PLA-based nanocomposites reinforced by fGNP and pGNP, respectively.

1.8 Structure of this thesis

There are five chapters in this thesis. The experimental approaches used in the research, including the preparation process of GNP/PLA nanocomposites, the method for GNP surface modification, and the properties characterization of samples, are described in Chapter 2. The structure testing of pGNP and fGNP powder, the microstructure, and macroscopic properties of pGNP/PLA and fGNP/PLA nanocomposites are discussed in Chapter 3. A study summary of the thesis is included in Chapter 4, and some research directions for future work are presented in Chapter 5.

Chapter 2 - Experimental Methodology

2.1 Experimental procedures

The materials, experimental procedures, and characterization techniques applied in this work are presented in Chapter 2, such as the functionalization of pure GNP, the preparation of GNP/PLA nanocomposites, and the testing of microstructure and macroscopic properties of the samples.

2.1.1 Materials

Commercially available type of graphene nanoplatelets (trade name xGNP-M15) was bought in XG Sciences Inc. (Lansing, MI, USA). This grade of GNP is described to have average thickness of 6 to 8 nm and a lateral dimension of 15 μm, with in-plane thermal conductivity of 3000 W/mK and through-plane value of 6 W/mK. The electrical conductivity in the in-plane direction is 10^7, compared with 10^2 S/m in the through-plane direction. Commercial poly(lactic acid) (PLA, type 4043D) was purchased from Filabot Co., Ltd. (Barre, VT, USA). The pellets are transparent and are described to have a specific mass of 1.25 g/cm^3, melting temperature of 150 to 180°C and decomposition temperature ~250°C, with the chemical structure shown in Figure 2.

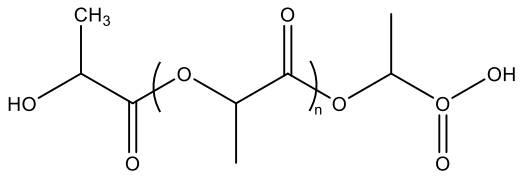

Figure 2. The structural formula of PLA polymer.

For GNP functionalization, tannic acid (TA), supplied by Fisher Scientific (Ottawa, ON, Canada), was used as interfacial modifier, with the structure illustrated in Figure 3. ACS reagent grade chloroform and other chemical materials, all purchased from Fisher Scientific, were used as delivered without any treatment.

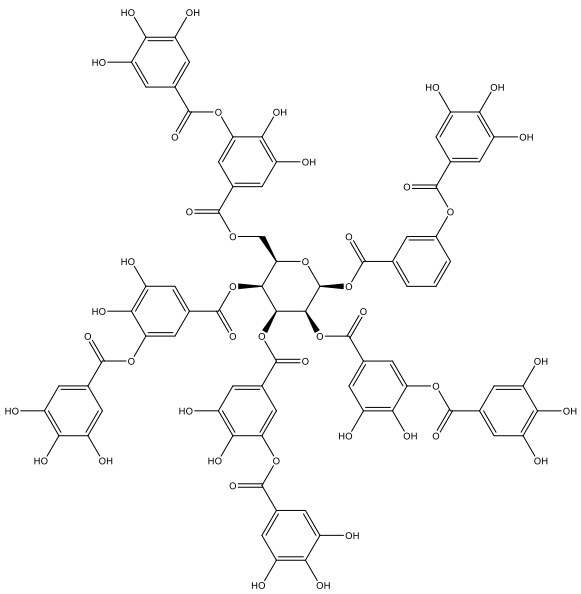

Figure 3. The structural formula of tannic acid (TA) molecular.

2.1.2 Preparation of functionalized GNP (fGNP)

A predetermined amount of pure graphene nanoplatelet (pGNP) was firstly dispersed in chloroform by magnetic stirring for about 10 minutes. Tannic acid (mass ratio of pGNP/TA at 5:1) was then added into the GNP/chloroform suspension under vigorously magnetic stirring for about 60 minutes at ambient temperature in the fume hood. Subsequently, the mixture was treated with an ultrasonic processor (type Q500 sonicator, Qsonica, Newtown, CT, USA) within a pause mode (40 seconds on/20 seconds off) at an output power of 50 to 60 W for 60 minutes. During sonication, the beaker was immersed into an ice bath to maintain the mixture temperature below 10°C, preventing quick evaporation of chloroform. After that, the suspension was further magnetic stirred for 4 to 5 hours at room temperature. The obtained suspension underwent vacuum filtration with a polyvinylidene difluoride filter (0.22 μm pore size, Durapore™ hydrophilic, MilliporeSigma, Burlington, MA, USA). Subsequently, the dark material collected on the membrane was washed three times by deionized water/isopropanol mixture (volume ratio 3:1) to remove unreacted tannic acid. The last step was to dry the material at 80°C overnight, resulting in the non-covalent functionalized GNP (fGNP), according to schematic illustrated in Figure 4.

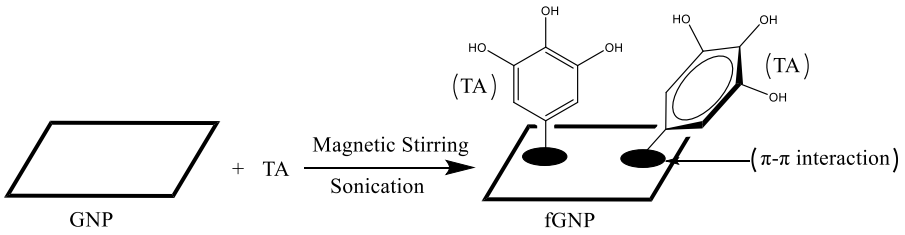

Figure 4. The schematic illustration of preparation of fGNP with tannic acid (TA).

2.1.3 Preparation of GNP/PLA nanocomposites

Before any processing steps, the as-received PLA and GNP powder were heated at 80°C more than 12 hours to minimize residual moisture. GNP/PLA nanocomposites were prepared via solution mixing method using chloroform as the solvent, followed by hot compression. The predetermined amount of GNP was dispersed in chloroform (concentration of 1 to 20 mg/mL), subjecting the suspension to ultrasonication with a cylindrical tip probe at an output power of 50 to 60 W with 40 second pulses alternating with 20 second rest periods for 3 hours. In this manner, a stable GNP/chloroform suspension was obtained. To prevent overheating and solvent evaporation, the beaker containing the suspension was immersed in an ice bath during the sonication process (shown in Figure 5a and Figure 30 in Appendix A). Continuously refilling the bath with fresh ice was required to maintain the desired cooling. At the same time, the PLA/chloroform solution (concentration of ~0.08 g/ml) was prepared by slowly pouring chloroform into a three-neck round-bottom flask prefilled with PLA. The flask content was then subjected to vigorous magnetic stirring at ambient temperature until forming a transparent solution, as depicted in Figure 5a' and Figure 31 in Appendix A.

After finishing GNP dispersion, the prepared PLA solution was added gradually into the GNP/chloroform suspension. The GNP/PLA/chloroform mixture was then homogenized by mechanical stirring at 950 rpm for 60 minutes (Figure 5b and Figure 32 in Appendix A). Further sonication in the ice bath for about 60 minutes was performed (Figure 5c) before the mixture was poured into a custom-made steel mold. The applied sonication time (1 h) is based on other works [149, 150]. Before filling the cuboid mold (Figure 35 in Appendix B) with the mixture, all walls of the mold were coated with a release agent (Frekote 700 NC, Henkel Corporation, Düsseldorf, Germany). Then the GNP/PLA/chloroform mixture was left overnight in a fume hood at ambient conditions in order to evaporate the bulk of the solvent (Figure 5d and Figure 33 in Appendix A).

A vacuum oven was subsequently used to remove any remaining chloroform in the nanocomposites for 5 to 12 hours at about 120°C. The resulting GNP/PLA nanocomposite plate was sectioned into smaller pieces, which were placed into a cylindrical steel mold with a diameter of 100 mm for hot compression molding (Figure 36 in Appendix B). The mold walls were also treated with the release agent. The smaller pieces were then shaped into the circular disc (with thicknesses ranging 2 to 4 mm) using a four-column Carver hydraulic press (model 4386, Wabash, IN, USA), as shown in Figure 5e and Figure 34 in Appendix A. During the hot-press, the material was preheated at 145°C for 5 minutes and then pressed at 15 MPa for 3 minutes. The mold was finally slowly cooled to the ambient temperature (20 to 30°C) in air under the applied pressure.

After compression molding, the prepared GNP/PLA nanocomposite specimens were then stored in sealed plastic bags and cut into the specific shape for characterization. Neat PLA plates were also fabricated in a similar process for the sake of comparison. Samples with different pGNP and fGNP loadings (4 wt%, 6 wt%, 8 wt%, 12 wt%, and 16 wt%) were prepared, which were designated as 'x-pGNP/PLA' and 'x-fGNP/PLA', respectively, where 'x' represented the weight percentage of pGNP and fGNP relative to PLA. For example, the sample with 4 wt% loading of pGNP and fGNP is designated as 4-pGNP/PLA and 4-fGNP/PLA, respectively.

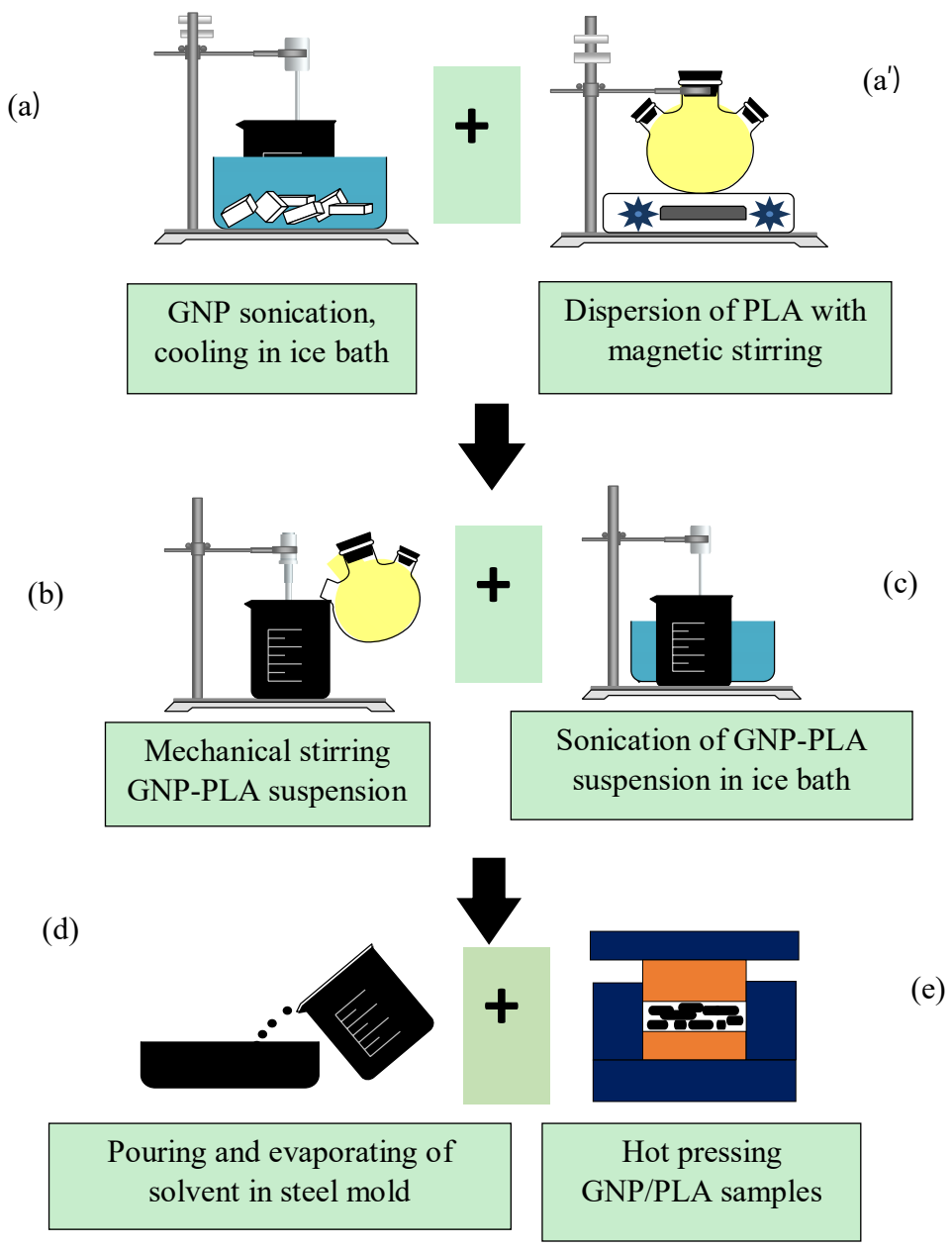

Figure 5. Fabrication processes of GNP/PLA nanocomposites.

2.2 Sample characterization

2.2.1 X-Ray diffraction

X-ray diffraction (XRD, Ultima IV, Rigaku, Tokyo, Japan) was applied to assess the crystal structure of pGNP and fGNP powders and the stacked state (single or multi-stacked layer) of GNP in PLA nanocomposites. Diffraction patterns were collected at 2θ angles ranging from 10° to 40° at a scan rate of 5°/minute and scan step size of ~0.05°. Scans were performed at 40 kV and 44 mA with Cu-Kα irradiation (λ = 1.542 Å).

2.2.2 Fourier-transform infrared spectroscopy

Fourier-transform infrared spectroscopy (FTIR) of pGNP and fGNP were performed to investigate their chemical structures. 32 scans were recorded at wavenumbers from 400 to 4000 cm^{-1} at a resolution of 4 cm^{-1} using an FTIR spectrometer (Nicolet 8700, Thermo Fisher Scientific, Waltham, MA, USA). Before FT-IR measurements, fGNP and pGNP powders mixing with potassium bromide were pressed into pellets.

2.2.3 Morphology characterization

Transmission electron microscopy (TEM) images of GNP/PLA nanocomposites were obtained using a JEM-ARM200CF S/TEM (JEOL, Tokyo, Japan) electron microscope performed at 200 kV accelerating voltage. TEM slices (90 nm in thickness) were sectioned using an ultramicrotome (model Ultracut 701704, Reichert-Jung/Leica Microsystems, Wetzlar, Germany) in the through-thickness direction.

Scanning electron microscopy (SEM) of tensile-fractured surfaces of GNP/PLA samples was conducted using a Zeiss Sigma Field Emission Scanning Electron Microscope (FE-SEM) with EDX & EBSD (Carl Zeiss Microscopy, Jena, Thüringen, Germany). Before the SEM observations, the sample surfaces were coated with gold (Leica ACE600 Carbon/Metal coater). Gold-coated samples for SEM testing are shown in Figure 6.

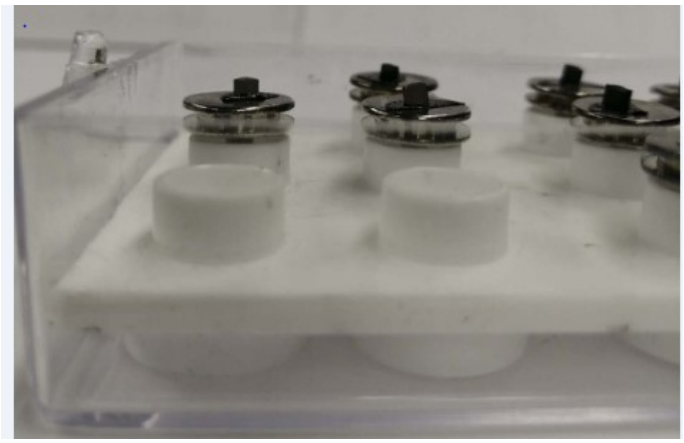

Figure 6. Gold-coated tensile fractured specimens for SEM testing.

2.2.4 Thermal conductivity testing

The thermal conductivity of GNP/PLA samples was tested at atmospheric pressure by a transient plane source (TPS) device (type 2500S, Thermtest, Fredericton, NB, Canada) with a Kapton sensor (model 5465, Thermtest). The sample dimensions were 35 mm by 35 mm by 4 mm. The sensor was placed between two samples (as shown in Figure 37 in Appendix C), and measurement time and heating power were set before testing to obtain the maximum axial and radial depth but to be still within the boundaries of the sample. Four samples were tested for each GNP loading to obtain averaged thermal conductivity values. It is required to supply the specific heat capacity of the tested materials for measuring the anisotropic thermal conductivity. Samples with a mass of 5 to 10 mg, prepared in platinum pans, were heated from 0°C to 50°C in a differential scanning calorimeter (DSC, Mettler Toledo, Switzerland), under dry nitrogen flow (50 mL/minute) at a heating ramp of 10°C/minute. Three separate runs were performed, i.e., empty pan, sample, and sapphire reference (Perkin Elmer, Shelton, CT, USA) for calculating the heat capacity. The volumetric heat capacity for each GNP loading was calculated using the value of the averaged specific heat capacity and density.

2.2.5 Dynamic mechanical analysis

The thermo-mechanical property of PLA and GNP/PLA nanocomposites was characterized by dynamic mechanical analysis (DMA 8000, Perkin-Elmer, Waltham, MA, USA). Tests were performed in single-cantilever mode at the frequency of 1 Hz, with deformation of 0.05 mm and a ramp of 2°C/minute from ambient temperature to about 130°C. Rectangular sample strips had a

gauge length of ~10 mm (total length of ~20 mm), a width of ~5 mm and thickness ranging from 2 to 4 mm. The dynamic storage and loss modulus (E' and E'', respectively) and damping factor (tan δ) were recorded as a function of the temperature. The temperature at tan δ peaks was considered as the glass transition temperature (T_g).

2.2.6 Thermal analysis

The thermal stability of pure PLA and PLA nanocomposites was characterized using thermogravimetric analysis (TGA, Q500, TA Instruments, Lindon, UT, USA). Samples with a mass of about 5 to 10 mg were isothermally treated at 30°C for 5 minutes. Then, specimens were heated to 470°C at an increasing rate of 10°C/minute under nitrogen flow (25 ml/minute).

The thermal transition of PLA samples was studied using differential scanning calorimeter (DSC, TA Instrument, DSC-Q 1000, New Castle, DE, USA) under nitrogen atmosphere (60 mL/min). The 5 to 7 mg samples were sealed in standard Tzero aluminum pans, and the same empty encapsulated aluminum pan was used as the reference. The thermograms were recorded following a heating-cooling-heating procedure. The specimens were firstly heated to 180°C from 30ºC at a heating ramp of 10°C/min and then kept isotherm at 180°C for 5 minutes to eliminate the anterior thermal memory of samples. The system was then cooled to 30°C at a cooling ramp of 20°C/min, kept at 30 °C for 3 minutes. The temperature of the system was finally heated again to 180°C at a heating rate of 2°C/min in the second heating scan. Only the results in the second heating scan were considered for evaluating the thermal characteristics of the GNP/PLA nanocomposites.

2.2.7 Tensile properties

The mechanical properties of PLA and GNP/PLA samples were carried out in accordance with the ISO527-2:1BB standard. Dumbbell shaped samples were prepared by cutting the compression-molded sheet using a waterjet cutter. Measurements were conducted using a dual column Instron 5966 Universal Testing Machine (Norwood, MA, US), with a constant crosshead rate of 0.1 mm/min at room temperature. For every composition, tests were conducted in triplicate to obtain the average and standard deviation of tensile strength, elongation at break, and Young's modulus.

2.2.8 Electrical conductivity measurements

The electrical conductivity of compression-molded GNP/PLA nanocomposites were measured using two different testing devices. When the electrical conductivity of samples is higher than 10^{-2} S/m, the ESP four‐pin probe (type: MCPTP08P) coupled with the Loresta GP (model: CP-T610) resistivity meter (Mitsubishi Chemical Co., Japan) was applied. When the electrical conductivities is smaller than 10^{-2} S/m, the testing was employed on a Keithley 6517A electrometer.

2.2.9 Electromagnetic interference (EMI) shielding

EMI shielding of the nanocomposites was analyzed in the X-band frequency range (8.2 to 12.4 GHz) with an Agilent E5071C wave guided network analyzer (ENA series, Keysight Technologies, Santa Rosa, CA, USA) coupled with a rectangular waveguide WR-90. During the measurements, the rectangular specimens under test (average length × width × thickness of 25 mm × 14 mm × 2 mm) were sandwich-placed between the two standard X-band waveguides WR-90 of the network analyzer. The analyzer sent a signal incident to the material, and then the relevant scattering parameters (S-parameters) were detected and recorded by the wave receivers. For each formulation, at least three specimens were tested. At least three samples were tested for each GNP loading during the EMI characterization process.

Chapter 3 - Results and Discussions

The structural analysis of the fGNP and pGNP powders, and the discussion of properties of fGNP/PLA and pGNP/PLA nanocomposites are presented in this chapter.

3.1 FT-IR characterization of pGNP and fGNP powders

The aromatic rings of tannic acid molecules can form non-covalent bonds with GNP by π–π stacking interactions [146]. As shown in Figure 7 of the FT-IR spectra, the peaks at 1200 cm^{-1} (phenolic O-H stretch vibration), 1320 cm^{-1} (ester C-O stretch vibration), and 1707 cm^{-1} (C=O stretch vibration) were the characteristic chemical groups of tannic acid [151, 152].

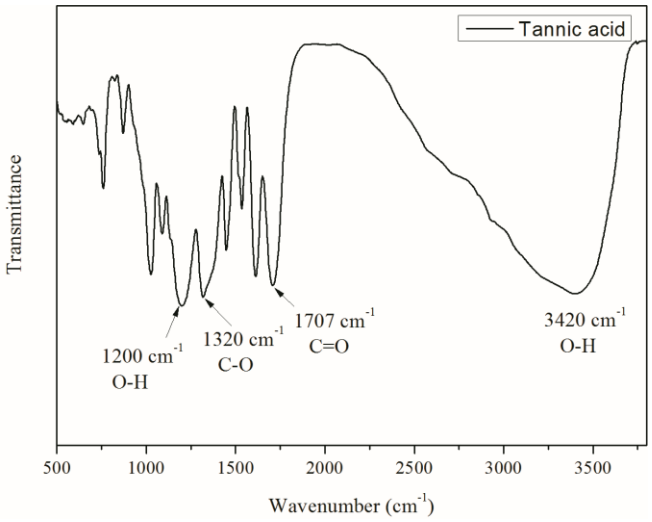

Figure 7. FT-IR spectra of tannic acid molecules.

From the FT-IR spectra of pGNP and fGNP, shown in Figure 8, the characteristic sharp peak at 3430 cm^{-1} was attributed to the stretching vibrations of O-H. Notably, the peaks at 1320 cm^{-1} and 1705 cm^{-1} of tannic acid molecules were only presented on fGNP surface, indicating the absorption of tannic acid molecules on the surface of unmodified GNP. Moreover, the intensity of some peaks (such as 2924, 2854, 1630, 1112 cm^{-1}) in fGNP curves were increased due to the introduction of tannic acid [152].

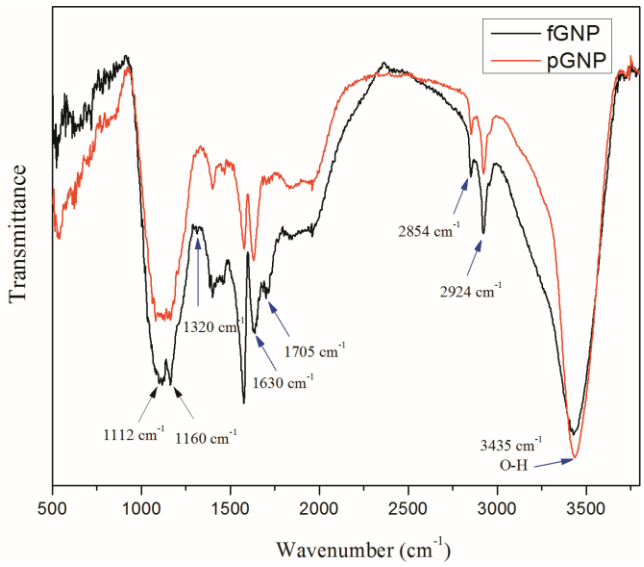

Figure 8. FT-IR spectra of pGNP and fGNP powders.

3.2 XRD analysis of pGNP and fGNP powders

XRD analysis was conducted to characterize the crystal structure of pristine pGNP and fGNP. The diffraction patterns of pGNP and fGNP, as shown in Figure 9, all demonstrate a peak at 2θ of ~26.5°, which is associated with the d_{002} graphitic plane with d-spacing of 0.34 nm [153]. The intensity of this peak for fGNP decreased sharply, indicating fGNP was much less ordered than pGNP [154].

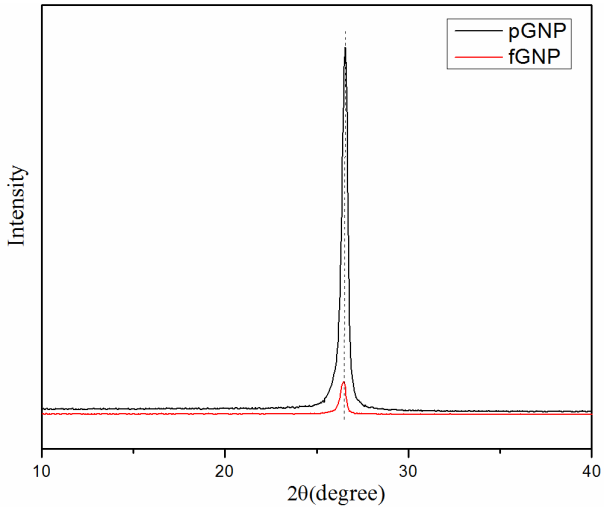

Figure 9. XRD patterns of pGNP and fGNP powders.

3.3 Morphology of PLA nanocomposites

The SEM morphology studies may provide information about the nanofillers dispersion state in the polymer nanocomposites and the interfacial bonding between them. Figures 10a), b) and c) show SEM morphologies of the tensile-fractured cross-section of pure PLA, 4-pGNP/PLA, and 4-fGNP/PLA samples, respectively. As indicated in Figure 10a), the tensile-fractured surface of neat PLA exhibited a smooth and featureless characteristic without any polymer yielding lines under the tensile loading. Compared with the image of 4-fGNP/PLA sample, more stacked nanoplatelets (the blue circles), and micro-holes as the result of pGNP pullout from PLA surfaces (green rectangles) were shown in Figure 10b) for the PLA nanocomposite with pGnP. As seen in the image of Figure 10c), most of the fGNP nanofillers were embedded in the PLA matrix after tensile loading. These characteristics for pGNP/PLA and fGNP/PLA samples might suggest improved interfacial strength between fGNP and PLA matrix after the non-covalent functionalization. Moreover, it was found that GNP nanofillers were aligned in the polymeric matrix (the red arrows) in pGNP/PLA and fGNP/PLA nanocomposites. It is conceivable that nanofillers may overlap and interconnect under the intense compression loads during hot pressing.

While not directly evident in SEM images, the interfacial compatibilizer tannic acid may significantly promote surface interactions between the PLA matrix and fGNP nanofillers, based on the theoretically reactions depicted in Figure 11. On the one hand, π–π interactions between GNP and the aromatic tannic acid can form stable features of tannic acid on the surface of fGNP. On the other hand, the presence of active functional phenolic hydroxyl groups on the structure of tannic acid may result in chemical interactions, i.e., hydrogen bonding with the PLA matrix to promote interfacial adhesion [146]. In contrast, interfacial reactions are likely much less prominent between pGNPs and the PLA matrix.

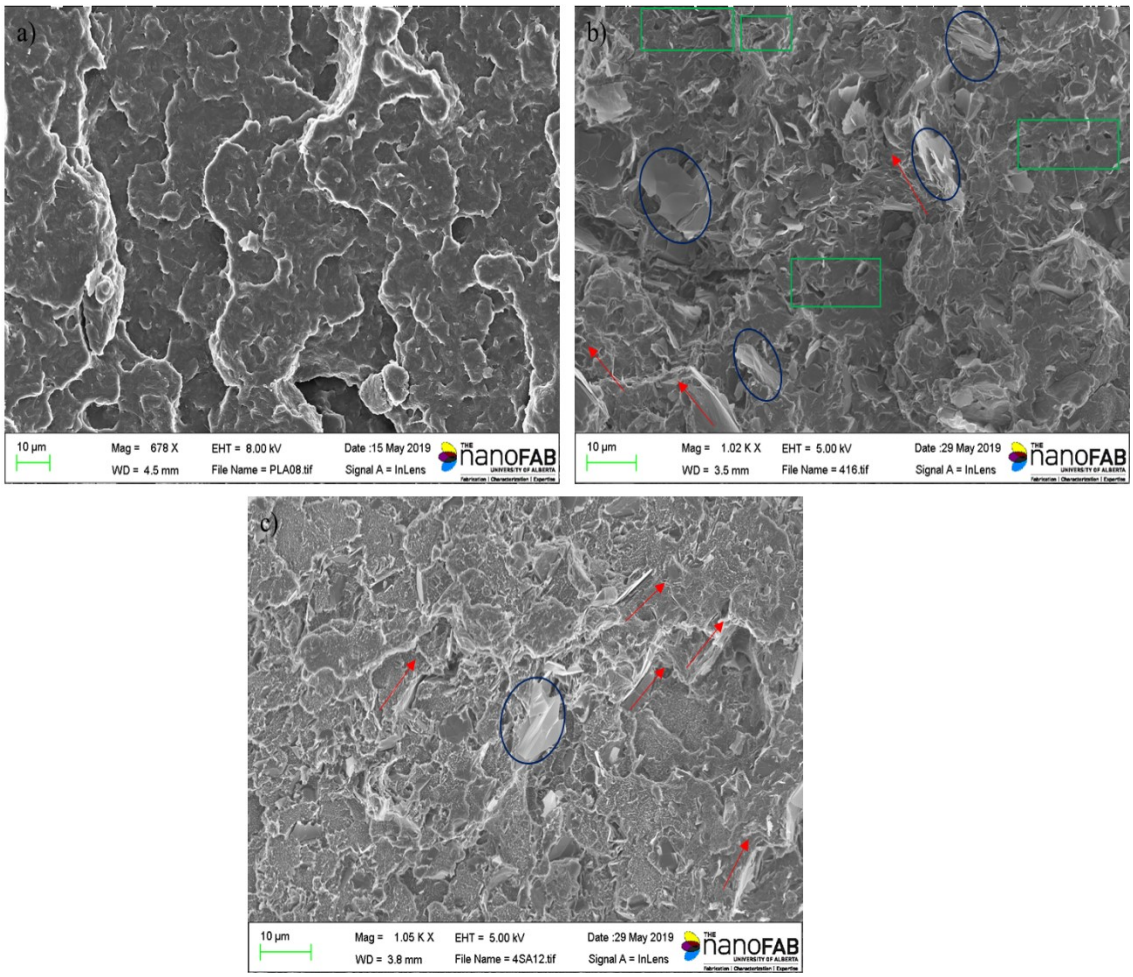

Figure 10. Scanning electron micrographs of tensile-fractured surfaces of a) neat PLA, b) 4-pGNP/PLA nanocomposites, and c) 4-fGNP/PLA nanocomposites.

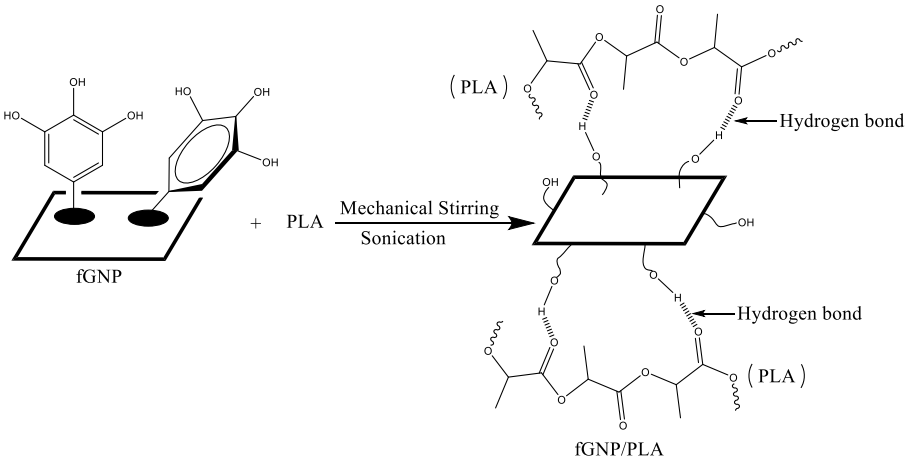

Figure 11. Schematic illustration of possible interactions of fGNP particles and PLA matrix by using tannic acid (TA) as bridging agent.

Figures 12a to 12e show representative TEM images of pGNP/PLA (Figures 12a_1 to 12e_1) and fGNP/PLA nanocomposites (Figures 12a_2 to 12e_2), respectively, corresponding to 4 wt%, 6 wt%, 8 wt%, 12 wt%, and 16 wt% GNP loading. Notably, the TEM images also indicate nanofiller alignment above 6 wt% GNP. It was hypothesized that GNP alignment was facilitated by the intense compression and excluded volume effects between adjacent GNP nanofillers during hot pressing [130, 155]. Noting some visible holes in the micrographs, it is presumed these to be artifacts of the ultramicrotomy process. The dispersion of fGNP in the PLA matrix appears to be more homogenous, and interconnected pathways between adjacent nanofillers seem to be more significant.

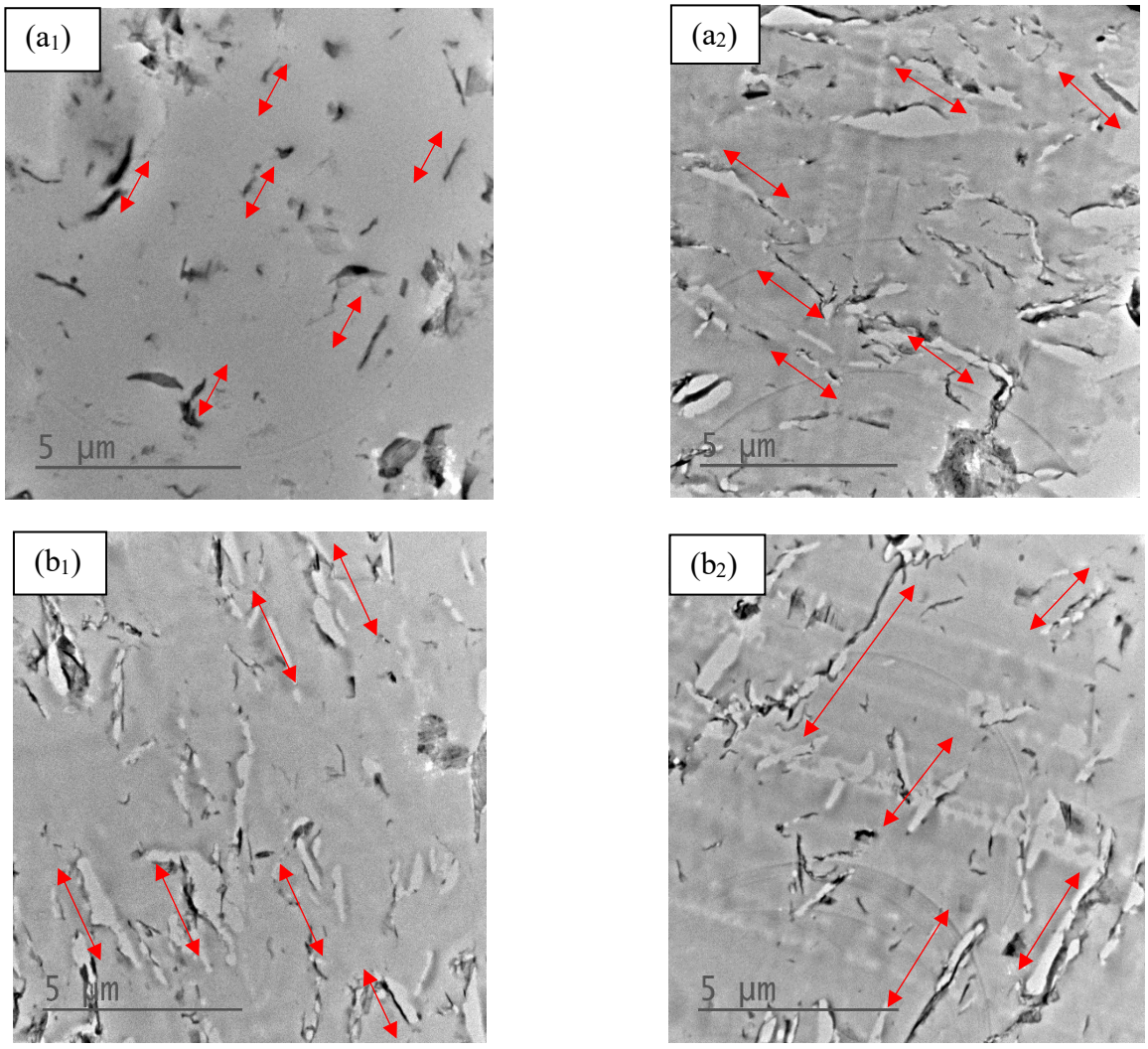

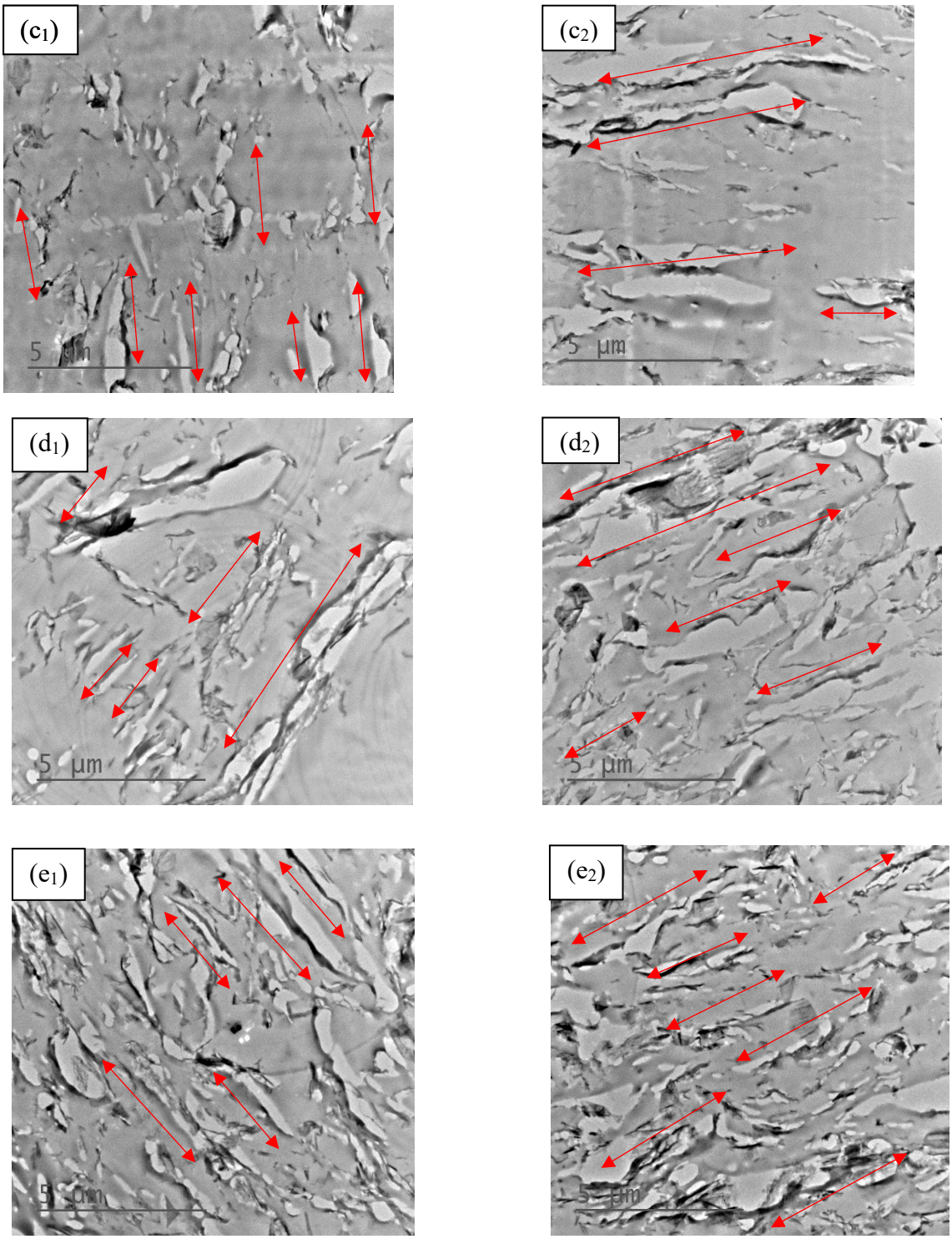

Figure 12. TEM images of a_1) 4-pGNP/PLA, b_1) 6-pGNP/PLA, c_1) 8-pGNP/PLA, d_1) 12-pGNP/PLA, e_1)16-pGNP/PLA and a_2) 4-fGNP/PLA, b_2) 6-fGNP/PLA, c_2) 8-fGNP/PLA, d_2) 12-fGNP/PLA, e_2)16-fGNP/PLA.

3.4 DSC analysis of PLA nanocomposites

The crystallinity degree (χ) of neat PLA and GNP/PLA specimens is calculated using the following equation.

$$\chi = \frac{\Delta H_m - \Delta H_{cc}}{\Delta H_m^0 \times (1 - \varphi_f)} \times 100$$

In this formula, ΔH_m and ΔH_{cc} are the enthalpies of melting and cold crystallization of samples respectively, ΔH_m^0 is the melting enthalpy of 100% crystalline PLA (set as 93.0 J/g [156]), and φ_f is the weight fraction of GNP relative to PLA matrix.

The DSC curves of pGNP/PLA and fGNP/PLA nanocomposites with GNP loading are depicted in Figures 13 and 14, respectively. All these thermograms show the thermal behavior of glass transition, cold crystallization, and double melting of samples.

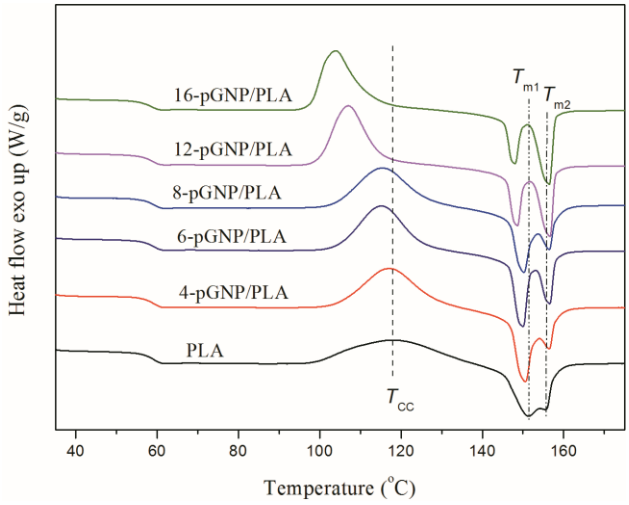

Figure 13. DSC thermograms of pGNP/PLA samples versus temperature for different filler loadings.

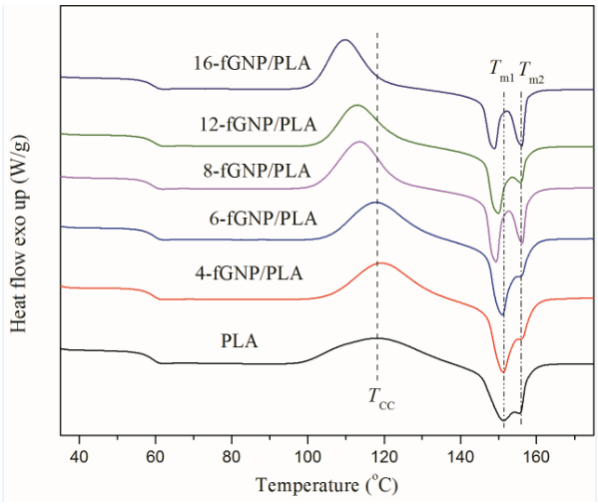

Figure 14. DSC thermograms of fGNP/PLA samples versus temperature for different filler loadings.

Data derived from the curves in Figures 13 and 14 for glass transition temperature (T_g), cold crystallization temperatures (T_{cc}), melting temperatures (T_m), exothermic enthalpy of cold crystallization (ΔH_{cc}), and endothermic enthalpy of melting (ΔH_m) of pGNP/PLA and fGNP/PLA nanocomposites are summarized in Table 2 and Table 3, respectively.

Table 2. Thermal properties of neat PLA and its pGNP-based nanocomposites

Sample	T_g (°C)	T_{cc} (°C)	ΔH_{cc} (J/g)	T_{m1} (°C)	T_{m2} (°C)	ΔH_m (J/g)	Crystallinity (%)
PLA	57.24	118.03	26.08	150.75	155.84	28.76	2.88
4-pGNP/PLA	57.73	117.11	25.17	150.63	156.58	33.18	8.97
6-pGNP/PLA	57.5	115.12	25.15	149.89	156.56	32.88	8.84
8-pGNP/PLA	58.00	115.48	24.67	150.24	156.52	31.04	7.44
12-pGNP/PLA	58.15	107.03	28.32	148.64	156.62	33.52	6.35
16-pGNP/PLA	57.5	103.87	30.35	148.03	156.48	33.46	3.98

Table 3. Thermal properties of neat PLA and its fGNP-based nanocomposites

Sample	T_g (°C)	T_{cc} (°C)	ΔH_{cc} (J/g)	T_{m1} (°C)	T_{m2} (°C)	ΔH_m (J/g)	Crystallinity (%)
PLA	57.24	118.03	26.08	150.75	155.84	28.76	2.88
4-fGNP/PLA	57.77	119.14	25.09	151.34	156.54	33.23	9.11
6-fGNP/PLA	57.90	117.91	22.6	151.07	156.21	30.49	9.03
8-fGNP/PLA	58.13	113.48	26.13	149.42	156.26	33.27	8.35
12-fGNP/PLA	58.24	112.86	24.84	150.02	156.03	31.26	7.84
16-fGNP/PLA	58.20	109.68	24.53	149	156.15	29.94	6.92

As presented in Tables 2 and 3, the crystallinity (2.88%) of pure PLA was low. Values increased to 8.97% and 9.11% for 4-pGNP/PLA and 4-fGNP/PLA nanocomposites, respectively. The increased crystallinity may be due to the a nucleation effect of GNP nanofillers, which can facilitate the crystallization process and induce the growth of crystallites [157]. Slightly larger value for fGNP/PLA nanocomposites can probably be attributed to the formation of uniform crystalline structure. Although the crystallinity (3.98%) for 16-pGNP/PLA was the smallest among all nanocomposites, it was still higher than that of PLA. The decreased crystallinity at high GNP loading may result from poor dispersion of GNP.

As seen from Figures 13 and 14, the cold-crystallization temperatures exhibited a downward trend with increasing GNP concentration, which indicates that the addition of GNP might promote the extent of cold crystallization and accelerate the crystallization kinetics of PLA polymer [158, 159]. From Table 2 and Table 3, the glass transition and melting temperatures of all PLA samples were found to have no considerable change. The similar melting temperature (T_{m1} and T_{m2}) of fGNP/PLA and pGNP/PLA nanocomposites suggests the lamellar thickness of these samples was almost identical [160, 161].

According to Figures 13 and 14, it becomes apparent that neat PLA and PLA nanocomposites are characterized by bimodal or shoulder-shaped melting behavior. The characteristic peaks were attributed to either melt recrystallization of α-crystals structures, heterogeneous crystal phases, or polymorphism [83]. The melting temperature (T_{m1}) was slightly decreased while T_{m2} was a

marginally increased compared with the peaks of neat PLA. Because of the nucleation effect of GNP, imperfect crystals that formed at the primary phase of cold crystallization would melt at a lower temperature (T_{m1}). The higher perfect crystals developed at the secondary phase of cold crystallization would melt at high temperature (T_{m2}) [162].

3.5 XRD analysis of PLA nanocomposites

The XRD method was employed to evaluate the crystal structure of PLA and the exfoliation state of GNP within the polymer. The diffractograms of pure PLA and nanocomposites for pGNP/PLA and fGNP/PLA are depicted in Figure 15 and Figure 16, respectively. The comparisons of pGNP/PLA and fGNP/PLA samples with the same GNP loading are illustrated in Figures 17a), b), and c), respectively. Note that, in order to clearly show the relative intensity of diffraction peaks, only XRD results for nanocomposites with 4 wt%, 6 wt%, and 16 wt% GNP loading are plotted. The other XRD curves are provided in Figures 38 and 39 in Appendix D.

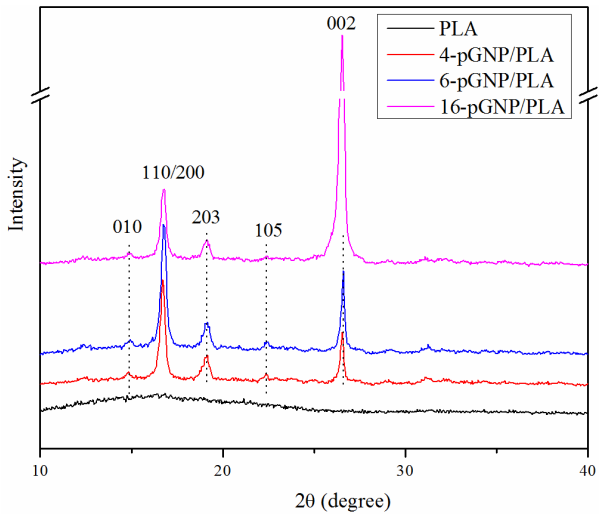

Figure 15. XRD patterns for neat PLA and its representative pGNP/PLA nanocomposites.

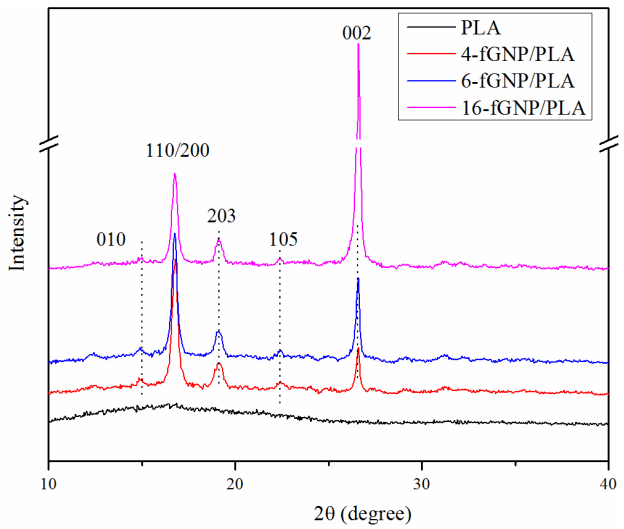

Figure 16. XRD patterns for neat PLA and its representative fGNP/PLA nanocomposites.

As seen in Figures 15 and 16, the profiles of pGNP-based and fGNP-based nanocomposites were similar. The intense peak at $2\theta = 26.5°$ was assigned to the d_{002} diffraction plane of GNP with a d-spacing of 0.34 nm. Moreover, the relative intensity of this peak became more robust with increased GNP loading. Based on Bragg's Law (i.e., $2d\sin\theta=n\lambda$), the d-spacing of peak at 26.5° for all GNP/PLA samples was the same with that of GNP powders, suggesting that pGNP and fGNP were not subjected to polymer intercalation after ultrasonication and mechanical stirring steps during the fabrication process of PLA nanocomposites.

The neat PLA exhibited only a broad diffraction distribution from approximately $2\theta = 12°$ to 20° with maximum intensity but no obvious peak at about 16.7°, which demonstrates the amorphous structure of PLA polymer. With GNP incorporation, an apparent peak appears at 16.7° in PLA nanocomposites, indicating distinct crystallinity with neat PLA. Besides the prominent peak at 16.7°, additional minor peaks can also be observed for GNP/PLA nanocomposites. For example, the peaks occurring at 2θ of 15.0°, 16.7°, 19.0° and 22.5° were characteristic of the stable planes of semi-crystalline α phase crystals of PLA matrix, corresponding to (010), (110) and (200), (203) and (015) planes [163, 164], respectively. Based on XRD results, only α-phase crystals of PLA presented in the GNP/PLA nanocomposites. Thus the double melting endotherms observed in Figures 13 and 14 of Section 3.4 were due to melt recrystallization and not the result of polymorphism.

As shown in Figures 17a), b), and c), the relative peak intensity at 26.5° of pGNP/PLA was stronger than that of fGNP/PLA counterparts at the same nanofiller loading, which may be due to more aggregation of pGNP than fGNP particles [147]. Besides, the non-covalent adsorption of tannic acid onto the surface of GNP may increase the disordered stacking structures of fGNP, which was shown in the XRD results of fGNP and pGNP powders in Section 3.2.

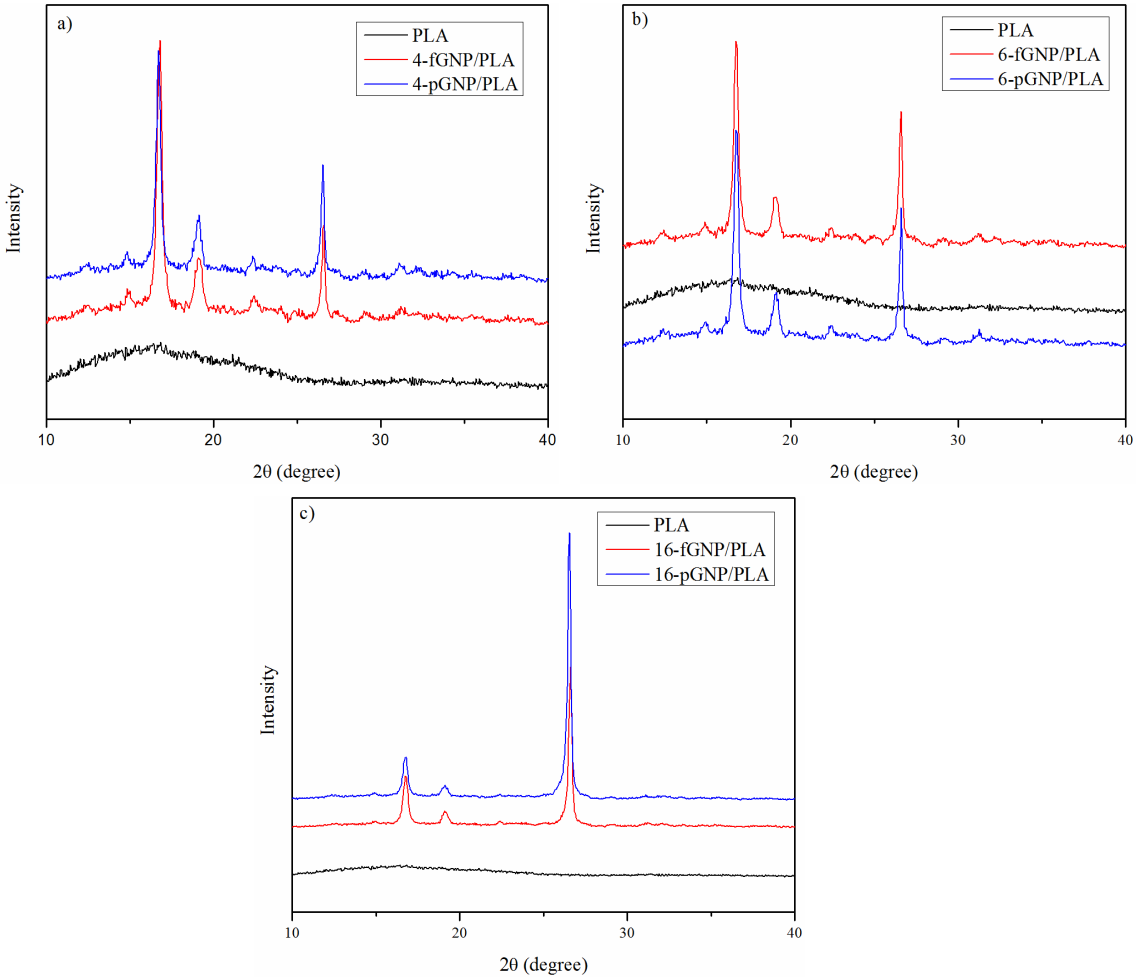

Figure 17. The comparison of XRD profiles of pGNP/PLA and fGNP/PLA nanocomposites at different GNP loading a) 4 wt%, b) 6 wt%, and c) 16 wt%, including the neat PLA sample.

3.6 Thermal conductivity of PLA nanocomposites

The thermal conductivities of GNP/PLA specimens were measured with the TPS analyzer in cross-plane and in-plane direction. As shown by TEM images in Figure 12, GNP exhibited a preferential orientation, especially for high GNP loadings. The filler alignment appears to be accompanied by

the formation of preferred continuous thermal conduction networks along the alignment direction, thus permitting efficient phonon transport and heat flow [165, 166]. Therefore, it would be expected high thermal conductivity in the specimen planar direction associated with the alignment of GNP.

Indeed, the experimental results of GNP/PLA nanocomposite presented in Figures 18 and 19 supported this notion. At room temperature (25 ^{o}C), with a thermal conductivity of 0.21 W/mK, neat PLA can be considered a thermal insulator. The in-plane thermal conductivity of PLA nanocomposites nonlinearly increased with increasing GNP fraction, exhibiting a two-stage trend. For example, upon slowly rising to 0.81 W/mK and 0.67 W/mK for 6-pGNP/PLA and 4-fGNP/PLA nanocomposites, the thermal conductivity then increased at a higher rate, reaching up to 3.41 W/mK and 3.56 W/mK for 12-pGNP/PLA and 8-fGNP/PLA nanocomposites, respectively. The thermal conductivity in the through-thickness direction remained between 0.21 W/mK and 0.58 W/mK. For both pGNP and fGNP based nanocomposites, the in-plane thermal conductivity was higher than that in through-plane direction. Pronounced anisotropic thermal conductivity can be observed beyond 4 wt% fGNP and 6 wt% pGNP. For example, the anisotropy index (the ratio of in-plane to through-plane thermal conductivity) was about 18.5 and 21.6 for the 16-pGNP/PLA and 16-fGNP/PLA, respectively, further corroborating GNP alignment in the PLA matrix.

For heat conduction in polymer nanocomposites, phonons are the dominant transfer mechanism. Along the in-plane direction, heat transfer was mainly dominated by GNP-GNP linkages [143]. As shown in Figure 12 of TEM images, at low filler concentrations, GNP particles were suggested to be spatially separated with little to no interfacial contacts, which would maximize ITR effects and thus reduce heat flow. Increasing GNP loading led to greater filler alignment and an increased formation of continuous thermal conduction networks, allowing for more effective phonon transfer along these pathways because of the lower thermal and contact resistance. While, in the through-plane direction, heat flow continues to be dominated by graphene-polymer-graphene linkages [143], which was actively obstructed because of the significant thermal resistance effects associated with the insulating behavior of PLA polymer. Therefore, thermally conductive pathways were discontinuous, and GNP fillers had only a minor influence on the through-thickness thermal conductivity.

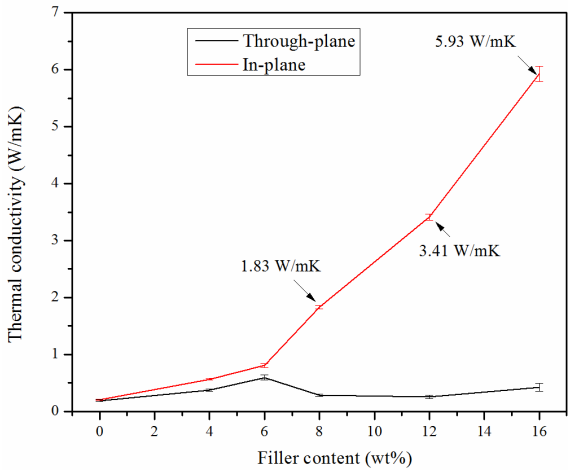

Figure 18. In-plane and through-plane thermal conductivity of pGNP/PLA nanocomposites versus pGNP loading.

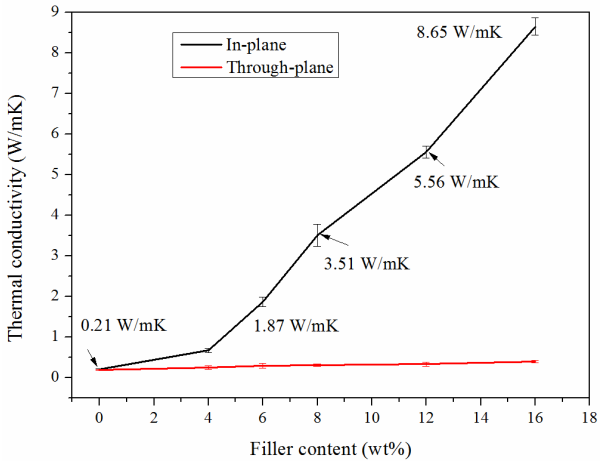

Figure 19. In-plane and through-plane thermal conductivity of fGNP/PLA nanocomposites versus fGNP loading.

At any given content of GNP, the in-plane thermal conductivity value for fGNP/PLA nanocomposites was higher than that of pGNP/PLA counterparts. With 16 wt% fGNP, the in-plane thermal conductivity was enhanced to 8.65 W/mK, which is 1.46 and 43.2 times that of 16-pGNP/PLA nanocomposite and neat PLA, respectively. After non-covalent modification, an enhanced interfacial adhesion between fGNP and PLA may promote the more uniform dispersion of fGNP in the PLA matrix compared with pGNP. Improved bonding and dispersion may reduce phonon scattering between the fGNP-PLA interface and induce ease phonon transport between

GNP nanofillers, and hence, thermal conductivity was effectively improved [119]. A variety of previous thermal conductivity studies of GNP/PLA nanocomposites are summarized in Table 4 [85, 144-146]. It can be concluded that thermal conductivity values in this work are at a higher level.

There are several contributing factors for the observed higher thermal conductivity. Referring to the work by Lin et al. [146], one of differences is that in their experiments a coagulation process was incorporated after mixing the GNP suspension and PLA solution, whereas in the present work, an evaporation method was performed. The evaporation process may promote the alignment of GNP in the polymer matrix due to the excluded volume effect and steric hindrance between adjacent GNP particles [155, 167]. Moreover, the lower viscosity of the chloroform/PLA solution in this study, compared to the N, N-dimethylformamide (DMF)/PLA solution in the work of Lin et al. [146] may have promoted a more homogenous dispersion of GNP nanosheets in the nanocomposites, which may further reduce phonon scattering at the GNP/PLA interface.

The higher thermal conductivity may also be attributed to the larger size of GNP nanosheets (~15 μm) used in this study compared to the smaller size (~3-6 μm) in the work of Lin el at. [146]. As shown in the study by Wang and Drzal [94], the thermal conductivity (0.38 W/mK) of polyethersulfone/epoxy composites reinforced by larger GNP (~5 μm) is higher than the value (0.28 W/mK) of composites reinforced by smaller GNP (less than 1 μm). The higher thermal conductivity in the case of large-sized GNP may be ascribed to a lower GNP/GNP and GNP/polymer contact resistance, more interconnected thermal conductive networks, and ease of phonon diffusion at the GNP/polymer interface [94].

Cooling of hot-pressed samples was conducted in this study by leaving the mold at the powered-off Carver hydraulic press, termed herein the “slow-cooling” method. Slow-cooling can impart higher crystallinity and more perfect crystals, which would ease phonon transport, thus leading to higher thermal conductivity [168]. The thermal conductivity of GNP/UHMWPE (ultra-high molecular weight polyethylene) nanocomposites prepared by slow-cooling reached to 4.624 W/mK at 21.4% volume fraction of GNP, compared to value of about 4.1 W/mK for the counterparts prepared by a “fast-cooling” method (direct cooling away from the Carver hydraulic press) [168].

Table 4. The comparison of thermal conductivity for GNP/PLA nanocomposites in previous literature and this work

Matrix	Filler	Filler content (wt%)	Thermal conductivity (W/mK)	Preparation method	Ref.
PLA	GNP and hBN	hBN:24.7 GNP:21.7	2.77	Melt compounding	[144]
PLLA	GNP	5	0.94	Melt mixing	[145]
PLA	GNP	30	0.61	Solution mixing+ coagulation+hot-press	[146]
PLA	GNP	12	0.664	3D Printing	[85]
PLA	fGNP	16	8.65	Non-covalnet modification+solution mixing+ evaporation+hot-press	This work

PLLA: Poly(L-lactide), hBN: Hexagonal boron nitride

3.7 Thermal stability of PLA and GNP/PLA nanocomposites

The thermal stability of samples is investigated via the TGA method. Figures 20 and 21 depict the thermal degradation behaviors for pGNP/PLA and fGNP/PLA nanocomposites, respectively. To clearly show the change of thermal stability, only TGA results for nanocomposites with 4 wt%, 8 wt%, and 16 wt% GNP loading are plotted, and the other TGA curves are provided in Figures 40 and 41 in Appendix E.

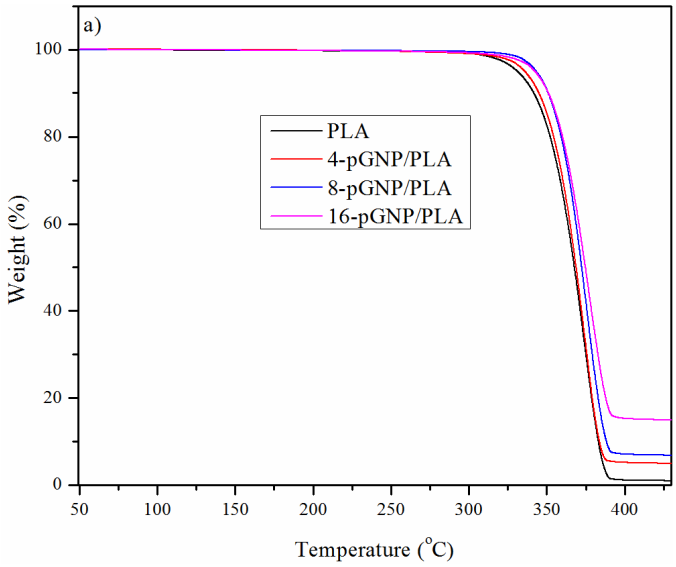

Figure 20. TGA curves of neat PLA and pGNP/PLA nanocomposites.

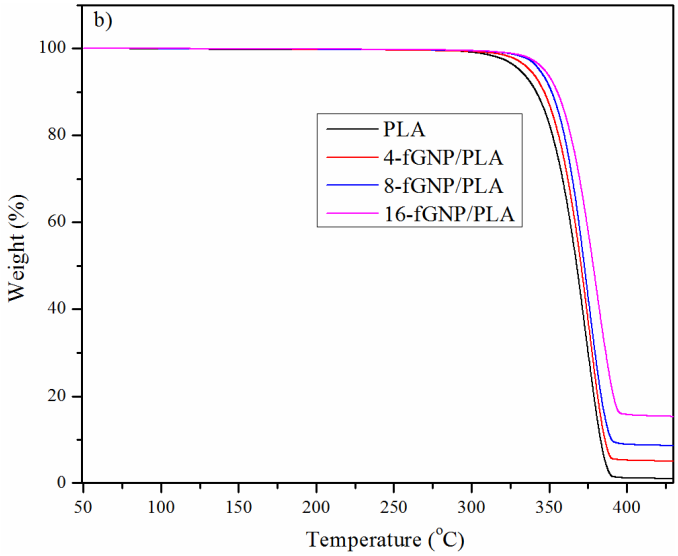

Figure 21. TGA curves of neat PLA and fGNP/PLA nanocomposites.

For quantitative evaluation, some characteristic temperatures, i.e., $T_{5\%}$, $T_{10\%}$, $T_{50\%}$, T_{max}, and char yields (%) at 400°C are summarized in Table 5 and Table 6, where $T_{5\%}$, $T_{10\%}$, and $T_{50\%}$ are defined as the thermal decomposition temperature at the weight loss of 5%, 10%, and 50%, respectively. And, T_{max} represents the temperature of the maximum weight loss rate.

Table 5. TGA data of pristine PLA and pGNP/PLA nanocomposites

Sample	$T_{5\%}$ (ºC)	$T_{10\%}$ (ºC)	$T_{50\%}$ (ºC)	T_{max} (ºC)	Char residue (%) at 400 ºC
Pure PLA	331	342	368	373	1.2
4-pGNP/PLA	336	345	369	374	5.2
6-pGNP/PLA	341	348	372	377	7.1
8-pGNP/PLA	343	350	372	376	7.2
12-pGNP/PLA	343	351	373	376	11.5
16-pGNP/PLA	342	351	373	378	15.3

Table 6. TGA data of pristine PLA and fGNP/PLA nanocomposites

Sample	$T_{5\%}$ (ºC)	$T_{10\%}$ (ºC)	$T_{50\%}$ (ºC)	T_{max} (ºC)	Char residue (%) at 400 ºC
Pure PLA	331	342	368	373	1.2
4-fGNP/PLA	338	347	371	376	5.3
6-fGNP/PLA	341	350	373	377	8.2
8-fGNP/PLA	344	352	373	376	8.9
12-fGNP/PLA	346	354	375	378	12.2
16-fGNP/PLA	347	355	378	381	15.8

Observing the degradation thermograms in Figures 20 and 21, they resemble a one-step decomposition process, showing decomposition commencing at about 300°C and rapidly continuing until about 400°C.

For neat PLA, the $T_{5\%}$ and T_{max} appeared at 331°C and 373°C, respectively, with an ash content of 1.2% at 400°C. With the addition of GNP, $T_{5\%}$, $T_{10\%}$, $T_{50\%}$, and T_{max} all shifted towards higher temperatures compared with the corresponding temperature of neat PLA, confirming somewhat higher thermal stabilities. For example, the $T_{5\%}$ of nanocomposites incorporating 12 wt% fGNP

and pGNP were 346°C and 343°C, with an increase of 15°C and 12°C compared to pure PLA, respectively.

The retardation of thermal degradation after GNP inclusion presumably stems from several effects. Firstly, the inherent thermal stability of GNP platelets is high. Besides, the high aspect ratio, and 2-D structure of aligned GNP may impart a mass barrier effect by increasing the escape paths of volatile pyrolyzed products, effectively restraining the release of these decomposition materials [169]. Also, GNP can form a char layer acting as a heat barrier effect during the thermal degradation process, which may further inhibit the heat transfer between the volatile gas and undecomposed PLA matrix [29]. Recorded higher T_{max} temperatures of nanocomposites supported the notion of mass and heat barrier effects of GNP.

Comparing the data in Table 5 and Table 6, adding fGNP into the PLA matrix displayed more improved thermal stability compared to samples reinforced with pGNP for the same GNP loading. The higher thermal conductivity of fGNP/PLA nanocomposites may be more favorable in terms of external heat energy transfer and dissipation than pGNP/PLA samples. Moreover, because of the enhanced fGNP/PLA interfacial compatibility, more homogeneous dispersion of fGNP could further limit the heat accumulation in the PLA matrix [170].

3.8 Thermo-mechanical properties of PLA nanocomposites

Long molecular chains endow polymers with viscoelastic behavior, combining the characteristics of a viscous fluid (loss modulus) and elastic solid (storage modulus). Therefore, studying a polymer's viscoelastic properties is important to assess its usability for intended applications. Moreover, the storage modulus of polymer nanocomposites is closely related to the interfacial bonding between the nanofillers and polymer matrix [171]. Consequently, DMA was conducted in this study to assess the viscoelastic properties of GNP/PLA nanocomposites.

The storage modulus (E'), damping factor (tan δ), and loss modulus (E'') for the pGNP/PLA and the fGNP/PLA samples are displayed in Figures 22 and 23, respectively, as a function of temperature. To clearly show the change of values, only DMA results for nanocomposites with 6 wt%, 12 wt%, and 16 wt% GNP loading are plotted, and the other DMA curves are provided in Figures 42 and 43 in Appendix F.

For quantitative comparison, the E' values of each sample at the temperature of 40°C and 70°C are listed in Table 7 and Table 8, along with glass transition temperature. Recalling the peak temperature of tan δ plots is herein considered to be the T_g of samples.

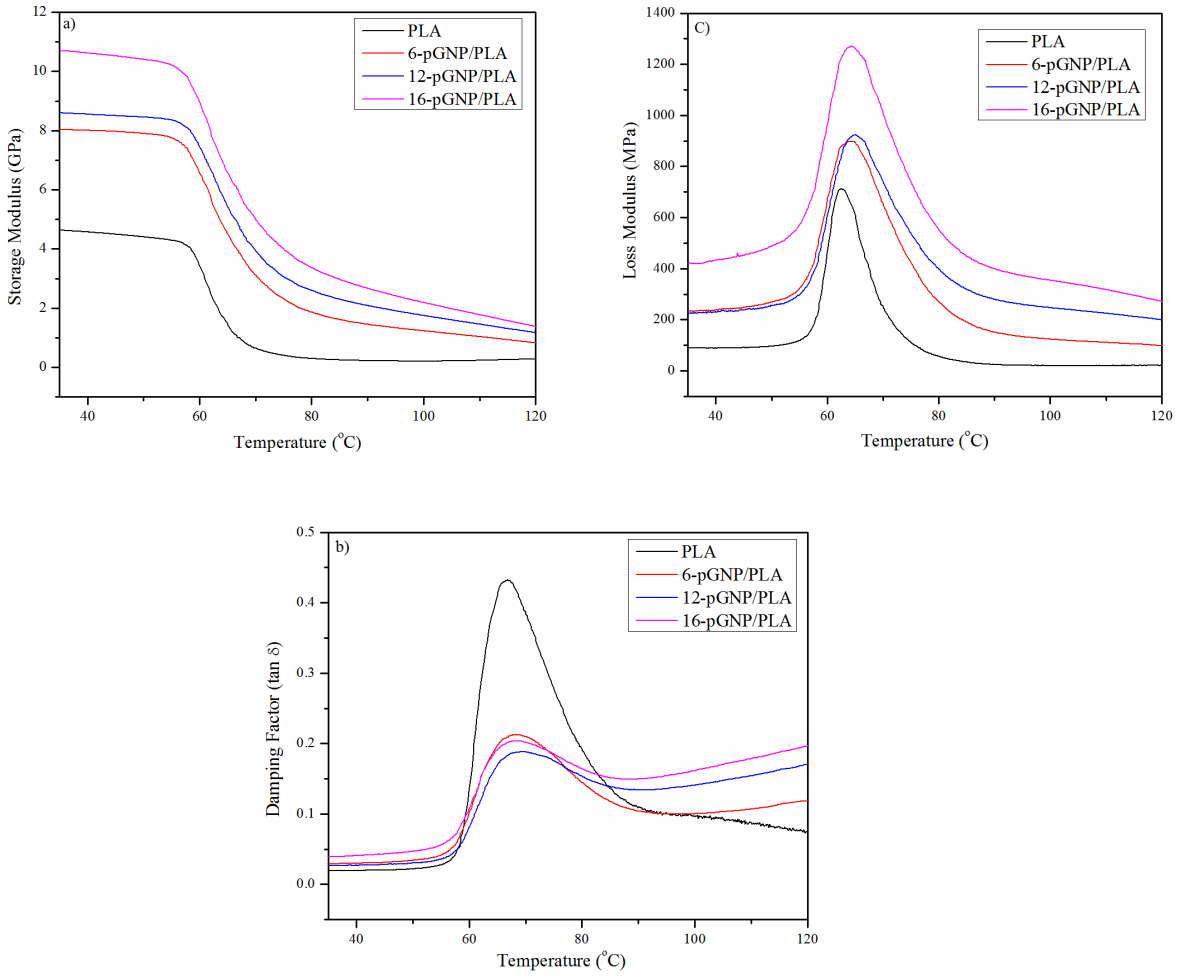

Figure 22. Dynamic mechanical properties of neat PLA and pGNP/PLA nanocomposites as a function of temperature: a) storage modulus, b) loss factor, and c) loss modulus.

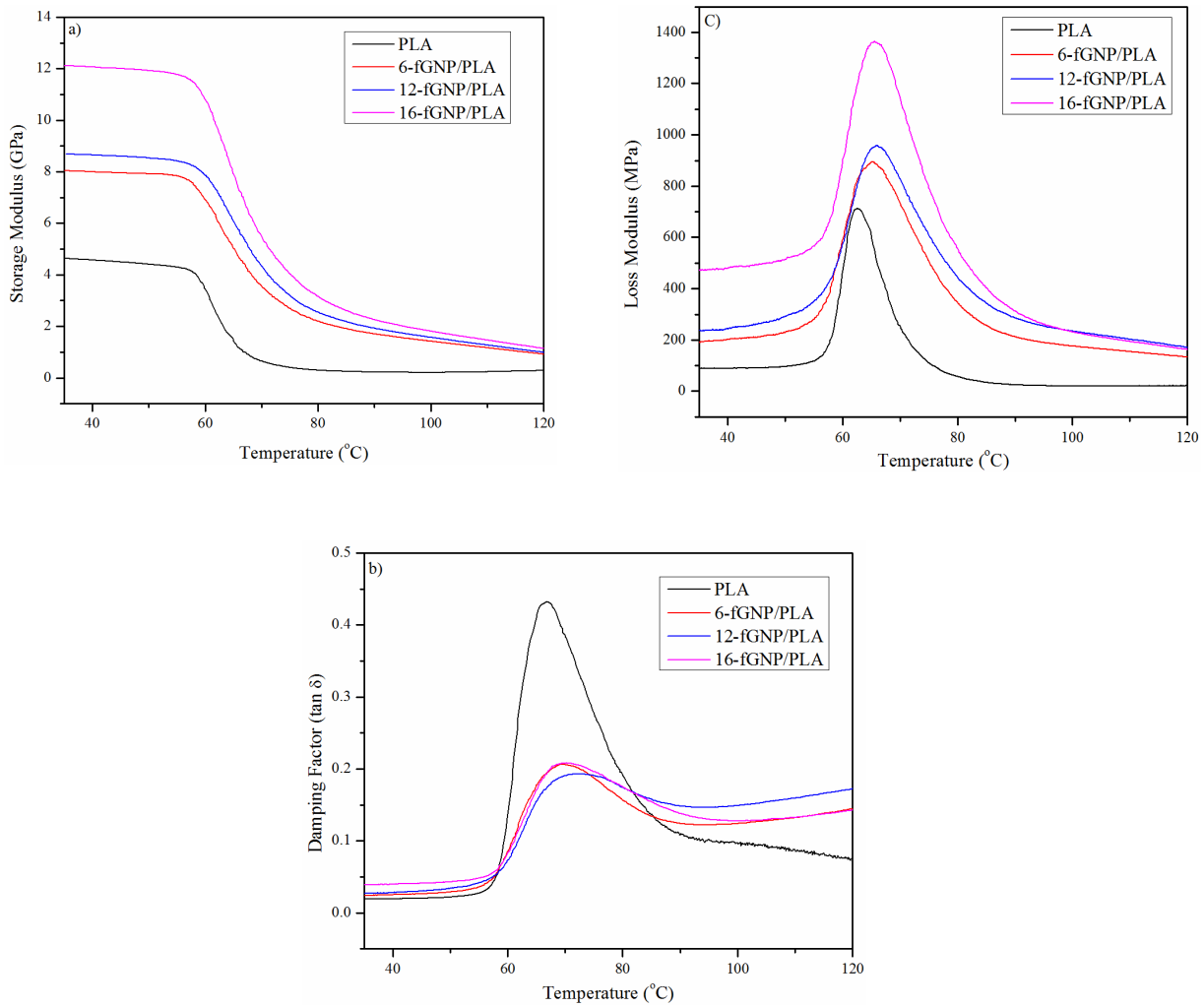

Figure 23. Dynamic mechanical properties of neat PLA and fGNP/PLA nanocomposites as a function of temperature: a) storage modulus, b) loss factor, and c) loss modulus.

Table 7. Storage modulus at different temperatures (40°C, 70°C) and glass transition temperature of PLA and pGNP/PLA nanocomposites

Sample	Storage modulus E' (GPa)		Glass transition temperature T_g (°C)
	40°C	70°C	
Pure PLA	4.6	0.65	66.7
4-pGNP/PLA	6.6	2.3	68.7
6-pGNP/PLA	8.0	3.1	68.2
8-pGNP/PLA	8.3	3.6	69.4
12-pGNP/PLA	8.6	3.9	69.7
16-pGNP/PLA	10.6	5.0	68.4

Table 8. Storage modulus at different temperatures (40°C, 70°C) and glass transition temperature of PLA and fGNP/PLA nanocomposites

Sample	Storage modulus E' (GPa)		Glass transition temperature T_g (°C)
	40 °C	70 °C	
Pure PLA	4.6	0.65	66.7
4-fGNP/PLA	6.9	3.3	68.9
6-fGNP/PLA	8.0	3.6	69.2
8-fGNP/PLA	8.3	3.7	69.1
12-fGNP/PLA	8.7	4.4	71.7
16-fGNP/PLA	12.1	5.4	70.1

As depicted in Figures 22 and 23, both the storage modulus and the loss modulus of PLA nanocomposites were higher than that of neat PLA. Besides, the storage modulus substantially increased with GNP contents increase over the full temperature range studied, regardless of

functionalization. An increased storage modulus of nanocomposites can improve the load-bearing ability by effectively transferring the load to GNP nanofillers from PLA polymer. The enhancements in storage modulus possibly were attributed to a mechanical reinforced capability imparted by stiff GNP and increased crystallinity of PLA with GNP addition [83, 172, 173].

At the same GNP loading, the storage modulus enhancements of samples reinforced by fGNP were more pronounced than that of counterparts containing pGNP (which is consistent with the trend of Young's modulus discussed in Section 3.9). For example, as listed in Table 7 and Table 8, at 16 wt% filler inclusion and 40°C, E' increased by a factor of 2.3 and 2.6 over neat PLA (4.6 GPa) to 10.6 GPa and 12.1 GPa for pGNP/PLA and fGNP/PLA nanocomposites, respectively. At a higher temperature, such as the rubbery region (70°C), the storage modulus of 12-fGNP/PLA increased to 4.4 GPa, showing an about 1.13 times reinforced performance compared with that of 12-pGNP/PLA (3.9 GPa). The higher reinforcing effect may be attributed to the enhanced fGNP-PLA adhesion strength, which can further hinder the chain motivation around fGNP and improve the load transfer capability [171, 174]. As shown in Figure 22a) and Figure 23a), a gradual decrease in storage modulus was ascertained with rising temperatures for all tested materials. And the samples exhibited a sharp drop in storage modulus between 60°C and 70°C, indicating the transition from a glassy to a rubbery state.

Glass transition temperatures of the samples, as derived from tan δ peaks, were found to increase with the addition of GNP, enhancing up to the maximum of 71.7°C for 12-fGNP/PLA compared to 66.7°C for neat PLA. Compared with pGNP-based samples, the slightly higher T_g values of fGNP-based systems may be ascribed to the more significant restriction effect on PLA chains mobility under the load due to robust bonding interactions between fGNP and polymer matrix and more uniform dispersion of fGNP [175]. As depicted in Figure 22c) and Figure 23c), the loss modulus of GNP/PLA nanocomposites became slightly broader, indicating an extension of the glass transition region, owing to the increased motion limitation of PLA chain and additional energy dissipation [83, 176].

Comparing the T_g obtained by DMA and DSC technique, it is found that the T_g of all samples in DMA analysis is notably larger, which may be due to different sample sizes used between these two methods [177]. During DMA testing, the heat transfer hysteresis may happen in the bulk cuboid sample. While during DSC operation, only about 5 mg samples were used, constituting a

relatively small sample weight and size. Thus, the transition of smaller-scaled polymer chain motion may occur at a lower temperature. The difference in T_g for DMA and DSC testing was consistent with previous works [81, 178].

3.9 Mechanical properties of PLA nanocomposites

Tables 9 and 10 present the experimental results (with mean and standard deviation) of the elongation at break, tensile strength, and modulus of PLA nanocomposites. The representative stress-strain plots of pure PLA and GNP/PLA samples are shown in Figure 24, and others are presented in Figures 44 to 54 in Appendix G (where number of test replicates is indicated as "1", "2", "3", and so on; for example, the four replicates of 16-fGNP/PLA are termed "16-fGNP/PLA-1", "16-fGNP/PLA-2", "16-fGNP/PLA-3" and "16-fGNP/PLA-4").

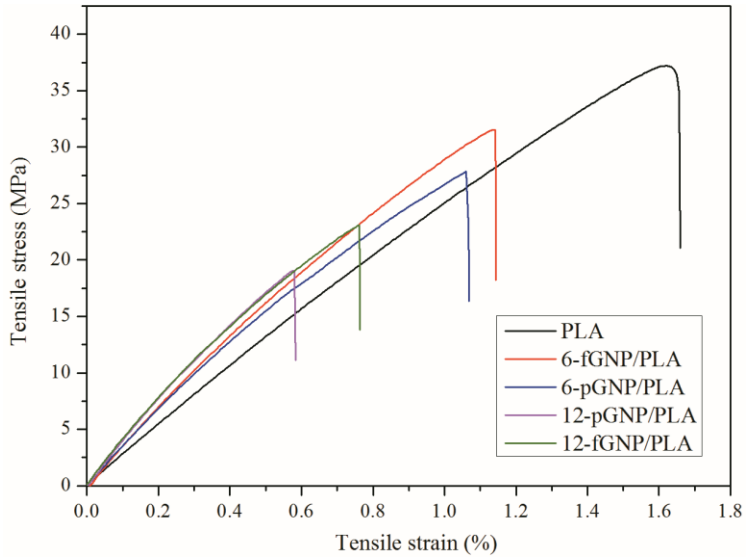

Figure 24. Tensile stress-tensile strain curves for PLA and some GNP/PLA nanocomposites.

It is observed from Tables 9 and 10 that Young's moduli of PLA nanocomposites showed a steadily increasing trend compared with pure PLA, meaning the material became stiffer with GNP loading. Generally, the enhancement of Young's moduli was more pronounced in fGNP/PLA nanocomposites than for pGNP-based counterparts. For example, the modulus increased from 2.21 GPa of pure PLA to 2.65 GPa and 2.90 GPa for nanocomposites with 8 wt% pGNP and fGNP, respectively. The modulus reached to a maximum of 3.51 GPa for 16-fGNP/PLA, which is an improvement of 1.59 and 1.05 times over neat PLA and 16-pGNP/PLA, respectively. The modulus enhancement of fGNP/PLA nanocomposites is attributed mainly to the high intrinsic stiffness of

GNP and the strong interfacial interactions between fGNP and PLA matrix. Notably, despite higher mean values for fGNP/PLA samples some overlaps exists considering standard deviations for fGNP/PLA and pGNP/PLA samples. Therefore, statistical analysis (such as t-testing) should be performed in the future work.

Table 9. Mechanical properties of pure PLA and pGNP/PLA nanocomposites

Samples	Tensile strength (MPa)	Elongation at break (%)	Young's modulus (GPa)
PLA	37.4±1.7	1.70±0.09	2.21±0.03
4-pGNP/PLA	30.7±1.8	1.25±0.20	2.47±0.05
6-pGNP/PLA	27.5±2.5	1.08±0.27	2.58±0.18
8-pGNP/PLA	26.8±2.5	1.01±0.10	2.65±0.02
12-pGNP/PLA	19.8±2.3	0.63±0.09	3.16±0.14
16-pGNP/PLA	18.1±0.8	0.54±0.04	3.34±0.16

Table 10. Mechanical properties of pure PLA and fGNP/PLA nanocomposites

Samples	Tensile strength (MPa)	Elongation at break (%)	Young's modulus (GPa)
PLA	37.4±1.7	1.70±0.09	2.21±0.03
4-fGNP/PLA	36.2±1.3	1.41±0.11	2.57±0.14
6-fGNP/PLA	32.5±2.0	1.18±0.07	2.76±0.14
8-fGNP/PLA	29.7±1.2	1.10±0.03	2.95±0.07
12-fGNP/PLA	22.3±0.8	0.68±0.07	3.28±0.23
16-fGNP/PLA	21.4±1.6	0.61±0.05	3.56±0.05

Similar to the previous analysis in Section 3.3, the phenolic hydroxyl groups across the surface of fGNP may form hydrogen bonding with the PLA chain, thereby improving interfacial

compatibility to produce more efficient stress transfer from matrix to fGNP phase [179]; therefore the reinforcing effect was stronger for fGNP/PLA nanocomposites.

Based on the data in Table 9 and Table 10, an inverse trend for tensile strength and elongation at break for PLA nanocomposites was observed compared to the Young's modulus, i.e., tensile strength and elongation at break were reduced as the GNP content rose from 4.0 wt% to 16.0 wt%. The observed trend in tensile strength and elongation at break is consistence with the works by Narimissa et al. [180, 181]. Adding 16 wt% pGNP and fGNP caused a decrease of tensile strength from 37.4 MPa of pristine PLA to 18.1 MPa and 22.5 MPa, respectively. The increasing deterioration in tensile strength for pGNP/PLA samples may be attributed to an insufficient stress transfer resulting from weak PLA-pGNP interfacial adhesion and agglomeration of pGNP.

Table 9 shows that the elongation at break value of PLA was 1.7%, which is in the same order of magnitude with data (i.e. 3.5%) reported by Narimissa et al. [180]. The addition of GNP decreased the elongation at break, indicating a toughness decrease of PLA polymer. At 16 wt% GNP loading, the ultimate values of elongation at break reduced to respective 0.54% and 0.64% for pGNP/PLA and fGNP/PLA samples, corresponding to a decrease of 68.2% and 62.3% compared to neat PLA, respectively. The increase in embrittlement behavior upon the addition of GNP could be ascribed to the prohibition of PLA chain mobility and relaxation by the rigid characteristics of GNP [182].

3.10 Electrical conductivity of PLA nanocomposites

For polymer nanocomposites, at a critical amount of conductive particles, there is a dramatic rise in electrical conductivity (usually several orders of magnitude). The minimum content of nanofillers required to result in this sudden jump is called the percolation threshold.

The electrical conductivity of PLA nanocomposites versus pGNP and fGNP loading is illustrated in Figure 25. The electrical conductivity of neat PLA was about 10^{-14} S/m; hence, PLA can be considered an electrical insulator. As expected, the conductivity of PLA nanocomposites increased with GNP incorporation. It is interesting to note that the change rate was significantly different below and above 6 wt% pGNP loading.

At content less than 6 wt%, conductivity gradually increased from 1.34×10^{-14} S/cm (neat PLA) to 1.6×10^{-7} S/cm of 6-pGNP/PLA nanocomposites. Further adding pGNP, reaching a critical concentration between 6 wt% and 8 wt%, the electrical percolation threshold emerged, with a

dramatic increase by three to four orders of magnitude to the value to 0.0015 S/cm for 8-pGNP/PLA. Therefore, it was conjectured that electron conduction networks were established within the PLA at 6 wt% to 8 wt% pGNP weight fraction. When pGNP content was more than 12 wt%, the rate of electrical conductivity rise slowed. As the inclusion of 16 wt% GNP, the conductivity of pGNP/PLA (0.5 S cm^{-1}) and fGNP/PLA (0.8 S cm^{-1}, corresponding to an electric resistivity of 1.25 Ω/cm) was more than 13 orders of magnitude higher than that of pure PLA. The percolation threshold of fGNP/PLA nanocomposites also appeared in the range between 6 wt% and 8 wt% fGNP.

Comparing to the same nanofiller loading, the electrical conductivity of fGNP/PLA was higher than that of pGNP/PLA, which may be attributed to better dispersion of fGNP within the polymeric matrix and the increased contact area between the overlapping surfaces of fGNP. Therefore, more interconnected electron conduction networks may be formed, favoring electron transfer. It should be noted that electrical resistivity of ~1.25 Ω/cm is low enough for potential applications in electrostatic and electromagnetic dissipation area or other electronic devices requiring high electrical conductivity [183].

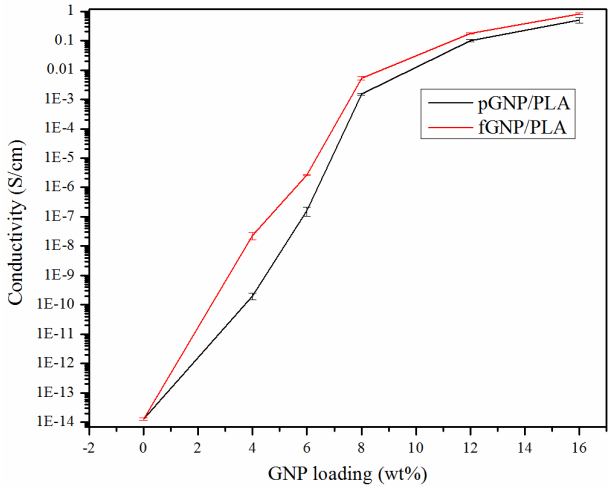

Figure 25. The electrical conductivity of GNP/PLA nanocomposites. Error bars represent the standard deviation.

There are two dominated electron transport modes for the electrical conductivity of polymer nanocomposites [184, 185]. One is called leakage current, and in that, nanofillers contact each other to form interconnected pathways inside the polymer. Then electrons can migrate across these

networks. The other is tunneling current, and for that, there is no physical contact between the nanofillers. But the distances between these fillers are small for quantum mechanical electron transfer effects to occur in which electrons 'tunnel' from one particle to nearby ones.

At low GNP loading, the number of conductive pathways is limited since the distance between nanofillers is larger than the tunneling distance and nanoparticles are surrounded and separated by polymer chains. Thus, electrons transport and electrical contact between nanofillers hardly occur. As a result, conductivity increases only slightly with GNP content increase. With GNP concentration rising to above 6 wt%, the sharp jump in electrical conductivity could be ascribed primarily to the rapid increase in electron migrating and hopping [186]. The determining conduction mechanism for the further remarkable rise in charge conduction has been attributed to the leakage current effect instead of tunneling conduction [187].

At high GNP loading, particle-particle contacts are more accessible, and much denser electron conduction networks are formed between the connected GNP nanofillers, which may significantly increase the leakage current. TEM images in Figure 12 may confirm the rationale for this supposition. Below 6 wt% GNP, the nanoparticles were surrounded by PLA chains, whereas for higher loadings, physical contacts between them were significantly increased, which was supposed to assist the movement of electrons within the polymer nanocomposites.

3.11 Electromagnetic interference shielding effectiveness

The electromagnetic interference (EMI) shielding effectiveness (*SE*), expressed in decibel, is commonly applied to assess the shielding ability of materials to attenuate incident electromagnetic radiation energy. The value of total EMI *SE* (SE_T) of a material can be used to evaluate the shielding efficiency in the electromagnetic microwave. The higher SE_T represents less transmitted energy and more efficiency in shielding waves.

Figures 26 and 27 display SE_T values of pGNP/PLA and fGNP/PLA nanocomposites, respectively, over the X-band frequency range of 8.2 to 12.4 GHz. The higher the GNP content, the larger the SE_T. For instance, the SE_T of 8-pGNP/PLA and 8-fGNP/PLA varied between 8.4 dB to 13.2 dB and 13.3 dB to 15.8 dB, respectively. Adding 12 wt% GNP endowed nanocomposites with an average SE_T value of 20.7 dB and 27.9 dB for pGNP/PLA and fGNP/PLA, respectively, which are both higher than that of the required minimum value (20.0 dB) for commercial electromagnetic

interference shielding products [188]. When fGNP content increased to 16 wt%, SE_T reached a maximum and average value of 43.99 dB and 40.61 dB, respectively. The average SE_T of 37.81 dB (16-pGNP/PLA) and 40.61 dB (16-fGNP/PLA) represents 99.979% and 99.991% blockage of incident EMI radiation, respectively.

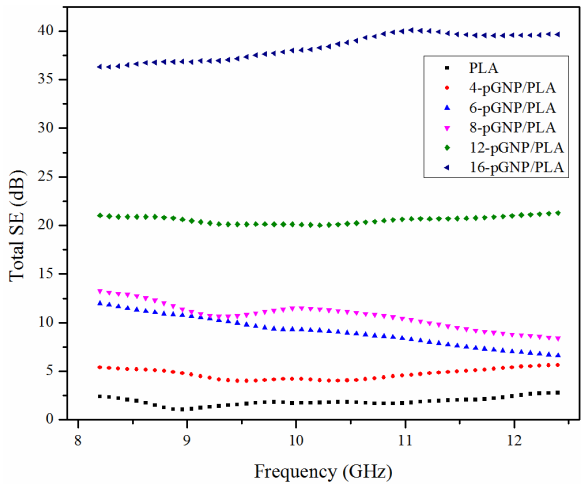

Figure 26. The SE_T of pGNP/PLA nanocomposite as a function of frequency and pGNP concentration.

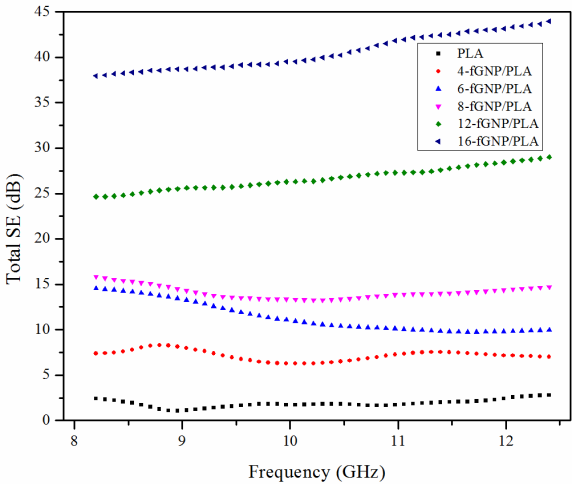

Figure 27. The SE_T of fGNP/PLA nanocomposite as a function of frequency and fGNP concentration.

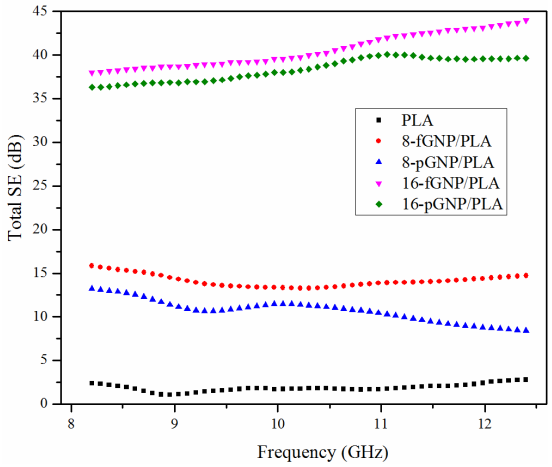

Figure 28. The comparison of SE_T of pGNP/PLA and fGNP/PLA nanocomposite.

The remarkable shielding features of PLA nanocomposites may be ascribed to the significant improvement in electrical conductivity (revealed in Figure 25) and the formation of many interconnected conductive networks (shown in Figure 12). These networks may increase the interactions between the mobile charge carriers and incident radiation [187], thus leading to enhanced attenuation of the electromagnetic microwave. Moreover, the layered structure resulting from the GNP alignment in the PLA matrix may cause effective multi-reflection and multi-absorption of the incident waves [189]. The more enhanced shielding effectiveness for fGNP/PLA nanocomposites may be because of higher electrical conductivity and the better dispersion of fGNP in the PLA matrix.

While SE_T is a significant parameter, two important contribution mechanisms of the total EMI shielding performance, the absorption and reflection effects, should be further quantified. Therefore, the reflection shielding effectiveness (SE_R) and absorption shielding effectiveness (SE_A) were calculated separately according to directly obtained scattering parameters (S_{11}, S_{21} or S_{12} and S_{22}) [190]. Total electromagnetic interference shielding effectiveness is set as the logarithm of the ratio of incident microwave power to transmitted counterparts.

$$SE_R = 10 \times \log\left(\frac{1}{1-R}\right) = 10 \times \log\left(\frac{1}{1-|S_{11}|^2}\right) = 10 \times \log\left(\frac{1}{1-|S_{22}|^2}\right) \quad (1)$$

$$SE_A = 10 \times \log\left(\frac{1-R}{T}\right) = 10 \times \log\left(\frac{1-|S_{11}|^2}{|S_{21}|^2}\right) = 10 \times \log\left(\frac{1-|S_{22}|^2}{|S_{12}|^2}\right) \quad (2)$$

$$SE_T = 10 \times \log\left(\frac{I}{T}\right) \text{ with } 1 = R + T + A \quad (3)$$

Where I, R, T, and A are the incident, reflected, transmitted and absorbed power counterparts, respectively. The incident electromagnetic power is divided into reflected, absorbed, and transmitted power.

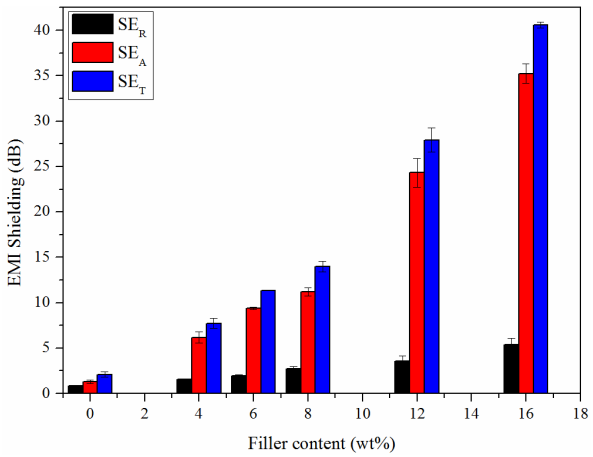

Figure 29. The value of SE_T, SE_A, and SE_R at different fGNP loading. Error bars represent the standard deviation.

Results of frequency-averaged SE_T, SE_A, and SE_R with different fGNP loadings are shown in Figure 29, with further data for pGNP/PLA nanocomposites depicted in Figure 55 in Appendix H. As indicated in Figure 29, the SE_T, and SE_A all became larger with increasing GNP loading. By comparing the values of SE_A and SE_R, it was worth noting that for any GNP concentration, the average SE_A was higher than SE_R. For example, as shown in Figure 29, at 12 wt%, the average SE_A and SE_R were 24.32 dB and 3.59 dB, respectively. At low fGNP content (less than 8 wt%), SE_A indicated only a slight change from 6.19 dB at 4 wt% to 11.22 dB at 8 wt% loading. As fGNP concentration increased to 12 wt% and 16 wt%, SE_A data demonstrates a significant increasing trend, while the increment for SE_R was negligible as compared to SE_A. For instance, SE_A increased from a value of 11.22 dB to 35.25 dB (214% increments), with fGNP addition rising from 8 to 16 wt%, whereas SE_R was raised from 2.74 dB to 5.36 dB (increased only by 95.6%) for the same change in fGNP content. Thus, for 16 wt% fGNP, there was a much smaller contribution to EMI shielding effectiveness from reflection (13.2%) than that contributed by absorption (86.8%).

It was evident that absorption shielding dominated EMI shielding behavior, indicating most of the incident energy was converted to heat among all GNP contents [191], regardless of functionalization. Because of the 2-D structure, large surface area, and alignment morphology of

GNP, the interactions between the mobile charge carriers and incident radiation were significantly increased, resulting in efficient wave absorption. This absorption-dominated shielding behavior showed superiority in commercial EMI shielding applications of PLA nanocomposites compared with the conventional reflection-dominated counterparts because the reflected electromagnetic microwaves can affect or even damage the functionality of the vulnerable electronic or electric components [192].

Chapter 4 - Conclusions

The presented study was undertaken to prepare multifunctional graphene nanoplatelets (GNP)/polylactide (PLA) sustainable nanocomposites with high conductivities and comparable mechanical properties by aligning GNP in the polymer matrix. To improve the dispersion of GNP and GNP/PLA interfacial adhesion, a tannic acid modifier was used to non-covalent modify pure GNP (pGNP) to obtain functionalized graphene nanoplatelets (fGNP). The fGNP/PLA and pGNP/PLA nanocomposites were prepared in a two-step scalable fabrication process, i.e., solution-blending followed by hot compression molding, at various GNP weight fractions up to 16 wt%. The crystal structure and chemical groups of fGNP and pGNP powders were assessed. In addition, the morphologies, structures, thermal properties (including the thermal transition, thermal stability, and thermo-mechanical behavior), electrical and thermal conductivities, electromagnetic interference shielding effectiveness and mechanical strength of GNP/PLA nanocomposites were systematically investigated.

FTIR testing revealed the successful absorption of tannic acid molecules on the surface of GNP by π–π interactions, while XRD analyses indicated fGNP was much less ordered than pGNP powder. Consequently, the relative peak intensity at 26.5° of pGNP/PLA was stronger than that of fGNP/PLA counterparts at the same nanofiller loading. The amorphous form of pure PLA was changed to a semi-crystalline state in nanocomposites due to an efficient nucleation ability of GNP nanofillers.

An enhanced interfacial bonding and better dispersion for fGNP in the PLA matrix were conjectured by the SEM and TEM measurements. Moreover, after the hot-compression process, indications of GNP alignment in nanocomposites were ascertained, especially for high filler loadings, as indicated by TEM analysis and thermal conductivity testing.

For both pGNP and fGNP based nanocomposites, the in-plane thermal conductivity was substantially higher than that in the through-plane direction due to the formation of preferred continuous thermal conduction networks along the alignment direction and diminished interfacial thermal resistance. The specific anisotropic thermal conductivity can be observed beyond 4 wt% fGNP and 6 wt% pGNP. For example, the anisotropy index (the ratio of in-plane to through-plane thermal conductivity) was about 18.5 and 21.6 for the 16-pGNP/PLA and 16-fGNP/PLA,

respectively. Because of reduced phonon scattering at the fGNP-PLA interface and easy phonon transport, thermal conductivity was effectively improved for fGNP/PLA nanocomposites compared with pGNP/PLA counterparts. With 16 wt% fGNP, the in-plane thermal conductivity was enhanced to 8.65 W/mK, which is a 1.46 and 43.2 times of 16-pGNP/PLA nanocomposites and neat PLA, respectively. With substantially improved thermal conductivity, oriented GNP/PLA nanocomposites may meet the requirements for commercial use in components requiring thermal management functionality.

Furthermore, the enhanced thermal stability was more pronounced because of the higher thermal conductivity of fGNP/PLA samples and the more homogeneous dispersion of fGNP. In addition, improved Young's and storage moduli of fGNP/PLA nanocomposites were attributed to the strong interfacial interactions by forming hydrogen bonding between PLA and fGNP, which can ensure more efficient stress-transfer from matrix to fGNP phase. An increased modulus can improve the load-bearing ability of nanocomposites. But, tensile strength and elongation at break were reduced, which was attributed to the high intrinsic stiffness of GNP.

As expected, the electrical conductivity of PLA nanocomposites also increased with GNP incorporation, displaying the formation of percolating networks between 6 wt% to 8 wt% GNP. The conductivity at 16 wt% fGNP was detected to be 0.8 S/cm (corresponding to an electric resistivity of 1.25 Ω/cm), which was an increase of more than 13 orders of magnitude over pure PLA. It should be noted that electrical resistivity of ~1.25 Ω/cm is low enough for potential applications requiring electrostatic dissipation or other electronic devices requiring electrical conductivity. EMI shielding performance of PLA nanocomposites was also explored. When GNP content increased to 16 wt%, an average total shielding effectiveness of 37.81 dB (16-pGNP/PLA) and 40.61 dB (16-fGNP/PLA) represents 99.979% and 99.991% blockage of incident EMI radiation, respectively, which are both larger than the required minimum value (20.0 dB) for industrial EMI shielding products. Among all GNP contents, absorption shielding was the primary shielding mechanism.

The demonstrated high-performance of bio-based PLA nanocomposites may create new opportunities for these materials with high commercial and industrial demand and thus decrease the dependency on petroleum-based products in the future.

Chapter 5 - Suggested Future Studies

5.1 Incorporating two or more nanofillers into the polymer matrix

Besides modifying PLA polymer with only individual type of GNP, simultaneously combining two or more different nanofillers into the polymer matrix may be an effective strategy for realizing high thermal conductivity enhancement. Synergistic effects between different fillers may construct more efficient three-dimensional conductive networks in the nanocomposites [96, 193]. For example, continuous hybrid interconnected networks can be formed by bridging the two-dimensional GNP with one-dimensional CNT if using a combination of CNT and GNP in the polymer nanocomposites [96]. Inspired by this notion, a future study direction can focus on alignment of synergistic nanofillers in the polymer, including different dimensional nano-reinforcement (such as zero- and one-dimensional nanoparticles and GNP), various aspect ratios of GNP, and different two-dimensional nanofillers (such as graphene oxide and GNP, or boron nitride and GNP). Furthermore, the microstructure and other macroscopic properties, such as the thermal, mechanical properties, and electrical conductivity, should be explored to understand the synergistic effect thoroughly.

5.2 Using analytic modeling to assess the thermal conductivity

An experiment can directly provide values for various properties, but experimentation is typically time and cost consuming. It is therefore desirable to develop theoretical models to estimate and predict the properties and reveal underlying mechanisms. Existing models for thermal conductivity published in the technical literature can be categorized into two groups.

1) Model based on the idea that nanofillers are randomly distributed in the nanocomposites: These powerful models include the Maxwell-Eucken model [194], Bruggeman model [195], and Halpin-Tsai model [196]. Moreover, some researchers have proposed analytical approaches for predicting the thermal conductivity of GNP/polymer nanocomposites [197].
2) Models considering the alignment distribution of nanofillers in the nanocomposites: Such models include the effective medium approximation theory [198, 199], the model

presented in studies of Balandin et al. [200, 201] and the Lewis and Nielsen model [202-204].

Schemes for modeling thermal conductivity can be divided into two possible tasks.

1) Comparing the values of thermal conductivity obtained from existing analytical models and experimental results to evaluate their effectiveness.

2) Based on the analysis of theoretical and experimental values, developing a new modeling approach to assess the thermal conductivity of GNP/PLA nanocomposites. Many factors should be considered in the theoretic model, including the thermal conductivity of nanofillers and matrix, the microstructure, the interfacial thermal resistance between nanofillers and polymer matrix, and the volume fraction, geometric dimension, orientation of nanofillers.

5.3 Further study of mechanical properties

1) In this study, elongation at break of neat PLA and GNP/PLA nanocomposites was found to be comparatively low, which may be ascribed to the hot-compression preparation method. After hot-pressing, the bottom surface of sample is smoother than the top surface, which may influence the elongation at break due to surface roughness effects. The effect of roughness on the mechanical properties (especially the elongation at break) should be examined.
2) In this study, some overlap between the range of test data was observed for the mechanical properties for fGNP/PLA and pGNP/PLA samples at the same filler loading (such as tensile strength, elongation at break and Young's modulus). At this point, it is thus not clear if certain properties of fGNP/PLA are statistically significantly different from pGNP/PLA for the same filler loading. Therefore t-testing or similar statistical analysis should be conducted.

References

[1] S. Kashi, R.K. Gupta, T. Baum, N. Kao, S.N. Bhattacharya, Dielectric properties and electromagnetic interference shielding effectiveness of graphene-based biodegradable nanocomposites, Materials & Design 109 (2016) 68-78.

[2] V. Ojijo, S. Sinha Ray, Processing strategies in bionanocomposites, Progress in Polymer Science 38(10) (2013) 1543-1589.

[3] Z. Lule, H. Ju, J. Kim, Thermomechanical properties of alumina-filled plasticized polylactic acid: Effect of alumina loading percentage, Ceramics International 44(18) (2018) 22767-22776.

[4] A. Nanni, M. Messori, Effect of the wine lees wastes as cost-advantage and natural fillers on the thermal and mechanical properties of poly(3-hydroxybutyrate-co-hydroxyhexanoate) (PHBH) and poly(3-hydroxybutyrate-co-hydroxyvalerate) (PHBV), Journal of Applied Polymer Science 137(28) (2020) 48869.

[5] M. Sabzi, L. Jiang, F. Liu, I. Ghasemi, M. Atai, Graphene nanoplatelets as poly(lactic acid) modifier: linear rheological behavior and electrical conductivity, Journal of Materials Chemistry A 1(28) (2013) 8253-8261.

[6] H. Norazlina, Y. Kamal, Graphene modifications in polylactic acid nanocomposites: a review, Polymer Bulletin 72(4) (2015) 931-961.

[7] C. Huang, X. Qian, R. Yang, Thermal conductivity of polymers and polymer nanocomposites, Materials Science and Engineering: R: Reports 132 (2018) 1-22.

[8] O.J. Botlhoko, J. Ramontja, S.S. Ray, Thermally shocked graphene oxide-containing biocomposite for thermal management applications, RSC Advances 7(54) (2017) 33751-33756.

[9] T. Wieme, L. Duan, N. Mys, L. Cardon, D.R. D'Hooge, Effect of Matrix and Graphite Filler on Thermal Conductivity of Industrially Feasible Injection Molded Thermoplastic Composites, Polymers 11(1) (2019) 87.

[10] G.-X. Chen, H.-S. Kim, E.-S. Kim, J.-S. Yoon, Synthesis of high-molecular-weight poly(l-lactic acid) through the direct condensation polymerization of l-lactic acid in bulk state, European Polymer Journal 42(2) (2006) 468-472.

[11] H. Zhao, Enzymatic ring-opening polymerization (ROP) of polylactones: roles of non-aqueous solvents, Journal of Chemical Technology & Biotechnology 93(1) (2018) 9-19.

[12] W.H. Carothers, G.L. Dorough, F.J.v. Natta, Studies of polymerization and ring formation. X. The reversible polymerization of six-membered cyclic esters, Journal of the American Chemical Society 54(2) (1932) 761-772.
[13] J.-M. Raquez, Y. Habibi, M. Murariu, P. Dubois, Polylactide (PLA)-based nanocomposites, Progress in Polymer Science 38(10) (2013) 1504-1542.
[14] R.M. Rasal, A.V. Janorkar, D.E. Hirt, Poly(lactic acid) modifications, Progress in Polymer Science 35(3) (2010) 338-356.
[15] S.Z. Rogovina, K.V. Aleksanyan, A.A. Kosarev, N.E. Ivanushkina, E.V. Prut, A.A. Berlin, Biodegradable polymer composites based on polylactide and cellulose, Polymer Science Series B 58(1) (2016) 38-46.
[16] C. Gonçalves, I.C. Gonçalves, F.D. Magalhães, A.M. Pinto, Poly(lactic acid) Composites Containing Carbon-Based Nanomaterials: A Review, Polymers 9(7) (2017) 269.
[17] T. Standau, C. Zhao, S. Murillo Castellón, C. Bonten, V. Altstädt, Chemical Modification and Foam Processing of Polylactide (PLA), Polymers 11(2) (2019) 306.
[18] A. Basu, M. Nazarkovsky, R. Ghadi, W. Khan, A.J. Domb, Poly(lactic acid)-based nanocomposites, Polymers for Advanced Technologies 28(8) (2017) 919-930.
[19] L.T. Lim, R. Auras, M. Rubino, Processing technologies for poly(lactic acid), Progress in Polymer Science 33(8) (2008) 820-852.
[20] K.S. Anderson, K.M. Schreck, M.A. Hillmyer, Toughening Polylactide, Polymer Reviews 48(1) (2008) 85-108.
[21] S. Inkinen, M. Hakkarainen, A.-C. Albertsson, A. Södergård, From Lactic Acid to Poly(lactic acid) (PLA): Characterization and Analysis of PLA and Its Precursors, Biomacromolecules 12(3) (2011) 523-532.
[22] A. Thabet, Y.A. Mobarak, Predictable Models and Experimental Measurements for Electric Properties of Polypropylene Nanocomposite Films, International Journal of Electrical and Computer Engineering 6 (2016) 120-129.
[23] https://omnexus.specialchem.com/selection-guide/polypropylene-pp-plastic.
[24] Clarinval AM, Halleux J (2005) Classification of biodegradable polymers. In: Smith R (ed) Biodegradable polymers for industrial applications, 1st edn. CRC Press, Boca Raton, FL, pp 3-31.

[25] M. Jonoobi, J. Harun, A.P. Mathew, K. Oksman, Mechanical properties of cellulose nanofiber (CNF) reinforced polylactic acid (PLA) prepared by twin screw extrusion, Composites Science and Technology 70(12) (2010) 1742-1747.
[26] A. Bher, I. Uysal Unalan, R. Auras, M. Rubino, C.E. Schvezov, Toughening of Poly(lactic acid) and Thermoplastic Cassava Starch Reactive Blends Using Graphene Nanoplatelets, Polymers 10(1) (2018) 95.
[27] S. Farah, D.G. Anderson, R. Langer, Physical and mechanical properties of PLA, and their functions in widespread applications — A comprehensive review, Advanced Drug Delivery Reviews 107 (2016) 367-392.
[28] B. Xue, J. Ye, J. Zhang, Highly conductive Poly(L-lactic acid) composites obtained via in situ expansion of graphite, Journal of Polymer Research 22(6) (2015) 112.
[29] A. Rostami, H. Nazockdast, M. Karimi, Graphene induced microstructural changes of PLA/MWCNT biodegradable nanocomposites: rheological, morphological, thermal and electrical properties, RSC Advances 6(55) (2016) 49747-49759.
[30] Z. Kulinski, E. Piorkowska, K. Gadzinowska, M. Stasiak, Plasticization of Poly(l-lactide) with Poly(propylene glycol), Biomacromolecules 7(7) (2006) 2128-2135.
[31] S. Boyacioglu, M. Kodal, G. Ozkoc, A comprehensive study on shape memory behavior of PEG plasticized PLA/TPU bio-blends, European Polymer Journal 122 (2020) 109372.
[32] X. Wen, Z. Liu, Z. Li, J. Zhang, D.-Y. Wang, K. Szymańska, X. Chen, E. Mijowska, T. Tang, Constructing multifunctional nanofiller with reactive interface in PLA/CB-g-DOPO composites for simultaneously improving flame retardancy, electrical conductivity and mechanical properties, Composites Science and Technology 188 (2020) 107988.
[33] A.S. Luyt, I. Kelnar, Effect of blend ratio and nanofiller localization on the thermal degradation of graphite nanoplatelets-modified PLA/PCL, Journal of Thermal Analysis and Calorimetry 136(6) (2019) 2373-2382.
[34] V. Mittal, A.U. Chaudhry, G.E. Luckachan, Biopolymer – Thermally reduced graphene nanocomposites: Structural characterization and properties, Materials Chemistry and Physics 147(1) (2014) 319-332.
[35] J. Sepulveda, C. Villegas, A. Torres, E. Vargas, F. Rodriguez, S. Baltazar, A. Prada, A. Rojas, J. Romero, S. Faba, M.J. Galotto, Effect of functionalized silica nanoparticles on the mass transfer

process in active PLA nanocomposite films obtained by supercritical impregnation for sustainable food packaging, The Journal of Supercritical Fluids 161 (2020) 104844.
[36] P. Ramesh, B.D. Prasad, K.L. Narayana, Influence of Montmorillonite Clay Content on Thermal, Mechanical, Water Absorption and Biodegradability Properties of Treated Kenaf Fiber/ PLA-Hybrid Biocomposites, Silicon (2020).
[37] S. Mohan Bhasney, K. Mondal, A. Kumar, V. Katiyar, Effect of microcrystalline cellulose [MCC] fibres on the morphological and crystalline behaviour of high density polyethylene [HDPE]/polylactic acid [PLA] blends, Composites Science and Technology 187 (2020) 107941.
[38] M. Bijarimi, M. Amirul, M. Norazmi, A. Ramli, M.S.Z. Desa, M.D.A. Desa, M.A. Abu Samah, Preparation and characterization of poly (lactic acid) (PLA)/polyamide 6 (PA6)/graphene nanoplatelet (GNP) blends bio-based nanocomposites, Materials Research Express 6(5) (2019) 055044.
[39] P. Wang, Z. Xiong, H. Xiong, J. Cai, Synergistic effects of modified TiO2/multifunctionalized graphene oxide nanosheets as functional hybrid nanofiller in enhancing the interface compatibility of PLA/starch nanocomposites, Journal of Applied Polymer Science 49094.
[40] S. Savaş, H. Üvez, Structure and resultant mechanical and tribological performance of PP/PLA/carbon fiber/ethylene-butyl acrylate composites, Journal of Composite Materials 53(10) (2019) 1299-1317.
[41] Y. Wang, Y. Mei, Q. Wang, W. Wei, F. Huang, Y. Li, J. Li, Z. Zhou, Improved fracture toughness and ductility of PLA composites by incorporating a small amount of surface-modified helical carbon nanotubes, Composites Part B: Engineering 162 (2019) 54-61.
[42] D. Pholharn, Y. Srithep, J. Morris, Melt compounding and characterization of poly(lactide) stereocomplex/natural rubber composites, Polymer Engineering & Science 58(5) (2018) 713-718.
[43] R. Patwa, N. Saha, P. Sáha, V. Katiyar, Biocomposites of poly(lactic acid) and lactic acid oligomer-grafted bacterial cellulose: It's preparation and characterization, Journal of Applied Polymer Science 136(35) (2019) 47903.
[44] A.H. Davoodi, S. Mazinani, F. Sharif, S.O. Ranaei-Siadat, GO nanosheets localization by morphological study on PLA-GO electrospun nanocomposite nanofibers, Journal of Polymer Research 25(9) (2018) 204.

[45] S. Gazzotti, H. Farina, G. Lesma, R. Rampazzo, L. Piergiovanni, M.A. Ortenzi, A. Silvani, Polylactide/cellulose nanocrystals: The in situ polymerization approach to improved nanocomposites, European Polymer Journal 94 (2017) 173-184.
[46] G. Mittal, V. Dhand, K.Y. Rhee, S.-J. Park, W.R. Lee, A review on carbon nanotubes and graphene as fillers in reinforced polymer nanocomposites, Journal of Industrial and Engineering Chemistry 21 (2015) 11-25.
[47] G. Haznedar, S. Cravanzola, M. Zanetti, D. Scarano, A. Zecchina, F. Cesano, Graphite nanoplatelets and carbon nanotubes based polyethylene composites: Electrical conductivity and morphology, Materials Chemistry and Physics 143(1) (2013) 47-52.
[48] W.K. Chee, H.N. Lim, N.M. Huang, I. Harrison, Nanocomposites of graphene/polymers: a review, RSC Advances 5(83) (2015) 68014-68051.
[49] M. Zhang, Y. Li, Z. Su, G. Wei, Recent advances in the synthesis and applications of graphene–polymer nanocomposites, Polymer Chemistry 6(34) (2015) 6107-6124.
[50] A.K. Geim, K.S. Novoselov, The rise of graphene, Nature Materials 6(3) (2007) 183-191.
[51] K.S. Novoselov, A.K. Geim, S.V. Morozov, D. Jiang, Y. Zhang, S.V. Dubonos, I.V. Grigorieva, A.A. Firsov, Electric Field Effect in Atomically Thin Carbon Films, Science 306(5696) (2004) 666-669.
[52] C.N.R. Rao, A.K. Sood, K.S. Subrahmanyam, A. Govindaraj, Graphene: The New Two-Dimensional Nanomaterial, Angewandte Chemie International Edition 48(42) (2009) 7752-7777.
[53] B. Jiang, C. Tian, L. Wang, L. Sun, C. Chen, X. Nong, Y. Qiao, H. Fu, Highly concentrated, stable nitrogen-doped graphene for supercapacitors: Simultaneous doping and reduction, Applied Surface Science 258(8) (2012) 3438-3443.
[54] A.A. Balandin, S. Ghosh, W. Bao, I. Calizo, D. Teweldebrhan, F. Miao, C.N. Lau, Superior Thermal Conductivity of Single-Layer Graphene, Nano Letters 8(3) (2008) 902-907.
[55] K.I. Bolotin, K.J. Sikes, Z. Jiang, M. Klima, G. Fudenberg, J. Hone, P. Kim, H.L. Stormer, Ultrahigh electron mobility in suspended graphene, Solid State Communications 146(9) (2008) 351-355.
[56] C. Lee, X. Wei, J.W. Kysar, J. Hone, Measurement of the Elastic Properties and Intrinsic Strength of Monolayer Graphene, Science 321(5887) (2008) 385-388.

[57] Y.S. Jun, J.G. Um, G. Jiang, A. Yu, A study on the effects of graphene nano-platelets (GnPs) sheet sizes from a few to hundred microns on the thermal, mechanical, and electrical properties of polypropylene (PP)/GnPs composites, Express Polymer Letters 12 (2018) 885-897.
[58] A. Yu, P. Ramesh, M.E. Itkis, E. Bekyarova, R.C. Haddon, Graphite Nanoplatelet−Epoxy Composite Thermal Interface Materials, The Journal of Physical Chemistry C 111(21) (2007) 7565-7569.
[59] S. Iranmanesh, H.C. Ong, B.C. Ang, E. Sadeghinezhad, A. Esmaeilzadeh, M. Mehrali, Thermal performance enhancement of an evacuated tube solar collector using graphene nanoplatelets nanofluid, Journal of Cleaner Production 162 (2017) 121-129.
[60] K. Honaker, F. Vautard, L.T. Drzal, Investigating the mechanical and barrier properties to oxygen and fuel of high density polyethylene–graphene nanoplatelet composites, Materials Science and Engineering: B 216 (2017) 23-30.
[61] H. Kim, A.A. Abdala, C.W. Macosko, Graphene/Polymer Nanocomposites, Macromolecules 43(16) (2010) 6515-6530.
[62] M. Mehrali, E. Sadeghinezhad, S.T. Latibari, S.N. Kazi, M. Mehrali, M.N.B.M. Zubir, H.S.C. Metselaar, Investigation of thermal conductivity and rheological properties of nanofluids containing graphene nanoplatelets, Nanoscale Research Letters 9(1) (2014) 15.
[63] C. Selvam, D. Mohan Lal, S. Harish, Thermal conductivity and specific heat capacity of water–ethylene glycol mixture-based nanofluids with graphene nanoplatelets, Journal of Thermal Analysis and Calorimetry 129(2) (2017) 947-955.
[64] X. Sun, Q. Wu, J. Zhang, Y. Qing, Y. Wu, S. Lee, Rheology, curing temperature and mechanical performance of oil well cement: Combined effect of cellulose nanofibers and graphene nano-platelets, Materials & Design 114 (2017) 92-101.
[65] M.A. Raza, A. Westwood, C. Stirling, Carbon black/graphite nanoplatelet/rubbery epoxy hybrid composites for thermal interface applications, Journal of Materials Science 47(2) (2012) 1059-1070.
[66] B. Li, W.-H. Zhong, Review on polymer/graphite nanoplatelet nanocomposites, Journal of Materials Science 46(17) (2011) 5595-5614.
[67] F. Wang, L.T. Drzal, Y. Qin, Z. Huang, Enhancement of fracture toughness, mechanical and thermal properties of rubber/epoxy composites by incorporation of graphene nanoplatelets, Composites Part A: Applied Science and Manufacturing 87 (2016) 10-22.

[68] R. Asmatulu, W.S. Khan, R.J. Reddy, M. Ceylan, Synthesis and analysis of injection-molded nanocomposites of recycled high-density polyethylene incorporated with graphene nanoflakes, Polymer Composites 36(9) (2015) 1565-1573.
[69] F. Wang, L.T. Drzal, Y. Qin, Z. Huang, Mechanical properties and thermal conductivity of graphene nanoplatelet/epoxy composites, Journal of Materials Science 50(3) (2015) 1082-1093.
[70] A. Nieto, D. Lahiri, A. Agarwal, Synthesis and properties of bulk graphene nanoplatelets consolidated by spark plasma sintering, Carbon 50(11) (2012) 4068-4077.
[71] J. Gu, X. Yang, Z. Lv, N. Li, C. Liang, Q. Zhang, Functionalized graphite nanoplatelets/epoxy resin nanocomposites with high thermal conductivity, International Journal of Heat and Mass Transfer 92 (2016) 15-22.
[72] S.G. Prolongo, R. Moriche, M. Sánchez, A. Ureña, Self-stratifying and orientation of exfoliated few-layer graphene nanoplatelets in epoxy composites, Composites Science and Technology 85 (2013) 136-141.
[73] M. El Achaby, A. Qaiss, Processing and properties of polyethylene reinforced by graphene nanosheets and carbon nanotubes, Materials & Design 44 (2013) 81-89.
[74] S. Chatterjee, F. Nafezarefi, N.H. Tai, L. Schlagenhauf, F.A. Nüesch, B.T.T. Chu, Size and synergy effects of nanofiller hybrids including graphene nanoplatelets and carbon nanotubes in mechanical properties of epoxy composites, Carbon 50(15) (2012) 5380-5386.
[75] M. Mehrali, S.T. Latibari, M. Mehrali, T.M. Indra Mahlia, H.S. Cornelis Metselaar, M.S. Naghavi, E. Sadeghinezhad, A.R. Akhiani, Preparation and characterization of palmitic acid/graphene nanoplatelets composite with remarkable thermal conductivity as a novel shape-stabilized phase change material, Applied Thermal Engineering 61(2) (2013) 633-640.
[76] I.S. Bayer, Thermomechanical Properties of Polylactic Acid-Graphene Composites: A State-of-the-Art Review for Biomedical Applications, Materials 10(7) (2017) 748.
[77] Y. Guo, X. Zuo, Y. Xue, J. Tang, M. Gouzman, Y. Fang, Y. Zhou, L. Wang, Y. Yu, M.H. Rafailovich, Engineering thermally and electrically conductive biodegradable polymer nanocomposites, Composites Part B: Engineering 189 (2020) 107905.
[78] B.W. Chieng, N.A. Ibrahim, W.M.Z.W. Yunus, M.Z. Hussein, Y.Y. Then, Y.Y. Loo, Reinforcement of graphene nanoplatelets on plasticized poly(lactic acid) nanocomposites: Mechanical, thermal, morphology, and antibacterial properties, Journal of Applied Polymer Science 132(11) (2015).

[79] M. Tait, A. Pegoretti, A. Dorigato, K. Kalaitzidou, The effect of filler type and content and the manufacturing process on the performance of multifunctional carbon/poly-lactide composites, Carbon 49(13) (2011) 4280-4290.
[80] S. Girdthep, W. Sankong, A. Pongmalee, T. Saelee, W. Punyodom, P. Meepowpan, P. Worajittiphon, Enhanced crystallization, thermal properties, and hydrolysis resistance of poly(l-lactic acid) and its stereocomplex by incorporation of graphene nanoplatelets, Polymer Testing 61 (2017) 229-239.
[81] C. Cai, L. Liu, Y. Fu, Processable conductive and mechanically reinforced polylactide/graphene bionanocomposites through interfacial compatibilizer, Polymer Composites 40(1) (2019) 389-400.
[82] S. Ganguli, A.K. Roy, D.P. Anderson, Improved thermal conductivity for chemically functionalized exfoliated graphite/epoxy composites, Carbon 46(5) (2008) 806-817.
[83] E.M. Sullivan, P. Karimineghlani, M. Naraghi, R.A. Gerhardt, K. Kalaitzidou, The effect of nanofiller geometry and compounding method on polylactic acid nanocomposite films, European Polymer Journal 77 (2016) 31-42.
[84] Y. Wang, C.-S. Lin, Preparation and characterization of maleated polylactide-functionalized graphite oxide nanocomposites, Journal of Polymer Research 21(1) (2013) 334.
[85] G. Spinelli, P. Lamberti, V. Tucci, R. Kotsilkova, E. Ivanov, D. Menseidov, C. Naddeo, V. Romano, L. Guadagno, R. Adami, D. Meisak, D. Bychanok, P. Kuzhir, Nanocarbon/Poly(Lactic) Acid for 3D Printing: Effect of Fillers Content on Electromagnetic and Thermal Properties, Materials 12(15) (2019) 2369.
[86] H. Park, Y.R. Jeong, J. Yun, S.Y. Hong, S. Jin, S.-J. Lee, G. Zi, J.S. Ha, Stretchable Array of Highly Sensitive Pressure Sensors Consisting of Polyaniline Nanofibers and Au-Coated Polydimethylsiloxane Micropillars, ACS Nano 9(10) (2015) 9974-9985.
[87] M. Kujawski, J.D. Pearse, E. Smela, Elastomers filled with exfoliated graphite as compliant electrodes, Carbon 48(9) (2010) 2409-2417.
[88] M.A. Raza, A.V.K. Westwood, A.P. Brown, C. Stirling, Texture, transport and mechanical properties of graphite nanoplatelet/silicone composites produced by three roll mill, Composites Science and Technology 72(3) (2012) 467-475.
[89] T.K. Das, S. Prusty, Graphene-Based Polymer Composites and Their Applications, Polymer-Plastics Technology and Engineering 52(4) (2013) 319-331.

[90] Z. Antar, H. Noel, J.F. Feller, P. Glouannec, K. Elleuch, Thermophysical and Radiative Properties of Conductive Biopolymer Composite, Materials Science Forum 714 (2012) 115-122.
[91] S. Herrmann, C. Ritchie, C. Streb, Polyoxometalate – conductive polymer composites for energy conversion, energy storage and nanostructured sensors, Dalton Transactions 44(16) (2015) 7092-7104.
[92] J.-E. An, Y.G. Jeong, Structure and electric heating performance of graphene/epoxy composite films, European Polymer Journal 49(6) (2013) 1322-1330.
[93] G. He, J. Liu, F. Gong, C. Lin, Z. Yang, Bioinspired mechanical and thermal conductivity reinforcement of highly explosive-filled polymer composites, Composites Part A: Applied Science and Manufacturing 107 (2018) 1-9.
[94] F. Wang, L.T. Drzal, Development of Stiff, Tough and Conductive Composites by the Addition of Graphene Nanoplatelets to Polyethersulfone/Epoxy Composites, Materials 11(11) (2018) 2137.
[95] Z. Antar, J.F. Feller, H. Noël, P. Glouannec, K. Elleuch, Thermoelectric behaviour of melt processed carbon nanotube/graphite/poly(lactic acid) conductive biopolymer nanocomposites (CPC), Materials Letters 67(1) (2012) 210-214.
[96] S.-Y. Yang, W.-N. Lin, Y.-L. Huang, H.-W. Tien, J.-Y. Wang, C.-C.M. Ma, S.-M. Li, Y.-S. Wang, Synergetic effects of graphene platelets and carbon nanotubes on the mechanical and thermal properties of epoxy composites, Carbon 49(3) (2011) 793-803.
[97] A. Tessema, D. Zhao, J. Moll, S. Xu, R. Yang, C. Li, S.K. Kumar, A. Kidane, Effect of filler loading, geometry, dispersion and temperature on thermal conductivity of polymer nanocomposites, Polymer Testing 57 (2017) 101-106.
[98] J. Yu, B. Sundqvist, B. Tonpheng, O. Andersson, Thermal conductivity of highly crystallized polyethylene, Polymer 55(1) (2014) 195-200.
[99] R. Kothari, C.T. Sun, R. Dinwiddie, H. Wang, Experimental and numerical study of the effective thermal conductivity of nano composites with thermal boundary resistance, International Journal of Heat and Mass Transfer 66 (2013) 823-829.
[100] N. Song, D. Jiao, S. Cui, X. Hou, P. Ding, L. Shi, Highly Anisotropic Thermal Conductivity of Layer-by-Layer Assembled Nanofibrillated Cellulose/Graphene Nanosheets Hybrid Films for Thermal Management, ACS Applied Materials & Interfaces 9(3) (2017) 2924-2932.

[101] M.A. Raza, A.V.K. Westwood, C. Stirling, Effect of processing technique on the transport and mechanical properties of graphite nanoplatelet/rubbery epoxy composites for thermal interface applications, Materials Chemistry and Physics 132(1) (2012) 63-73.
[102] E. Aram, M. Ehsani, H.A. Khonakdar, S.H. Jafari, N.R. Nouri, Functionalization of graphene nanosheets and its dispersion in PMMA/PEO blend: Thermal, electrical, morphological and rheological analyses, Fibers and Polymers 17(2) (2016) 174-180.
[103] Israelachvili, J. N. Intermolecular and Surface Forces, 2nd ed.; New York: Academic Press: 1991.
[104] D. Parviz, S. Das, H.S.T. Ahmed, F. Irin, S. Bhattacharia, M.J. Green, Dispersions of Non-Covalently Functionalized Graphene with Minimal Stabilizer, ACS Nano 6(10) (2012) 8857-8867.
[105] G.L. Pollack, Kapitza Resistance, Reviews of Modern Physics 41(1) (1969) 48-81.
[106] G. Zhang, F. Wang, J. Dai, Z. Huang, Effect of Functionalization of Graphene Nanoplatelets on the Mechanical and Thermal Properties of Silicone Rubber Composites, Materials 9(2) (2016) 92.
[107] A. Kausar, Z. Anwar, L.A. Khan, B. Muhammad, Functional graphene nanoplatelet reinforced epoxy resin and polystyrene-based block copolymer nanocomposite, Fullerenes, Nanotubes and Carbon Nanostructures 25(1) (2017) 47-57.
[108] S.S. Shazali, S. Rozali, A. Amiri, M.N.M. Zubir, M.F.M. Sabri, M.Z. Zabri, Evaluation on stability and thermophysical performances of covalently functionalized graphene nanoplatelets with xylitol and citric acid, Materials Chemistry and Physics 212 (2018) 363-371.
[109] J. Liu, J. Tang, J.J. Gooding, Strategies for chemical modification of graphene and applications of chemically modified graphene, Journal of Materials Chemistry 22(25) (2012) 12435-12452.
[110] A. Amiri, R. Sadri, M. Shanbedi, G. Ahmadi, B.T. Chew, S.N. Kazi, M. Dahari, Performance dependence of thermosyphon on the functionalization approaches: An experimental study on thermo-physical properties of graphene nanoplatelet-based water nanofluids, Energy Conversion and Management 92 (2015) 322-330.
[111] R.K. Layek, A.K. Nandi, A review on synthesis and properties of polymer functionalized graphene, Polymer 54(19) (2013) 5087-5103.

[112] R.M. Santos, S.T. Mould, P. Formánek, M.C. Paiva, J.A. Covas, Effects of Particle Size and Surface Chemistry on the Dispersion of Graphite Nanoplates in Polypropylene Composites, Polymers 10(2) (2018) 222.
[113] O. Zabihi, M. Ahmadi, T. Abdollahi, S. Nikafshar, M. Naebe, Collision-induced activation: Towards industrially scalable approach to graphite nanoplatelets functionalization for superior polymer nanocomposites, Scientific Reports 7(1) (2017) 3560.
[114] Tony McNally, Petra Pötschke. Polymer-Carbon Nanotube Composites: Preparation, Properties and Applications. Cambridge: Woodhead Publishing; 2011.
[115] V. Georgakilas, M. Otyepka, A.B. Bourlinos, V. Chandra, N. Kim, K.C. Kemp, P. Hobza, R. Zboril, K.S. Kim, Functionalization of Graphene: Covalent and Non-Covalent Approaches, Derivatives and Applications, Chemical Reviews 112(11) (2012) 6156-6214.
[116] R. Sadri, M. Hosseini, S.N. Kazi, S. Bagheri, S.M. Ahmed, G. Ahmadi, N. Zubir, M. Sayuti, M. Dahari, Study of environmentally friendly and facile functionalization of graphene nanoplatelet and its application in convective heat transfer, Energy Conversion and Management 150 (2017) 26-36.
[117] S.N. Kazi, A. Badarudin, M.N.M. Zubir, H.N. Ming, M. Misran, E. Sadeghinezhad, M. Mehrali, N.I. Syuhada, Investigation on the use of graphene oxide as novel surfactant to stabilize weakly charged graphene nanoplatelets, Nanoscale Research Letters 10(1) (2015) 212.
[118] X. Mu, X. Wu, T. Zhang, D.B. Go, T. Luo, Thermal Transport in Graphene Oxide – From Ballistic Extreme to Amorphous Limit, Scientific Reports 4(1) (2014) 3909.
[119] R. Gulotty, M. Castellino, P. Jagdale, A. Tagliaferro, A.A. Balandin, Effects of Functionalization on Thermal Properties of Single-Wall and Multi-Wall Carbon Nanotube–Polymer Nanocomposites, ACS Nano 7(6) (2013) 5114-5121.
[120] R. Sadri, M. Hosseini, S.N. Kazi, S. Bagheri, N. Zubir, G. Ahmadi, M. Dahari, T. Zaharinie, A novel, eco-friendly technique for covalent functionalization of graphene nanoplatelets and the potential of their nanofluids for heat transfer applications, Chemical Physics Letters 675 (2017) 92-97.
[121] T. Ardyani, A. Mohamed, S.A. Bakar, M. Sagisaka, Y. Umetsu, M.H. Mamat, M.K. Ahmad, H.P.S.A. Khalil, S. King, S.E. Rogers, J. Eastoe, Surfactants with aromatic headgroups for optimizing properties of graphene/natural rubber latex composites (NRL): Surfactants with aromatic amine polar heads, Journal of Colloid and Interface Science 545 (2019) 184-194.

[122] C.-C. Teng, C.-C.M. Ma, C.-H. Lu, S.-Y. Yang, S.-H. Lee, M.-C. Hsiao, M.-Y. Yen, K.-C. Chiou, T.-M. Lee, Thermal conductivity and structure of non-covalent functionalized graphene/epoxy composites, Carbon 49(15) (2011) 5107-5116.
[123] B. Li, S. Dong, X. Wu, C. Wang, X. Wang, J. Fang, Anisotropic thermal property of magnetically oriented carbon nanotube/graphene polymer composites, Composites Science and Technology 147 (2017) 52-61.
[124] W. Zhao, J. Kong, H. Liu, Q. Zhuang, J. Gu, Z. Guo, Ultra-high thermally conductive and rapid heat responsive poly(benzobisoxazole) nanocomposites with self-aligned graphene, Nanoscale 8(48) (2016) 19984-19993.
[125] G. Fugallo, A. Cepellotti, L. Paulatto, M. Lazzeri, N. Marzari, F. Mauri, Thermal Conductivity of Graphene and Graphite: Collective Excitations and Mean Free Paths, Nano Letters 14(11) (2014) 6109-6114.
[126] J. Xiang, L.T. Drzal, Investigation of exfoliated graphite nanoplatelets (xGnP) in improving thermal conductivity of paraffin wax-based phase change material, Solar Energy Materials and Solar Cells 95(7) (2011) 1811-1818.
[127] J. Xiang, L.T. Drzal, Thermal conductivity of exfoliated graphite nanoplatelet paper, Carbon 49(3) (2011) 773-778.
[128] X. Li, G.B. McKenna, G. Miquelard-Garnier, A. Guinault, C. Sollogoub, G. Regnier, A. Rozanski, Forced assembly by multilayer coextrusion to create oriented graphene reinforced polymer nanocomposites, Polymer 55(1) (2014) 248-257.
[129] K. Gaska, R. Kádár, A. Rybak, A. Siwek, S. Gubanski, Gas Barrier, Thermal, Mechanical and Rheological Properties of Highly Aligned Graphene-LDPE Nanocomposites, Polymers 9(7) (2017) 294.
[130] Y. Huang, Z. Liu, R. Chen, S. Zheng, C. Feng, L. Chen, W. Yang, M. Yang, Highly anisotropic functional conductors fabricated by multi-melt multi-injection molding (M3IM): A synergetic role of multiple melt flows and confined interface, Composites Science and Technology 171 (2019) 127-134.
[131] F. Wang, L.T. Drzal, Y. Qin, Z. Huang, Multifunctional graphene nanoplatelets/cellulose nanocrystals composite paper, Composites Part B: Engineering 79 (2015) 521-529.
[132] H. Jung, S. Yu, N.-S. Bae, S.M. Cho, R.H. Kim, S.H. Cho, I. Hwang, B. Jeong, J.S. Ryu, J. Hwang, S.M. Hong, C.M. Koo, C. Park, High Through-Plane Thermal Conduction of Graphene

Nanoflake Filled Polymer Composites Melt-Processed in an L-Shape Kinked Tube, ACS Applied Materials & Interfaces 7(28) (2015) 15256-15262.
[133] P. Ding, S. Su, N. Song, S. Tang, Y. Liu, L. Shi, Highly thermal conductive composites with polyamide-6 covalently-grafted graphene by an in situ polymerization and thermal reduction process, Carbon 66 (2014) 576-584.
[134] Q. Li, Y. Guo, W. Li, S. Qiu, C. Zhu, X. Wei, M. Chen, C. Liu, S. Liao, Y. Gong, A.K. Mishra, L. Liu, Ultrahigh Thermal Conductivity of Assembled Aligned Multilayer Graphene/Epoxy Composite, Chemistry of Materials 26(15) (2014) 4459-4465.
[135] F. An, X. Li, P. Min, P. Liu, Z.-G. Jiang, Z.-Z. Yu, Vertically Aligned High-Quality Graphene Foams for Anisotropically Conductive Polymer Composites with Ultrahigh Through-Plane Thermal Conductivities, ACS Applied Materials & Interfaces 10(20) (2018) 17383-17392.
[136] M. Saeidijavash, J. Garg, B. Grady, B. Smith, Z. Li, R.J. Young, F. Tarannum, N. Bel Bekri, High thermal conductivity through simultaneously aligned polyethylene lamellae and graphene nanoplatelets, Nanoscale 9(35) (2017) 12867-12873.
[137] S. Wu, R.B. Ladani, J. Zhang, E. Bafekrpour, K. Ghorbani, A.P. Mouritz, A.J. Kinloch, C.H. Wang, Aligning multilayer graphene flakes with an external electric field to improve multifunctional properties of epoxy nanocomposites, Carbon 94 (2015) 607-618.
[138] R.B. Ladani, S. Wu, A.J. Kinloch, K. Ghorbani, J. Zhang, A.P. Mouritz, C.H. Wang, Multifunctional properties of epoxy nanocomposites reinforced by aligned nanoscale carbon, Materials & Design 94 (2016) 554-564.
[139] D. Li, Y. Liu, H. Ma, Y. Wang, L. Wang, Z. Xie, Preparation and properties of aligned graphene composites, RSC Advances 5(40) (2015) 31670-31676.
[140] W. Jiao, M. Shioya, R. Wang, F. Yang, L. Hao, Y. Niu, W. Liu, L. Zheng, F. Yuan, L. Wan, X. He, Improving the gas barrier properties of Fe3O4/graphite nanoplatelet reinforced nanocomposites by a low magnetic field induced alignment, Composites Science and Technology 99 (2014) 124-130.
[141] S. Wu, J. Zhang, R.B. Ladani, K. Ghorbani, A.P. Mouritz, A.J. Kinloch, C.H. Wang, A novel route for tethering graphene with iron oxide and its magnetic field alignment in polymer nanocomposites, Polymer 97 (2016) 273-284.

[142] H.Y. Yan, R.R. Wang, Y.F. Li, W. Long, Thermal Conductivity of Magnetically Aligned Graphene-Polymer Composites with Fe3O4-Decorated Graphene Nanosheets, Journal of Electronic Materials 44(2) (2015) 658-666.
[143] P. Ding, J. Zhang, N. Song, S. Tang, Y. Liu, L. Shi, Anisotropic thermal conductive properties of hot-pressed polystyrene/graphene composites in the through-plane and in-plane directions, Composites Science and Technology 109 (2015) 25-31.
[144] S.G. Mosanenzadeh, S. Khalid, Y. Cui, H.E. Naguib, High thermally conductive PLA based composites with tailored hybrid network of hexagonal boron nitride and graphene nanoplatelets, Polymer Composites 37(7) (2016) 2196-2205.
[145] A. Fina, S. Colonna, L. Maddalena, M. Tortello, O. Monticelli, Facile and Low Environmental Impact Approach to Prepare Thermally Conductive Nanocomposites Based on Polylactide and Graphite Nanoplatelets, ACS Sustainable Chemistry & Engineering 6(11) (2018) 14340-14347.
[146] H. Lin, L. Pei, L. Zhang, Enhanced thermal conductivity of PLA-based nanocomposites by incorporation of graphite nanoplatelets functionalized by tannic acid, Journal of Applied Polymer Science 135(26) (2018) 46397.
[147] Q.-q. Bai, X. Wei, J.-h. Yang, N. Zhang, T. Huang, Y. Wang, Z.-w. Zhou, Dispersion and network formation of graphene platelets in polystyrene composites and the resultant conductive properties, Composites Part A: Applied Science and Manufacturing 96 (2017) 89-98.
[148] P.-C. Ma, N.A. Siddiqui, G. Marom, J.-K. Kim, Dispersion and functionalization of carbon nanotubes for polymer-based nanocomposites: A review, Composites Part A: Applied Science and Manufacturing 41(10) (2010) 1345-1367.
[149] P. Manafi, I. Ghasemi, M. Karrabi, H. Azizi, M.R. Manafi, P. Ehsaninamin, Thermal stability and thermal degradation kinetics (model-free kinetics) of nanocomposites based on poly (lactic acid)/graphene: the influence of functionalization, Polymer Bulletin 72(5) (2015) 1095-1112.
[150] M. Keramati, I. Ghasemi, M. Karrabi, H. Azizi, M. Sabzi, Incorporation of surface modified graphene nanoplatelets for development of shape memory PLA nanocomposite, Fibers and Polymers 17(7) (2016) 1062-1068.
[151] H.J. Kim, Y.-S. Choi, M.-Y. Lim, K.H. Jung, D.-G. Kim, J.-J. Kim, H. Kang, J.-C. Lee, Reverse osmosis nanocomposite membranes containing graphene oxides coated by tannic acid

with chlorine-tolerant and antimicrobial properties, Journal of Membrane Science 514 (2016) 25-34.
[152] R. Guo, Z. Ren, H. Bi, M. Xu, L. Cai, Electrical and Thermal Conductivity of Polylactic Acid (PLA)-Based Biocomposites by Incorporation of Nano-Graphite Fabricated with Fused Deposition Modeling, Polymers 11(3) (2019) 549.
[153] G. Wang, J. Yang, J. Park, X. Gou, B. Wang, H. Liu, J. Yao, Facile Synthesis and Characterization of Graphene Nanosheets, The Journal of Physical Chemistry C 112(22) (2008) 8192-8195.
[154] Y. Gao, O.T. Picot, E. Bilotti, T. Peijs, Influence of filler size on the properties of poly(lactic acid) (PLA)/graphene nanoplatelet (GNP) nanocomposites, European Polymer Journal 86 (2017) 117-131.
[155] N. Yousefi, X. Lin, Q. Zheng, X. Shen, J.R. Pothnis, J. Jia, E. Zussman, J.-K. Kim, Simultaneous in situ reduction, self-alignment and covalent bonding in graphene oxide/epoxy composites, Carbon 59 (2013) 406-417.
[156] M. Reghat, I. Ghasemi, E. Farno, H. Azizi, P.E. Namin, M. Karrabi, Investigation on shear induced isothermal crystallization of poly (lactic acid) nanocomposite based on graphene, Soft Materials 15(1) (2017) 103-112.
[157] E.M. Sullivan, Y.J. Oh, R.A. Gerhardt, B. Wang, K. Kalaitzidou, Understanding the effect of polymer crystallinity on the electrical conductivity of exfoliated graphite nanoplatelet/polylactic acid composite films, Journal of Polymer Research 21(10) (2014) 563.
[158] H. Wang, Z. Qiu, Crystallization behaviors of biodegradable poly(l-lactic acid)/graphene oxide nanocomposites from the amorphous state, Thermochimica Acta 526(1) (2011) 229-236.
[159] C. Hu, Z. Li, Y. Wang, J. Gao, K. Dai, G. Zheng, C. Liu, C. Shen, H. Song, Z. Guo, Comparative assessment of the strain-sensing behaviors of polylactic acid nanocomposites: reduced graphene oxide or carbon nanotubes, Journal of Materials Chemistry C 5(9) (2017) 2318-2328.
[160] K. Mezghani, R. Anderson Campbell, P.J. Phillips, Lamellar Thickening and the Equilibrium Melting Point of Polypropylene, Macromolecules 27(4) (1994) 997-1002.
[161] T. Konishi, W. Sakatsuji, K. Fukao, Y. Miyamoto, Temperature Dependence of Lamellar Thickness in Isothermally Crystallized Poly(butylene terephthalate), Macromolecules 49(6) (2016) 2272-2280.

[162] L. Zhang, Y. Li, H. Wang, Y. Qiao, J. Chen, S. Cao, Strong and ductile poly(lactic acid) nanocomposite films reinforced with alkylated graphene nanosheets, Chemical Engineering Journal 264 (2015) 538-546.
[163] H. Wang, Z. Qiu, Crystallization kinetics and morphology of biodegradable poly(l-lactic acid)/graphene oxide nanocomposites: Influences of graphene oxide loading and crystallization temperature, Thermochimica Acta 527 (2012) 40-46.
[164] J.F. Mano, Y. Wang, J.C. Viana, Z. Denchev, M.J. Oliveira, Cold Crystallization of PLLA Studied by Simultaneous SAXS and WAXS, Macromolecular Materials and Engineering 289(10) (2004) 910-915.
[165] Y. Guo, L. Pan, X. Yang, K. Ruan, Y. Han, J. Kong, J. Gu, Simultaneous improvement of thermal conductivities and electromagnetic interference shielding performances in polystyrene composites via constructing interconnection oriented networks based on electrospinning technology, Composites Part A: Applied Science and Manufacturing 124 (2019) 105484.
[166] N. Burger, A. Laachachi, M. Ferriol, M. Lutz, V. Toniazzo, D. Ruch, Review of thermal conductivity in composites: Mechanisms, parameters and theory, Progress in Polymer Science 61 (2016) 1-28.
[167] J.H. Park, N.R. Aluru, Self-assembly of graphenes, Surface Science 605(17) (2011) 1616-1620.
[168] J. Gu, N. Li, L. Tian, Z. Lv, Q. Zhang, High thermal conductivity graphite nanoplatelet/UHMWPE nanocomposites, RSC Advances 5(46) (2015) 36334-36339.
[169] B.W. Chieng, N.A. Ibrahim, W.M.Z. Wan Yunus, M.Z. Hussein, Y.Y. Loo, Effect of graphene nanoplatelets as nanofiller in plasticized poly(lactic acid) nanocomposites, Journal of Thermal Analysis and Calorimetry 118(3) (2014) 1551-1559.
[170] J.J. George, A.K. Bhowmick, Ethylene vinyl acetate/expanded graphite nanocomposites by solution intercalation: preparation, characterization and properties, Journal of Materials Science 43(2) (2008) 702-708.
[171] S. Wang, Z. Liang, T. Liu, B. Wang, C. Zhang, Effective amino-functionalization of carbon nanotubes for reinforcing epoxy polymer composites, Nanotechnology 17(6) (2006) 1551-1557.
[172] M. Seong, D.S. Kim, Effects of facile amine-functionalization on the physical properties of epoxy/graphene nanoplatelets nanocomposites, Journal of Applied Polymer Science 132(28) (2015).

[173] Robert F. Landel, Lawrence E. Nielsen. Mechanical properties of polymers and composites, 2nd ed.; London: CRC press: 1993.
[174] F. Wang, L.T. Drzal, Y. Qin, Z. Huang, Effects of functionalized graphene nanoplatelets on the morphology and properties of epoxy resins, High Performance Polymers 28(5) (2016) 525-536.
[175] M. Keramati, I. Ghasemi, M. Karrabi, H. Azizi, M. Sabzi, Dispersion of Graphene Nanoplatelets in Polylactic Acid with the Aid of a Zwitterionic Surfactant: Evaluation of the Shape Memory Behavior, Polymer-Plastics Technology and Engineering 55(10) (2016) 1039-1047.
[176] Z. Jin, K.P. Pramoda, G. Xu, S.H. Goh, Dynamic mechanical behavior of melt-processed multi-walled carbon nanotube/poly(methyl methacrylate) composites, Chemical Physics Letters 337(1) (2001) 43-47.
[177] J. Xu, W. Shi, W. Pang, Synthesis and shape memory effects of Si–O–Si cross-linked hybrid polyurethanes, Polymer 47(1) (2006) 457-465.
[178] S. Lashgari, M. Karrabi, I. Ghasemi, H. Azizi, M. Messori, Graphene nanoplatelets dispersion in poly(l-lactic acid): preparation method and its influence on electrical, crystallinity and thermomechanical properties, Iranian Polymer Journal 25(2) (2016) 193-202.
[179] Y. Zhang, Y. Wang, J. Yu, L. Chen, J. Zhu, Z. Hu, Tuning the interface of graphene platelets/epoxy composites by the covalent grafting of polybenzimidazole, Polymer 55(19) (2014) 4990-5000.
[180] E. Narimissa, R. Gupta, M. Bhaskaran, S. Sriram, Influence of nano-graphite platelet concentration on onset of crystalline degradation in polylactide composites, Polymer Degradation and Stability 97(5) (2012) 829-832.
[181] E. Narimissa, R.K. Gupta, H.J. Choi, N. Kao, M. Jollands, Morphological, mechanical, and thermal characterization of biopolymer composites based on polylactide and nanographite platelets, Polymer Composites 33(9) (2012) 1505-1515.
[182] S. Girdthep, N. Komrapit, R. Molloy, S. Lumyong, W. Punyodom, P. Worajittiphon, Effect of plate-like particles on properties of poly(lactic acid)/poly(butylene adipate-co-terephthalate) blend: A comparative study between modified montmorillonite and graphene nanoplatelets, Composites Science and Technology 119 (2015) 115-123.

[183] I.-H. Kim, Y.G. Jeong, Polylactide/exfoliated graphite nanocomposites with enhanced thermal stability, mechanical modulus, and electrical conductivity, Journal of Polymer Science Part B: Polymer Physics 48(8) (2010) 850-858.
[184] J. Chang, G. Liang, A. Gu, S. Cai, L. Yuan, The production of carbon nanotube/epoxy composites with a very high dielectric constant and low dielectric loss by microwave curing, Carbon 50(2) (2012) 689-698.
[185] W.Y. Zhao, W.M. Zhao, Y.J. Wang. The electrical properties and application of polymer materials. Beijing: Chemical Industry Press: 2006.
[186] S. Kashi, R.K. Gupta, N. Kao, S.A. Hadigheh, S.N. Bhattacharya, Influence of graphene nanoplatelet incorporation and dispersion state on thermal, mechanical and electrical properties of biodegradable matrices, Journal of Materials Science & Technology 34(6) (2018) 1026-1034.
[187] S. Kashi, R.K. Gupta, T. Baum, N. Kao, S.N. Bhattacharya, Morphology, electromagnetic properties and electromagnetic interference shielding performance of poly lactide/graphene nanoplatelet nanocomposites, Materials & Design 95 (2016) 119-126.
[188] S. Maiti, S. Suin, N.K. Shrivastava, B.B. Khatua, A strategy to achieve high electromagnetic interference shielding and ultra low percolation in multiwall carbon nanotube–polycarbonate composites through selective localization of carbon nanotubes, RSC Advances 4(16) (2014) 7979-7990.
[189] J. Chen, J. Xu, K. Wang, X. Qian, R. Sun, Highly Thermostable, Flexible, and Conductive Films Prepared from Cellulose, Graphite, and Polypyrrole Nanoparticles, ACS Applied Materials & Interfaces 7(28) (2015) 15641-15648.
[190] H. Zhang, G. Zhang, M. Tang, L. Zhou, J. Li, X. Fan, X. Shi, J. Qin, Synergistic effect of carbon nanotube and graphene nanoplates on the mechanical, electrical and electromagnetic interference shielding properties of polymer composites and polymer composite foams, Chemical Engineering Journal 353 (2018) 381-393.
[191] M.C. Hermant, N.M.B. Smeets, R.C.F.v. Hal, J. Meuldijk, H.P.A. Heuts, B. Klumperman, A.M.v. Herk, C.E. Koning, Influence of the molecular weight distribution on the percolation threshold of carbon nanotube – polystyrene composites, 9(1) (2009) 022.
[192] Z. Chen, C. Xu, C. Ma, W. Ren, H.-M. Cheng, Lightweight and Flexible Graphene Foam Composites for High-Performance Electromagnetic Interference Shielding, Advanced Materials 25(9) (2013) 1296-1300.

[193] A. Yu, P. Ramesh, X. Sun, E. Bekyarova, M.E. Itkis, R.C. Haddon, Enhanced Thermal Conductivity in a Hybrid Graphite Nanoplatelet – Carbon Nanotube Filler for Epoxy Composites, Advanced Materials 20(24) (2008) 4740-4744.
[194] R.C. Progelhof, J.L. Throne, R.R. Ruetsch, Methods for predicting the thermal conductivity of composite systems: A review, Polymer Engineering & Science 16(9) (1976) 615-625.
[195] D.A.G. Bruggeman, Berechnung verschiedener physikalischer Konstanten von heterogenen Substanzen. I. Dielektrizitätskonstanten und Leitfähigkeiten der Mischkörper aus isotropen Substanzen, Annalen der Physik 416(7) (1935) 636-664.
[196] J. Ashton, J. Halpin, P. Pett, Primer on Composite Materials: Analysis. Stamford, Connecticut: Technomic; 1969.
[197] K. Chu, C.-c. Jia, W.-s. Li, Effective thermal conductivity of graphene-based composites, Applied Physics Letters 101(12) (2012) 121916.
[198] C.-W. Nan, R. Birringer, D.R. Clarke, H. Gleiter, Effective thermal conductivity of particulate composites with interfacial thermal resistance, Journal of Applied Physics 81(10) (1997) 6692-6699.
[199] K. Chu, W.-s. Li, H.-f. Dong, F.-l. Tang, Modeling the thermal conductivity of graphene nanoplatelets reinforced composites, EPL (Europhysics Letters) 100(3) (2012) 36001.
[200] D.L. Nika, A.S. Askerov, A.A. Balandin, Anomalous Size Dependence of the Thermal Conductivity of Graphene Ribbons, Nano Letters 12(6) (2012) 3238-3244.
[201] J.D. Renteria, S. Ramirez, H. Malekpour, B. Alonso, A. Centeno, A. Zurutuza, A.I. Cocemasov, D.L. Nika, A.A. Balandin, Strongly Anisotropic Thermal Conductivity of Free-Standing Reduced Graphene Oxide Films Annealed at High Temperature, Advanced Functional Materials 25(29) (2015) 4664-4672.
[202] R.A. Hauser, J.M. Keith, J.A. King, J.L. Holdren, Thermal conductivity models for single and multiple filler carbon/liquid crystal polymer composites, Journal of Applied Polymer Science 110(5) (2008) 2914-2923.
[203] L.E. Nielsen, The Thermal and Electrical Conductivity of Two-Phase Systems, Industrial & Engineering Chemistry Fundamentals 13(1) (1974) 17-20.
[204] E.H. Weber, M.L. Clingerman, J.A. King, Thermally conductive nylon 6,6 and polycarbonate based resins. II. Modeling, Journal of Applied Polymer Science 88(1) (2003) 123-130.

Appendix A - Nanocomposite Fabrication Equipment

Figure 30. The sonication of GNP under the ice bath.

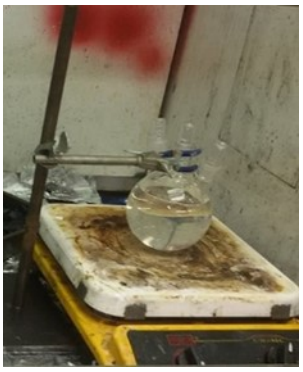

Figure 31. The magnetic stirring of PLA dispersion.

Figure 32. The mechanical stirring of GNP/PLA/chloroform mixture.

Figure 33. Evaporating the solvent in steel mold.

Figure 34. Hot pressing GNP/PLA samples.

Appendix B - Hot-Pressing Processing Equipment

Figure 35. The shape of the custom-made cuboid steel mold.

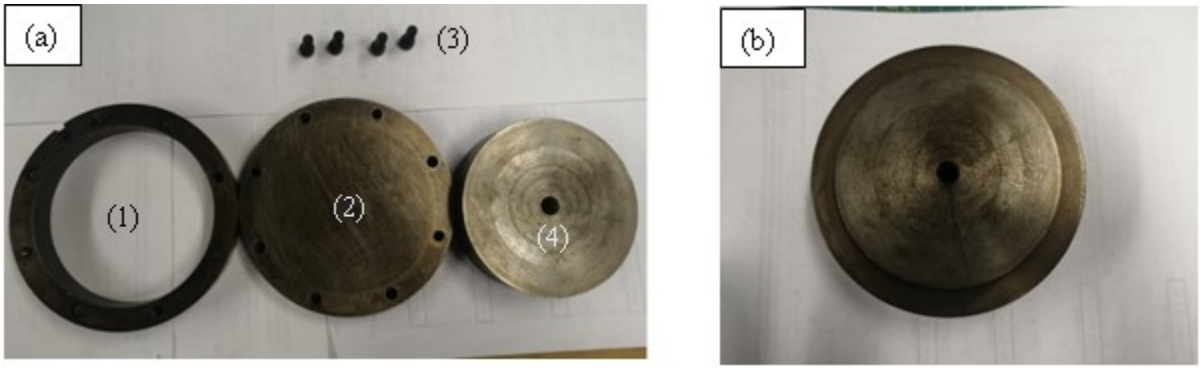

Figure 36. The shape of the custom-made cylindrical steel mold

a) The separate part of the hot-pressing mold, with (4) male die, the female die consisting of (1) cavity, (2) bottom, and (3) screws b) the shape of the whole mold combing the female die and male die.

Appendix C - Thermal Conductivity Testing Equipment

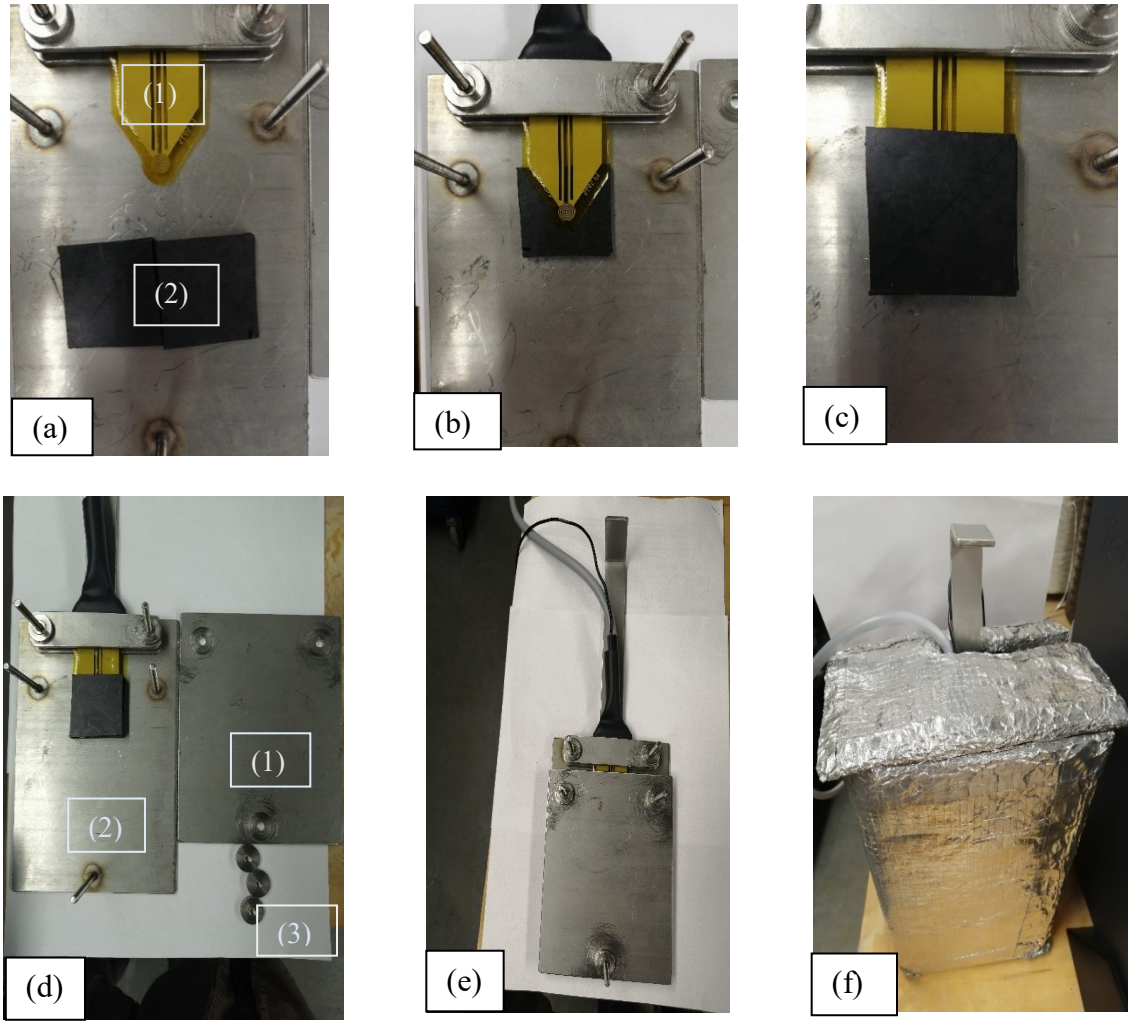

Figure 37. The process to sandwich the Kapton sensor with the two samples

a) the Kapton sensor (1) and two test specimens (2), b) putting one of the specimens under the sensor, c) putting the other one of the specimens above the sensor, d) the two parts of the holder (the bottom (1) and the top (2)) for compacting the sandwiched sensor, e) connecting the two parts of the holder with the screws in (3) of d), f) putting the holder into the cavity to maintain the testing temperature.

Appendix D - XRD Analysis Data

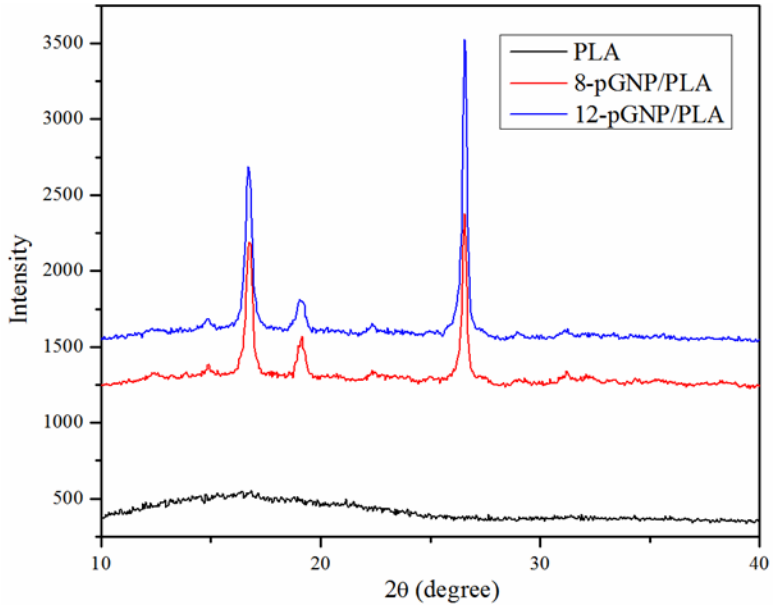

Figure 38. XRD pattern for neat PLA and its representative pGNP/PLA nanocomposites.

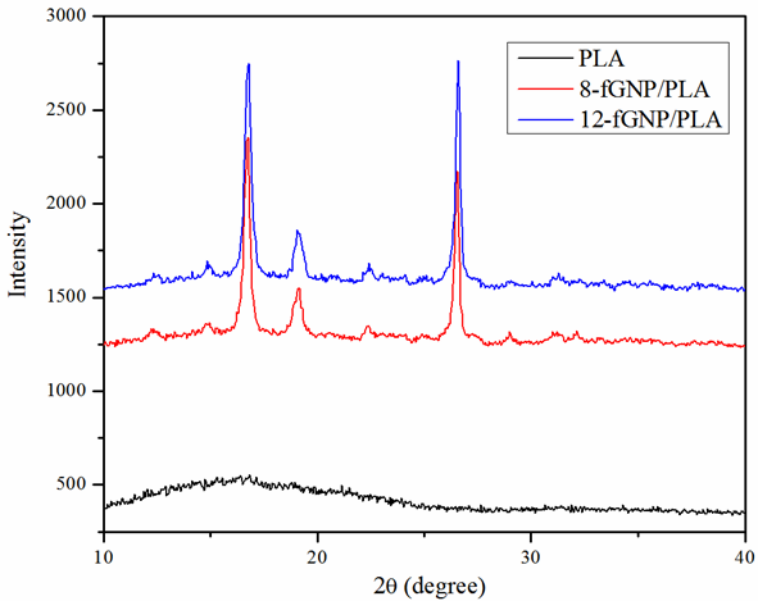

Figure 39. XRD pattern for neat PLA and its representative fGNP/PLA nanocomposites.

Appendix E - TGA Analysis Data

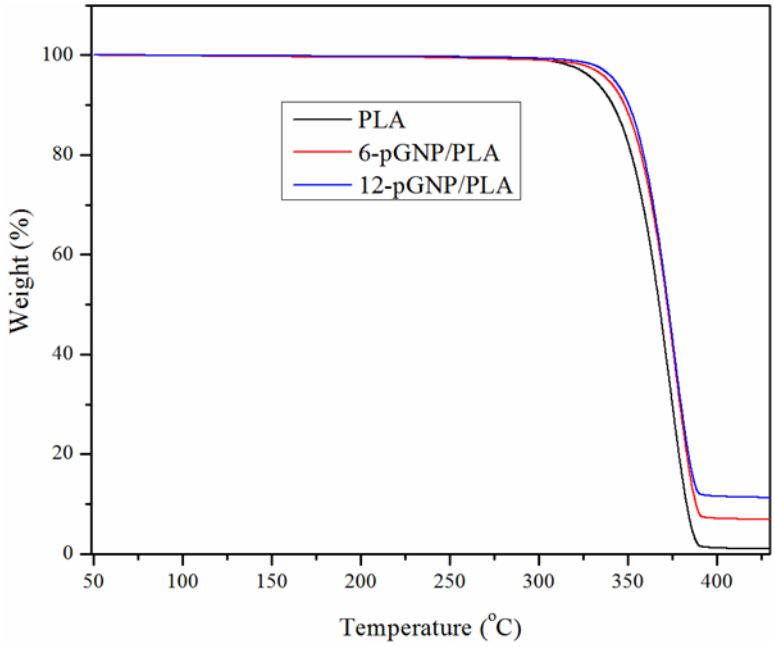

Figure 40.TGA curves of neat PLA and pGNP/PLA nanocomposites.

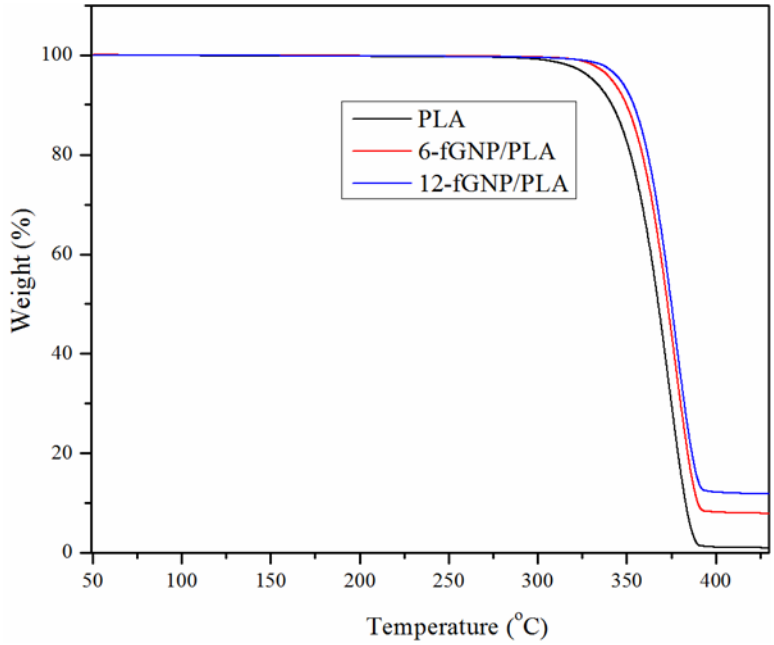

Figure 41. TGA curves of neat PLA and fGNP/PLA nanocomposites.

Appendix F - DMA Data

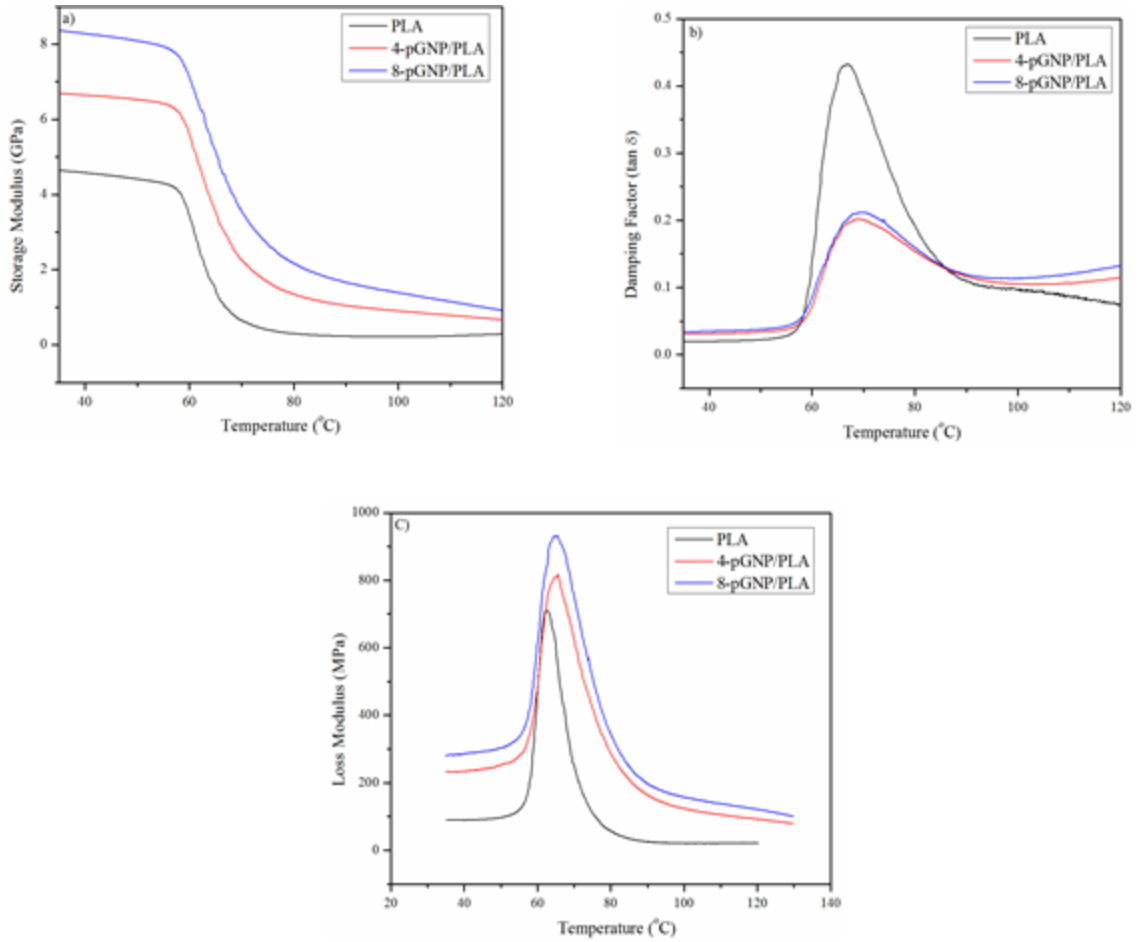

Figure 42. Dynamic mechanical properties of neat PLA and pGNP/PLA nanocomposites as a function of temperature: a) storage modulus, b) loss factor, and c) loss modulus.

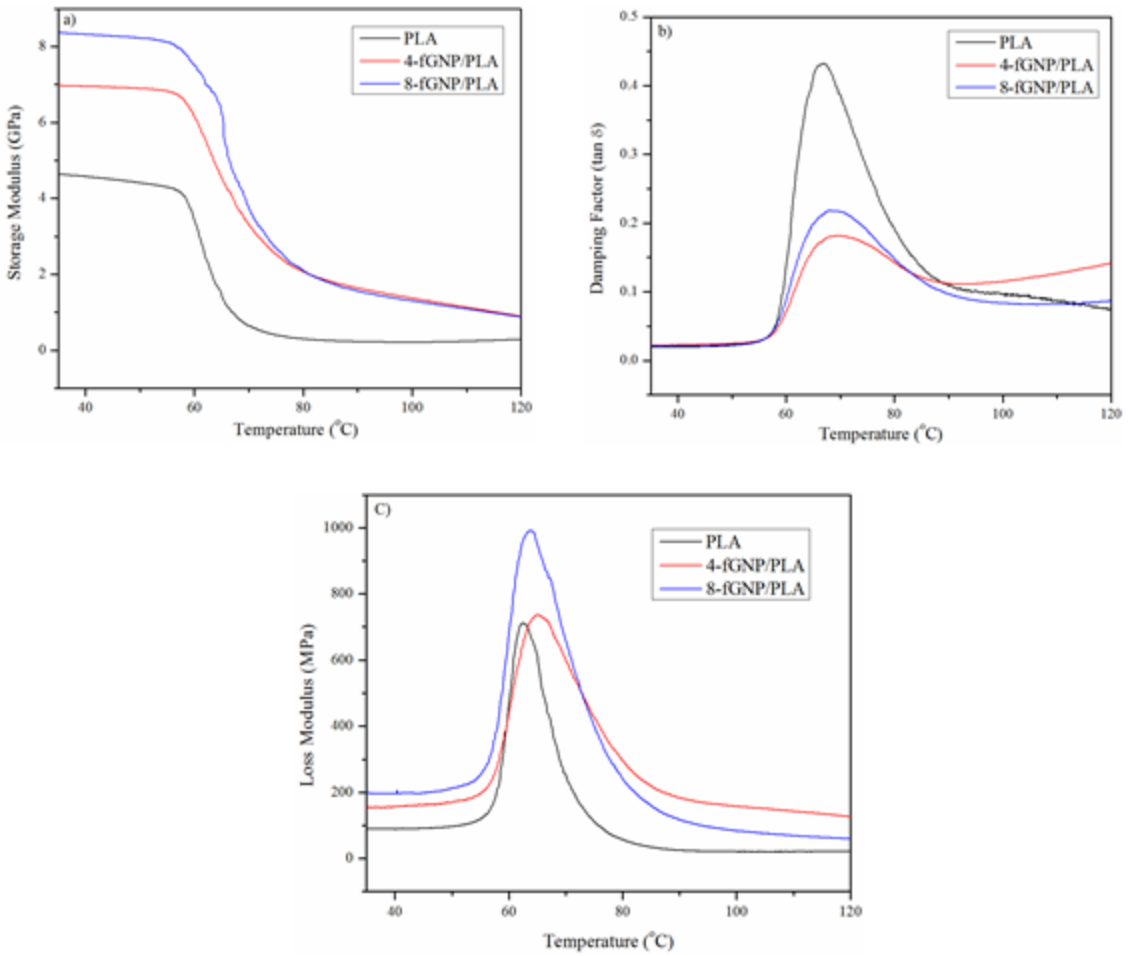

Figure 43. Dynamic mechanical properties of neat PLA and fGNP/PLA nanocomposites as a function of temperature: a) storage modulus, b) loss factor, and c) loss modulus.

Appendix G - Tensile Testing Data

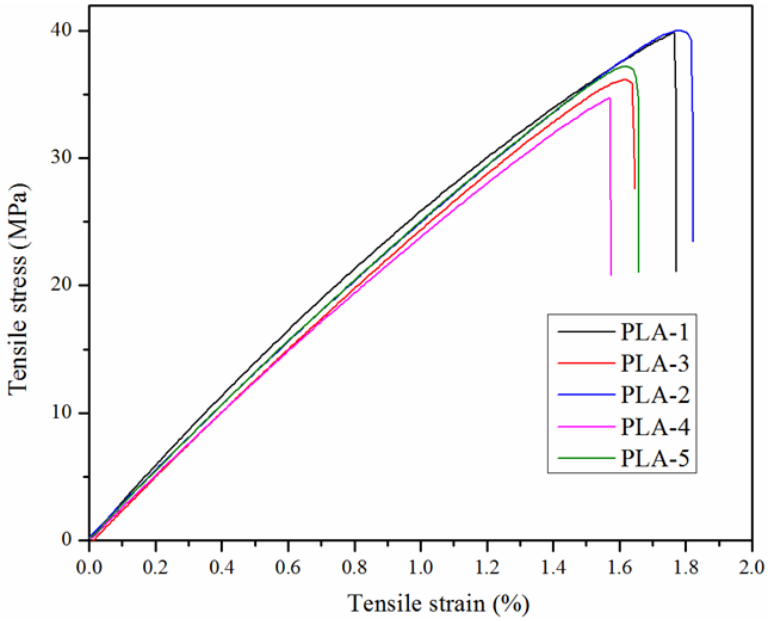

Figure 44. Representative stress-strain curves for neat PLA.

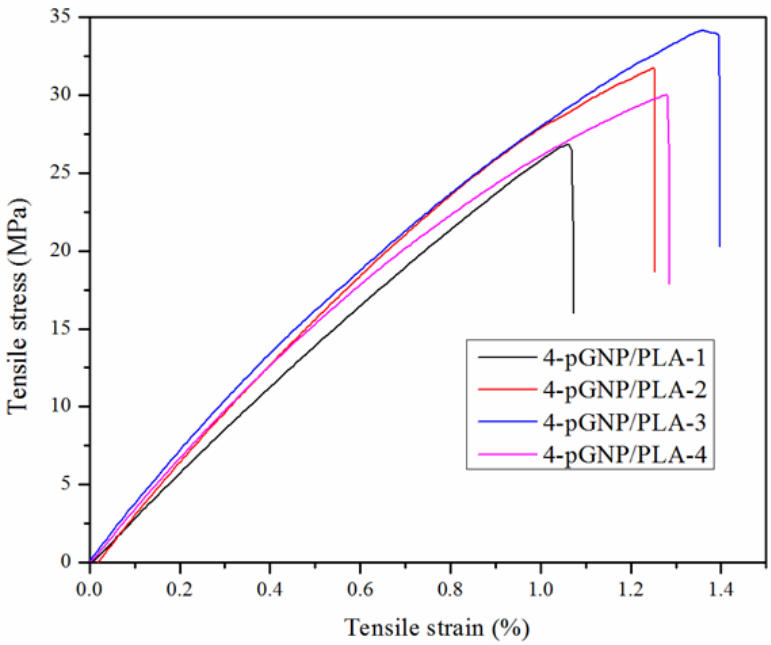

Figure 45. Representative stress-strain curves for 4-pGNP/PLA nanocomposites.

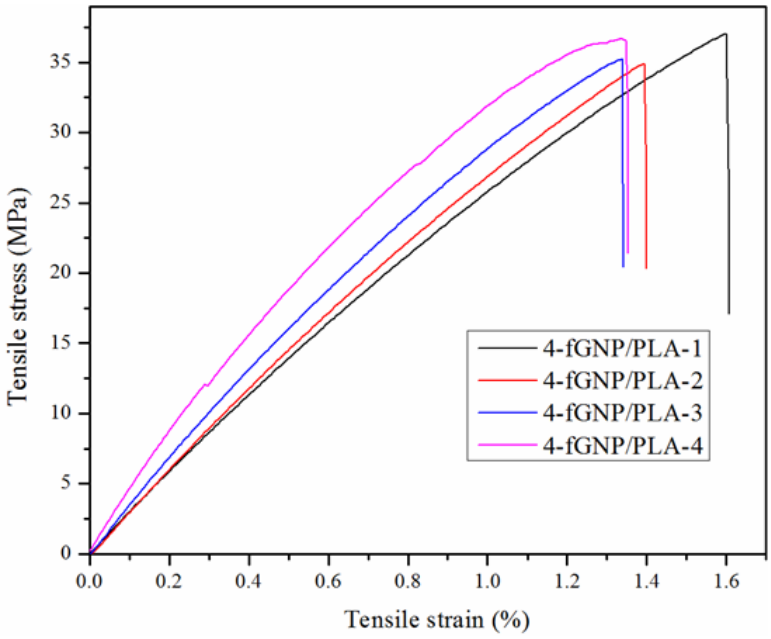

Figure 46. Representative stress-strain curves for 4-fGNP/PLA nanocomposites.

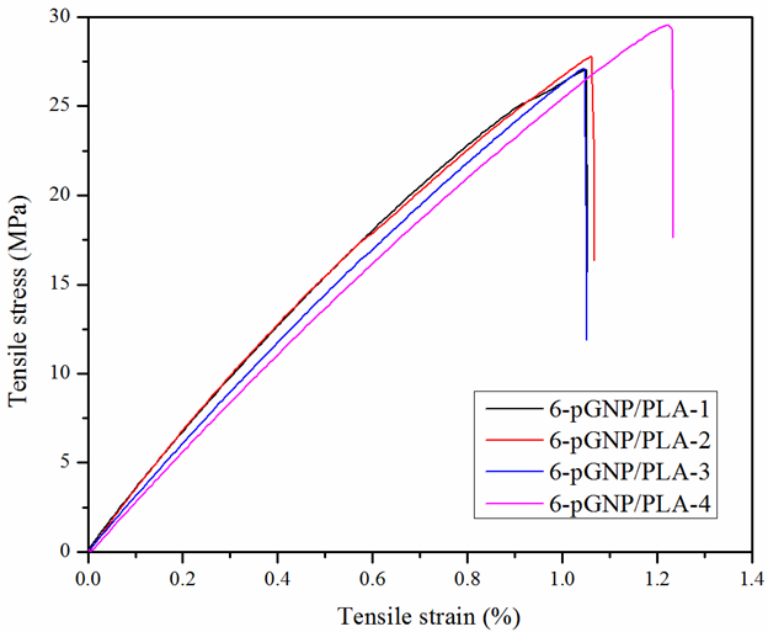

Figure 47. Representative stress-strain curves for 6-pGNP/PLA nanocomposites.

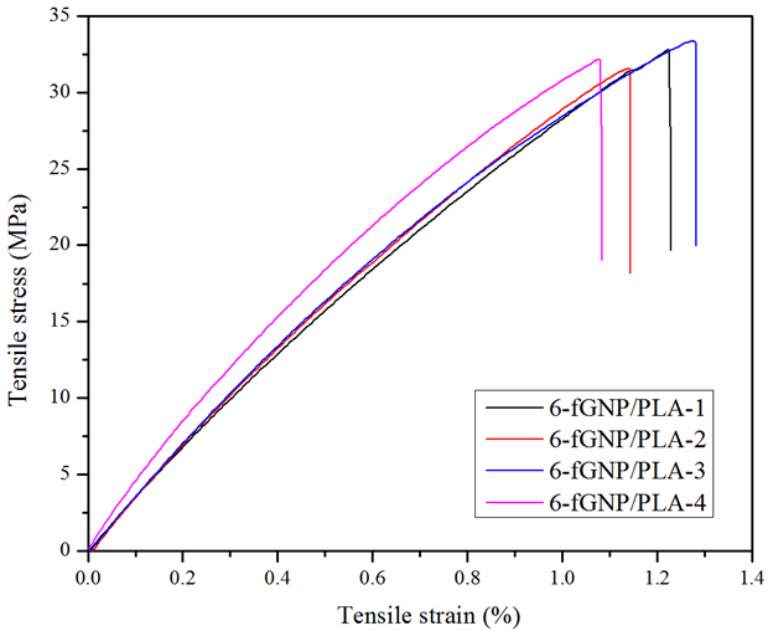

Figure 48. Representative stress-strain curves for 6-fGNP/PLA nanocomposites.

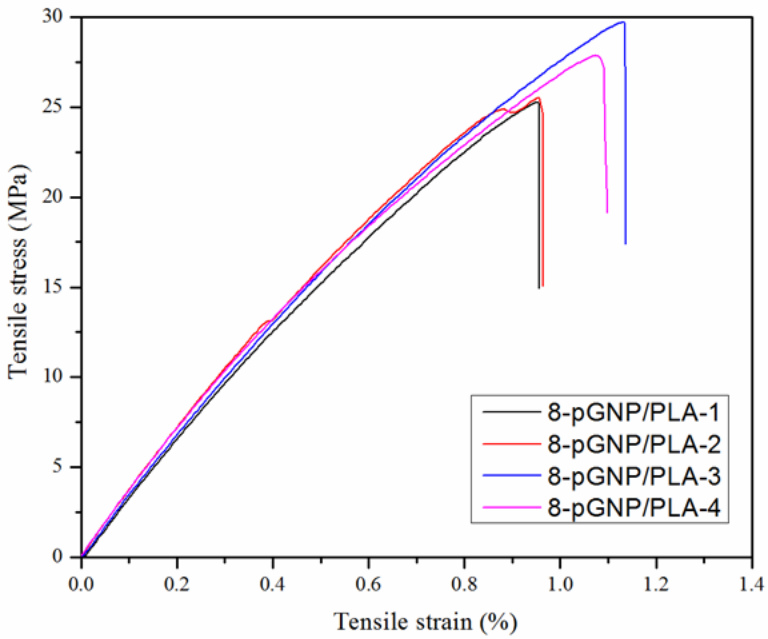

Figure 49. Representative stress-strain curves for 8-pGNP/PLA nanocomposites.

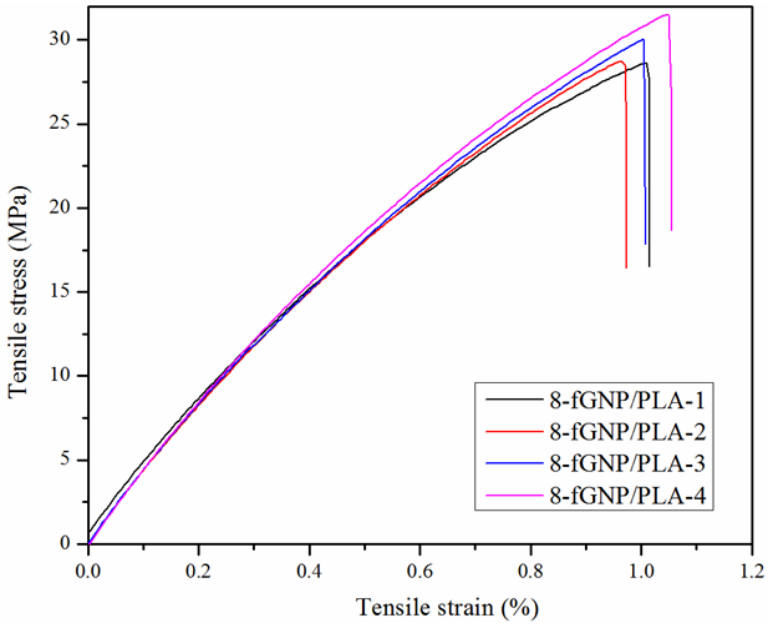

Figure 50. Representative stress-strain curves for 8-fGNP/PLA nanocomposites.

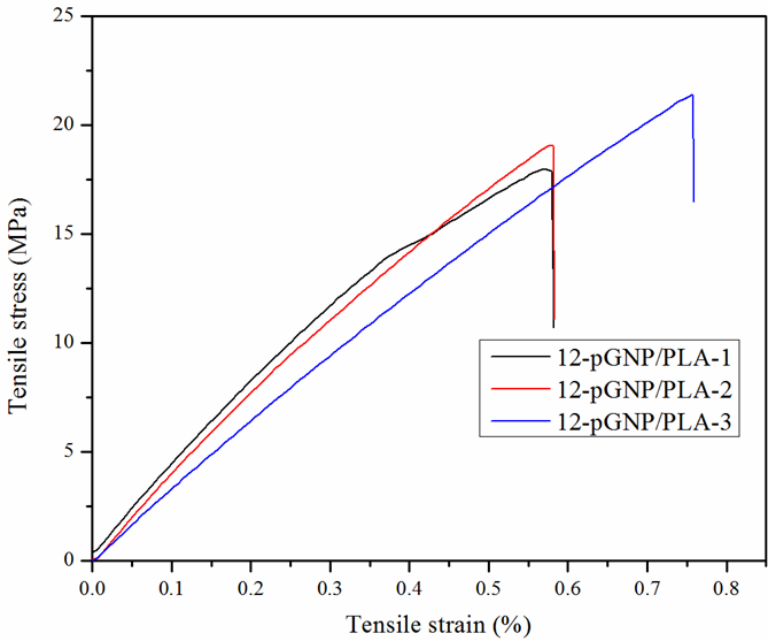

Figure 51. Representative stress-strain curves for 12-pGNP/PLA nanocomposites.

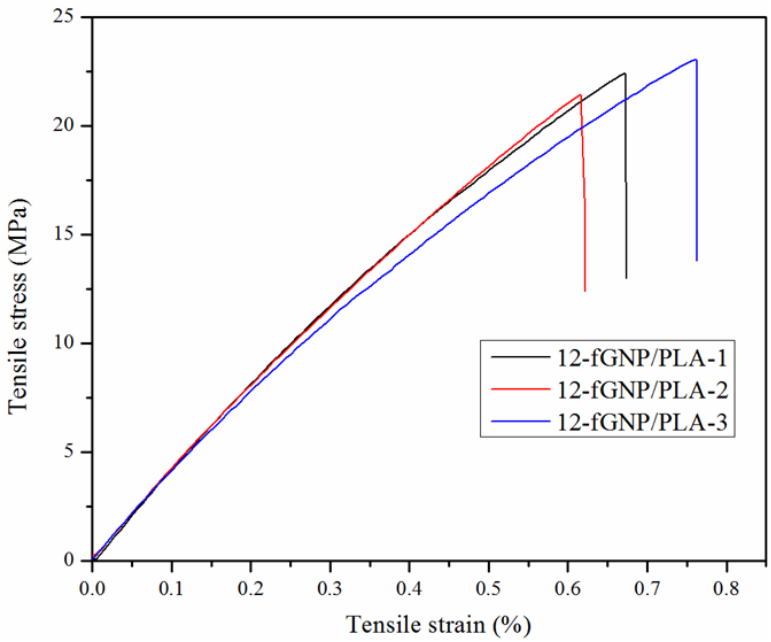

Figure 52. Representative stress-strain curves for 12-fGNP/PLA nanocomposites.

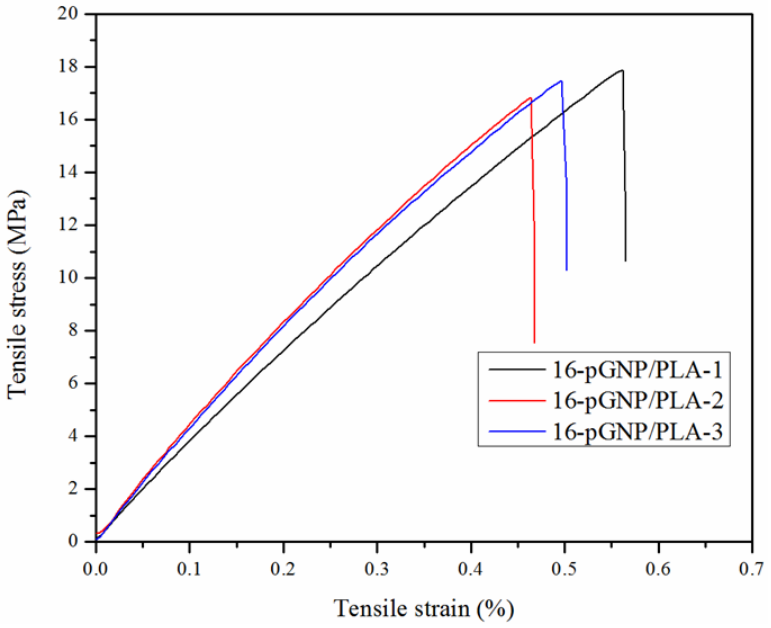

Figure 53. Representative stress-strain curves for 16-pGNP/PLA nanocomposites.

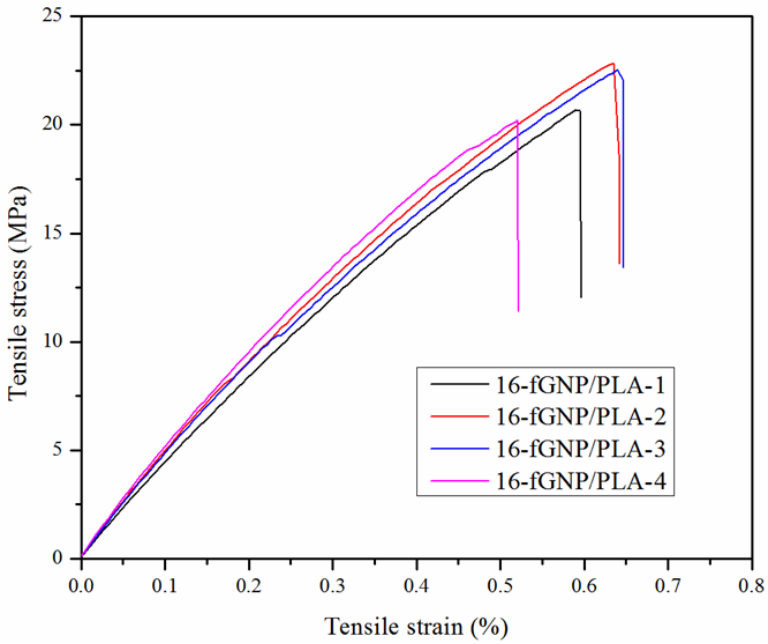

Figure 54. Representative stress-strain curves for 16-fGNP/PLA nanocomposites.

Appendix H - EMI Shielding Test Data

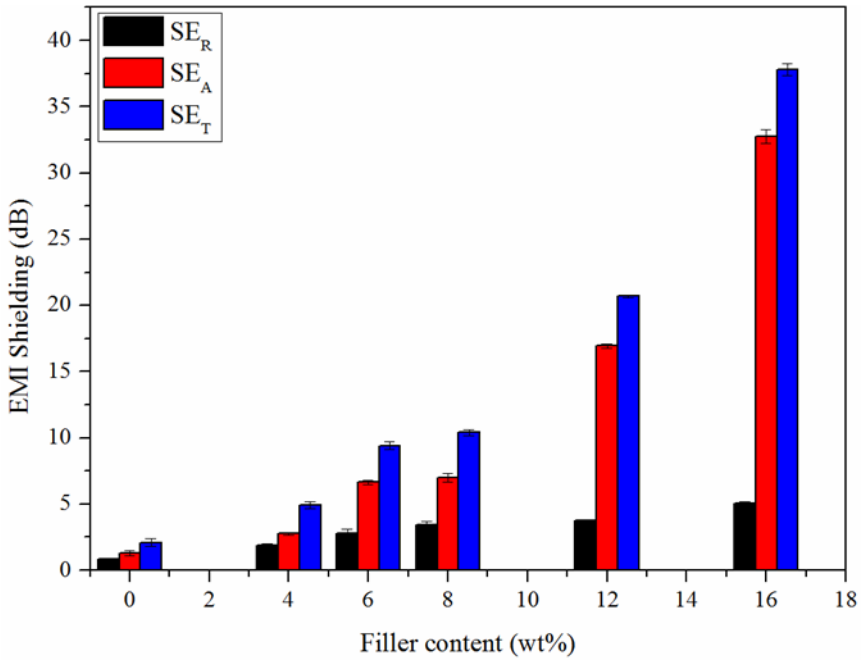

Figure 55. Values of SE_T, SE_A, and SE_R at different pGNP loading. Error bars represent standard deviations.